Rating Precast Prestressed Concrete Bridges for Shear

FINAL REPORT FHWA-OK-08-08

ODOT SPR ITEM 2186

By

Dr. Jin-Song Pei
Associate Professor

Mr. Randy D. Martin
Master's Candidate

Mr. Colby J. Sandburg
Former Master's Student

Dr. Thomas H.-K. Kang, P.E.
Assistant Professor

School of Civil Engineering and Environmental Science
University of Oklahoma
Norman, OK 73019

Technical Advisors:

Mr. Walter L. Peters, P.E.
Assistant Bridge Engineer

Mr. Robert J. Rusch, P.E.
Bridge Engineer

December 2008

TECHNICAL REPORT DOCUMENTATION PAGE

1. REPORT NO.	2. GOVERNMENT ACCESSION NO.	3. RECIPIENT'S CATALOG NO.
FHWA-OK-08-08		

4. TITLE AND SUBTITLE	5. REPORT DATE
Rating Precast Prestressed Concrete Bridges for Shear	December 2008
	6. PERFORMING ORGANIZATION CODE
7. AUTHOR(S)	8. PERFORMING ORGANIZATION REPORT
J.S. Pei, R.D. Martin, C.J. Sandburg, and T.H.-K. Kang	
9. PERFORMING ORGANIZATION NAME AND ADDRESS	10. WORK UNIT NO.
School of Civil Engineering and Environmental Science, University of Oklahoma, 202 W. Boyd St., Room 334, Norman, Oklahoma 73019-1024	11. CONTRACT OR GRANT NO. ODOT Item Number 2186
12. SPONSORING AGENCY NAME AND ADDRESS	13. TYPE OF REPORT AND PERIOD COVERED
Oklahoma Department of Transportation Planning and Research Division 200 N.E. 21st Street, Room 3A4 Oklahoma City, OK 73105	Final Report October 2005 – December 2008
	14. SPONSORING AGENCY CODE

15. SUPPLEMENTARY NOTES

16 . ABSTRACT

Shear capacity of real-world prestressed concrete girders designed in the 1960's and 1970's is a concern because AASHTO Standard Specifications (AASHTO-STD) employed the quarter-point rule for shear design, which is less conservative for shear demands than today's AASHTO LRFD.

Shear tests were conducted on two full sized AASHTO Type II girders, one of which had been in service for nearly forty years before being replaced due to irreparable damage.

The comparison of nominal shear capacities according to the 11th Edition AASHTO-STD (1973), AASHTO LRFD (2004), ACI 318-08 including provisions for strut and tie models is carried out. By examining the ratios of nominal shear capacity to demands for each code, considering all load and resistance factors, these code-to-code comparisons are better able to identify girders that may be deficient according to today's standards than a direct comparison of nominal capacities alone. Experimental results for shear capacity of real-world girders are compared with the codes' nominal capacities to check if the girders' are structurally sufficient. Additionally, LRFR is used to check the statistical safety for AASHTO inventory and legal loads.

Preliminary results are presented on the estimation of effective prestressing force using static test data. Nominal shear capacity is particularly sensitive to effective prestressing force under current design codes, so it's important to have accurate values when making calculations. In attempt to get more accurate results for effective prestressing force, span varying flexural stiffness is assumed. This assumption reflects that girders with long histories may be damaged, obvious or otherwise. Inverse problems are formulated where input and output are measured to determine system properties. Key challenges are discussed, and future work is identified.

For a given girder, the ratio of nominal shear capacity to demands has generally decreased with newer codes. Girders having this ratio near one for the 11th Edition AASHTO-STD may be structurally deficient according to newer codes, however, LRFR results show that the girders in this study are safe for all AASHTO legal loads. Experimental results indicate that the girders' actual capacity exceeds nominal capacity of current codes. Additional shear capacity tests should be performed on more real-world girders to get a more definitive conclusion.

17. KEY WORDS	18. DISTRIBUTION STATEMENT
Prestressed Concrete, Shear Capacity, Quart-Point Rule, Code Comparison, Testing & Inverse Problem of Aging Girder	No restrictions. This publication is available from The office of Planning & Research Division, Oklahoma DOT.

19. SECURITY CLASSIF. (OF THIS REPORT)	20. SECURITY CLASSIF. (OF THIS PAGE)	21. NO. OF PAGES	22. PRICE
Unclassified	Unclassified	118	

SI (METRIC) CONVERSION FACTORS									
Approximate Conversions to SI Units					**Approximate Conversions from SI Units**				
Symbol	**When you know**	**Multiply by**	**To Find**	**Symbol**	**Symbol**	**When you know**	**Multiply by**	**To Find**	**Symbol**
		LENGTH					**LENGTH**		
in	inches	25.40	millimeters	mm	mm	millimeters	0.0394	inches	in
ft	feet	0.3048	meters	m	m	meters	3.281	feet	ft
yd	yards	0.9144	meters	m	m	meters	1.094	yards	yds
mi	miles	1.609	kilometers	km	km	kilometers	0.6214	miles	mi
		AREA					**AREA**		
in^2	square inches	645.2	square millimeters	mm^2	mm^2	square millimeters	0.00155	square inches	in^2
ft^2	square feet	0.0929	square meters	m^2	m^2	square meters	10.764	square feet	ft^2
yd^2	square yards	0.8361	square meters	m^2	m^2	square meters	1.196	square yards	yd^2
ac	acres	0.4047	hectacres	ha	ha	hectacres	2.471	acres	ac
mi^2	square miles	2.590	square kilometers	km^2	km^2	square kilometers	0.3861	square miles	mi^2
		VOLUME					**VOLUME**		
fl oz	fluid ounces	29.57	milliliters	mL	mL	milliliters	0.0338	fluid ounces	fl oz
gal	gallon	3.785	liters	L	L	liters	0.2642	gallon	gal
ft^3	cubic feet	0.0283	cubic meters	m^3	m^3	cubic meters	35.315	cubic feet	ft^3
yd^3	cubic yards	0.7645	cubic meters	m^3	m^3	cubic meters	1.308	cubic yards	yd^3
		MASS					**MASS**		
oz	ounces	28.35	grams	g	g	grams	0.0353	ounces	oz
lb	pounds	0.4536	kilograms	kg	kg	kilograms	2.205	pounds	lb
T	short tons (2000 lb)	0.907	megagrams	Mg	Mg	megagrams	1.1023	short tons (2000 lb)	T
		TEMPERATURE (exact)					**TEMPERATURE (exact)**		
°F	degrees Fahrenheit	(°F-32)/1.8	degrees Celsius	°C	°C	degrees Fahrenheit	9/5(°C)+32	degrees Celsius	°F
		FORCE and PRESSURE or STRESS					**FORCE and PRESSURE or STRESS**		
lbf	poundforce	4.448	Newtons	N	N	Newtons	0.2248	poundforce	lbf
lbf/in^2	poundforce per square inch	6.895	kilopascals	kPa	kPa	kilopascals	0.1450	poundforce per square inch	lbf/in^2

TABLE OF CONTENTS

TABLE OF CONTENTS iv
LIST OF FIGURES vi
LIST OF TABLES ix
ACKNOWLEDGEMENT x
EXECUTIVE SUMMARY 1
1 INTRODUCTION 2
1.1 Motivation and Background 2
1.2 Technical Challenge and Proposed Solution 3
1.3 Structure of Report 6
2.1 Overview 7
2.2 Introduction to I-244 Bridge Girder 8
2.2.1 Brief History 8
2.2.2 Existing Damages and Reference System 14
2.3 Camber Measurements of Original I-244 Bridge Girder 17
2.4 Flexural Stiffness Tests of Original I-244 Bridge Girder 19
2.4.1 Test Configurations 19
2.4.2 Test Procedure 23
2.4.3 Results 24
2.5 Shear Tests of Original I-244 Bridge Girder 26
2.5.1 Test Configurations and Procedure 26
2.5.2 Results 29
2.6 Material Properties of Original I-244 Bridge Girder 31
2.7 Shortened I-244 Bridge Girder 32
2.7.1 Procedure 32
2.7.2 Results 34
2.8 Wild Horse Creek Bridge Girder 36
2.8.1 Introduction 36
2.8.2 Procedure 37
2.8.3 Results 39
3 ANALYTIC STUDY: SHEAR STRENGTH OF PRESTRESSED CONCRETE GIRDERS 41
3.1 Introduction 41
3.2 Overview of Codes 42
3.2.1 AASHTO Standard Specifications (1973) 42
3.2.2 AASHTO LRFD (2004) 46
3.2.3 ACI 318-08 48
3.3 Code Comparison 50
3.3.1 Design Philosophies 50
3.3.2 Minimum Shear Reinforcement 51
3.3.3 Shear Demands 51
3.3.4 Nominal Shear Strength 54
3.3.5 Margin of Safety 56
3.4 McCurtain County Bridge NBI #19257 58

3.5 Strut and Tie Models 59
3.6 Failure Modes 62
3.7 Comparison between Nominal and Experimental Shear Capacity 63
3.8 Load Posting based on LRFR 64
4 INVERSE PROBLEM: PRELIMINARY RESULTS OF IDENTIFICATION OF EI VALUE AND PRESTRESSING STRESS OF I-244 BRIDGE GIRDER 67
4.1 Motivations 67
4.2 Overview 67
4.2.1 Identification of Piecewise Constant EI Values 67
4.2.2 Identification of Prestressing Stress 68
4.3 Technical Challenges 69
4.3.1 Justification of Basic Assumption 69
4.3.2. Available Tests 69
4.3.3 Comparison of Various Types of Measurements 70
4.4 Estimating Flexural Stiffness 71
4.4.1 Data Cleansing 71
4.4.2 Problem Formulation 72
4.4.3 Programming Effort 74
4.4.4 Determining Initial Values 75
4.4.5 Linear Least-Squares Solutions 77
4.5 Processing Camber Measurements 81
4.5.1 Review of Time-Dependent Deformation 81
4.5.2 Overview of Proposed Research 82
4.5.3 Preliminary Analysis 86
4.5.4 Refined Analysis 89
4.6 Discussions 89
4.6.1 Derivation of Camber Formulas Related to Asymmetrical Strand Profiles 89
4.6.2 Other Means to Estimate Prestressing Stress 92
4.6.3 Future Work 94
5 CONCLUSION 97
REFERENCE 98

LIST OF FIGURES

Figure 1: Elevation of the Little River Overflow Bridge ("Bridge C", NBI No. 19257) and the details of the selected girder (ODOT [1967]). 3
Figure 2: Elevation and details of the selected I-244 Bridge girder (ODOT [2006]). 8
Figure 3: The I-244 Bridge girder (a) before (taken by Mr. Richard Moon) and (b) after the slab was removed by Concrete Services Corporation. 9
Figure 4: Track hoe used to demolish the girder from the I-244 Bridge. 9
Figure 5: Augustine, a Concrete Services Corporation employee, removing remaining slab on April 21, 2006 10
Figure 6: (a1) Front view, and (a2) side view of the depth gage. (b1) The depth gage being installed, and (b2) the depth gage being used. 10
Figure 7: Retrofitting process documented by Mr. Christopher Davis: (a1) using a pneumatic drill to remove unsound concrete; (a2) using a standard hammer to remove unsound concrete so that more damage was not done; (a3) original view of damage to the bottom of the girder; (b1) sandblasting the surface; (b2) using a pressure injection epoxy to repair existing cracks; (c1) applying the initial coat of the wet mortar; (c2) applying the second coat of the intermediate mortar; (c3) the final mortar being the thickest and the repaired end finally shaped; (c4) the burlap sack that was used during curing; (d1) rolling on the epoxy to the girder prior to install the FRP wrap; (d2) impregnating the three-layer FRP wrap prior to installing it, and (d3) rolling the FRP wrap onto the girder to avoid air voids in the finished product. 11
Figure 8: Girder unloading at Fears Lab: (a1) The girder on the delivery truck; (a2) the delivery truck backing into Fears lab; (a3) the cribbing built to support the girder while the truck left; (b1) the roller the girder was rolled on; (b2) the girder supported by the crane and the cribbing; (b3) the steel support the girder rested on after the truck left; (c1) the girder being lowered to the ground, and (c2) the girder being placed into the final location. 13
Figure 9: AutoCAD rendering with damages documented and highlighted. (a1) and (a2) Damages due to corrosion, and (b1) and (b2) damages caused when the girder was removed from the I-244 Bridge and perhaps, during the clean-up process. 14
Figure 10: Location and extent of some of damages of the I-244 Bridge girder. These damages include both caused by removing the girder from the bridge and clean-up process. 15
Figure 11: A schematic plan view of Fears Lab shows where the I-244 Bridge girder and loading frame are located as well as two photos to show where the diaphragm hole is located. 16
Figure 12: Grid system placed on the I-244 Bridge girder, where (a) shows the origin, i.e., the hole pointing to the diaphragm's location (circled), and (b) shows the grid system drawn by Mr. Aaron Landrum using Sharpie markers and the stirrups located by Mr. Krisda Piyawat using a pacometer borrowed from ODOT. 17
Figure 13: Summary of all measured camber profiles of the original I-244 Bridge girder before and after flexural stiffness tests 18
Figure 14: Summary of all measured camber profiles of the original I-244 Bridge girder before shear tests. 18
Figure 15: Instrumentation used in testing the original I-244 Bridge girder: (a1) Loading plate; (a2) one of the load cells used to determine the load applied to the girder; (a3) hydraulic pump to apply the load; (b1) front panel of the DAQ system; (b2) bracing used for stability; (b3)

loading frame used for flexural stiffness and shear tests; (c1) and (c 2) LVDTs, and (c3) wire potentiometers. 24
Figure 16: Illustration of data cleansing. (a) An original plot that shows the erroneous points, and (b) a modified plot that has the erroneous points removed and other data points averaged. 25
Figure 17: Results of flexural stiffness test 1B. 26
Figure 18: Illustrations of the setup and instrumentation for (a) the first set of shear tests on the non-retrofitted end of the girder, and (b) the second set of shear tests on the retrofitted end. 27
Figure 19: Crack pattern on the girder as a result of the two shear tests on the non-retrofitted end. 30
Figure 20: Crack pattern on the girder as a result of the two shear tests on the retrofitted end. 30
Figure 21: An illustration of softening trend from the first to second shear tests performed on the non-retrofitted end. 31
Figure 22: (a) Forney LC-1 testing machine (For [2005]) used for material testing, and (b) a view into the Forney machine with a concrete cylinder. 31
Figure 23: Flexure test configurations for shortened I-244 Bridge girder. 33
Figure 24: Shear test configurations for shortened I-244 Bridge girder. 34
Figure 26: Elevation and details of the selected Wild Horse Creek Bridge girder (Coreslab [2007]). 36
Figure 27: Flexural stiffness test configurations for the Wild Horse Creek Bridge girder. 37
Figure 28: Configuration for measuring camber of the Wild Horse Creek Bridge girder. 38
Figure 29: Shear test configurations of the Wild Horse Creek Bridge girder performed July 2008. 38
Figure 30: Camber profile of the Wild Horse Creek Bridge girder after Shear Test #1 failure 39
Figure 31: Lane loading for AASHTO-STD based on desired truck loading (AASHTO, 1973). 43
Figure 32: (a) H and (b) HS design trucks (AASHTO, 1973). 44
Figure 34: Minimum shear reinforcement with varying concrete compressive strength. 51
Figure 35: Comparison of ultimate shear demands between codes. 54
Figure 36: Nominal shear strength as affected by concrete compressive strength for AASHTO Types II, III and IV prestressed concrete girders, respectively. 55
Figure 37: Nominal shear strength of a Type II girder with varying stirrup spacing. 56
Figure 38: Margin of safety as affected by concrete compressive strength for AASHTO Types II, III and IV prestressed concrete girders, respectively. 57
Figure 39: Margin of safety of a Type II girder with varying stirrup spacing 58
Figure 40: (a) Design shear requirements, (b) nominal shear capacities, and (c) margins of safety for the Little River Overflow Bridge in McCurtain County, Oklahoma 59
Figure 41: Truss model used for analysis. 60
Figure 42: Nominal moment capacity for I-244 girder based on ACI-318. 63
Figure 43: Shear envelope based on nominal moment resistance (see Figure 42). 63
Figure 44: Comparison between the nominal shear strength and measured shear capacity of the selected I-244 Bridge girder. 64
Figure 45: Illustration of constant *EI* value vs. five piecewise constant *EI* values for a generic case. 68
Figure 46: An illustration of the quantities involved in Equation (28). 73
Figure 47: An illustration of multiple load-displacement relationships obtained from multiple flexural stiffness tests. 73

Figure 48: Flowchart for program to determine piecewise flexural stiffness. 75
Figure 50: Unconstrained linear least-squares results for piecewise flexural stiffness of the I-244 girder with initial values of zero. 77
Figure 51: (a) Various initial values defined in this study, and (b) the results obtained by using the initial values specified in (a). 79
Figure 52: (a) Random initial values adopted in this study, and (b) the results obtained by using the random initial values specified in (a). 80
Figure 53: Illustrations of the applied moment and camber histories for the I-244 Bridge girder to the best of our knowledge. 83
Figure 54: Breakdown of tasks. 85
Figure 55: Typical camber profiles of the I-244 Bridge girder in an original and a shortened condition. 87
Figure 56: Theoretical values of camber and deflection of the original I-244 girder based on the basic assumptions made for preliminary analysis as in Section 4.5.2. 88
Figure 58: Free body diagram shown in Figure 57 broken down into x- and y-components. 91
Figure 60: Mohr's Circle of an element at the neutral axis of a prestressed concrete girder when shear cracking begins. 93
Figure 61: Deflection profile of girder during flexure test 3A at multiple loads. 95
Figure 62: Deflection profile of girder during flexure test 4A at multiple loads. 95

LIST OF TABLES

Table 1: Pros and cons of possible options in this study 4
Table 2: Scope of work of this study. †Limited preliminary work conducted on finite element modeling of a bridge girder. ‡(1) An additional experimental study conducted on the shear capacity of a Type II girder reinforced with externally bonded glass fiber fabric. (2) another additional analytic study started on shear design using AASHTO-LRFR (AASHTO [2006]). 4
Table 3: Structure of this report 6
Table 4: Summary of experiments in this project 7
Table 5: All test configurations of flexural stiffness tests on the original I-244 Bridge girder. .. 20
Table 6: Summary of shear test results of the original I-244 Bridge girder. 29
Table 7: Failure loads, strengths, and adjusted strengths (according to Mindess et al. [2003]) of three 2.7" x 6" cylindrical concrete specimens cored during the cutting of the original I-244 Bridge girder and tested in compression according to ASTM [2001]. 32
Table 8: Results of shear tests of the shortened I-244 Bridge girder. 35
Table 9: Results from shear capacity tests conducted in summer 2008. 39
Table 11: Properties of model girders used in this section, unless specified otherwise. 55
Table 12: Nominal shear capacity based on capacity of strut S_1 and tie T_1. 62
Table 13: Rating factors of I-244 and LRO bridges for inventory and AASHTO legal loads 66
Table 14: Contrast between analyzing flexural stiffness test data and camber measurements .. 70
Table 15: Programs called by "piecewise_ei.m" to assist in calculating five *EI* values. 74
Table 16: Pros and cons of two distinctive choices of problem formulation in inverse analysis. 85
Table 17: Summary of available camber measurements. 86
Table 18: Quick analysis of peak camber measurements in Figure 55 89
Table 19: Project time line: Part 1 of 6. 103
Table 20: Project time line: Part 2 of 6. 104
Table 21: Project time line: Part 3 of 6. 105
Table 22: Project time line: Part 4 of 6. 106
Table 23: Project time line: Part 5 of 6. ..... **Error! Bookmark not defined.**
Table 24: Project time line: Part 6 of 6. ..... **Error! Bookmark not defined.**

ACKNOWLEDGEMENT

The authors would like to express their sincere gratitude to the following organization and personnel:

- Funding Agency: Oklahoma Department of Transportation (ODOT)
- Donations of girders for testing: Mr. Dewayne Jantz, Becco Inc. and Coreslab Structures Inc.
- Assistance is provided by the following engineers at ODOT: Mr. Walt Peters, Mr. Richard Moon, Ms. Annie Lombardo, Mr. Kenny Seward and Ms. Siv Sundaram
- Lab testing assistance provided by Mr. Michael Schmitz and Dr. Christopher Ramseyer at OU is greatly appreciated
- Thanks to Ms. Priyantha Wijesinghe, Mr. Aaron Landrum, Mr. Christopher Davis, Mr. Krisda Piyawat and Mr. Eric Mai for their assistance in experimental studies
- Thanks to Mr. Krisda Piyawat and Ms. Priyantha Wijesinghe for their preliminary numerical analysis
- The participation of REU students Ms. Sarah Zimmermann, Mr. Craig Borchard, Mr. Werner Stiegler and Mr. Archith Ramkumar in Summer 2007 and Mr. Joseph Howell in Summer 2008 is acknowledged
- The contributions made by Mr. Rami Akkari to produce an accessible report are greatly appreciated
- Discussions with Professor Luther White on his independent data processing are appreciated

EXECUTIVE SUMMARY

Shear capacity of real-world prestressed concrete girders designed in the 1960's and 1970's is a concern because AASHTO Standard Specifications (AASHTO-STD) employed the quarter-point rule for shear design, which is less conservative for shear demands than today's AASHTO LRFD.

Shear tests were conducted on two full sized AASHTO Type II girders, one of which had been in service for nearly forty years before being replaced due to irreparable damage. As a means to improve analysis, additional experimental data are used to determine the effective prestressing force of these specimens. Comparisons are then made between three design codes and experimental results to assess the condition and safety of similar girders currently in use.

The comparison of nominal shear capacities according to the 11th Edition AASHTO-STD (1973), AASHTO LRFD (2004), and ACI 318-08 including provisions for strut and tie models is carried out. Composite sections are analyzed with varying properties (concrete compressive strength, transverse reinforcement spacing, etc.) for AASHTO Type II, III and IV prestressed concrete girders. By examining the ratios of nominal shear capacity to demands for each code, considering all load and resistance factors, these code-to-code comparisons are better able to identify girders that may be deficient according to today's standards than a direct comparison of nominal capacities alone. Experimental results for shear capacity of real-world girders are compared with the codes' nominal capacities to check if the girders' are structurally sufficient. Girders are also rated according to AASHTO LRFR (2005) to check if AASHTO inventory and legal loads are permissible.

Preliminary results are presented on the estimation of effective prestressing force using static test data; an inverse problem is formulated where input and output are measured to determine system properties. Nominal shear capacity is particularly sensitive to effective prestressing force under current design codes, so it's important to have accurate values when making calculations. Although there are methods for determining long-term prestress losses, they apply to a wide variety of structural members and do not necessarily reflect the condition of girders and their uncertain histories studied here. In attempt to get more accurate results for effective prestressing force, span varying flexural stiffness is assumed. This assumption reflects that girders with long histories may be damaged, obvious or otherwise. The load balancing method is used in conjunction with the principle of virtual work to express camber and Δ/P in terms of effective prestressing force and/or piecewise-constant flexural stiffness. Least squares techniques are used to solve these overdetermined problems. The key challenges include the problem formulation considering time-dependent properties, the selection of appropriate initial values, and the interpretation the results.

For a given girder, the ratio of nominal shear capacity to demands has generally decreased with newer codes. Girders having this ratio near one for the 11th Edition AASHTO-STD may be structurally deficient. Experimental results from this study, however, indicate that the girders' actual capacity exceeds nominal capacity of current codes. Additional shear capacity tests should be performed on more real-world girders to get a more definitive conclusion.

1 INTRODUCTION

1.1 Motivation and Background

Bridges in Oklahoma are deteriorating, but replacements or even routine maintenance have been postponed due to inadequate funding. Some of the repairs of these bridges have been started, but before large scale repairs can be done, the current load-carrying capacities of these bridges need to be evaluated. The goal of this project is to help Oklahoma Department of Transportation (ODOT) engineers determine if the shear capacity of precast prestressed concrete bridge girders designed according to the "quarter-point rule" is adequate. The outcome of this research will lead to critical decisions made regarding load postings or retrofitting. It can be seen that this study has a significant economic and social impact.

Prestressed concrete has been one of the major construction forms used for highway bridges with precast pretensioned prestressed concrete being fairly popular in Oklahoma. This study targets precast pretensioned prestressed concrete bridge girders designed according to the American Association of State Highway and Transportation Officials (AASHTO) Standard Specifications prior to the 1979 interim. Several types of AASHTO prestressed concrete bridge girders are used by ODOT including Types II, III, and IV, each having a different typical span and cross-sectional dimensions. Type II girders are the focus of this study.

One of the major design requirements for prestressed concrete is shear capacity. Shear failure is an important failure mode due to its brittle nature. For decades, research on shear capacity has been very active. Noteworthy is the development of modified compression field theory (MCFT, Duthinh [1999], Bentz et al. [2006], Kuchma et al. [2008b]) and strut-tie model (Reineck [2007]). As a consequence, design codes on shear evolve with time. Ongoing debates are on safety/conservative nature of various shear design criteria (e.g., Shahawy and Batchelor [1996, 1997], Ma et al. [1997]). To contribute to this active research topic, our project provides experimental results of full-scale girders. In parallel, a spectrum of design codes for shear is compared including AASHTO [1973, 2004 and 2005] and ACI [2002]. They are applied to a series of typical and specific designs of AASHTO prestressed concrete bridge girders that are used on Oklahoma highway bridges.

D'Arcy et al. [2008] gives a review of the evolution of the design codes for AASHTO pre-stressed concrete bridge girders. We are concerned about the "quarter-point rule" that had been used in the shear design of highway bridge girders in Oklahoma following the AASHTO Standard Specifications prior to the 1979 interim. The "quarter-point rule" allows engineers to design an outer quarter span of a girder based on the shear at the quarter point. The current design codes in shear (AASHTO [2004]) are considered less conservative than the "quarter-point rule", which causes concerns on the safety of the bridge girders designed in the 1960's and 1970's. The deteriorating condition and often increased traffic load on these bridges have elevated the concerns on the actual shear capacity of these girders.

A critical case of the above-mentioned bridge girders in question is the interior Type II girders on the Little River Overflow Bridge as identified by ODOT engineers and shown in Figure 1. The drawing (ODOT [1967]) indicates these Type II girders with a large beam spacing of 11'9".

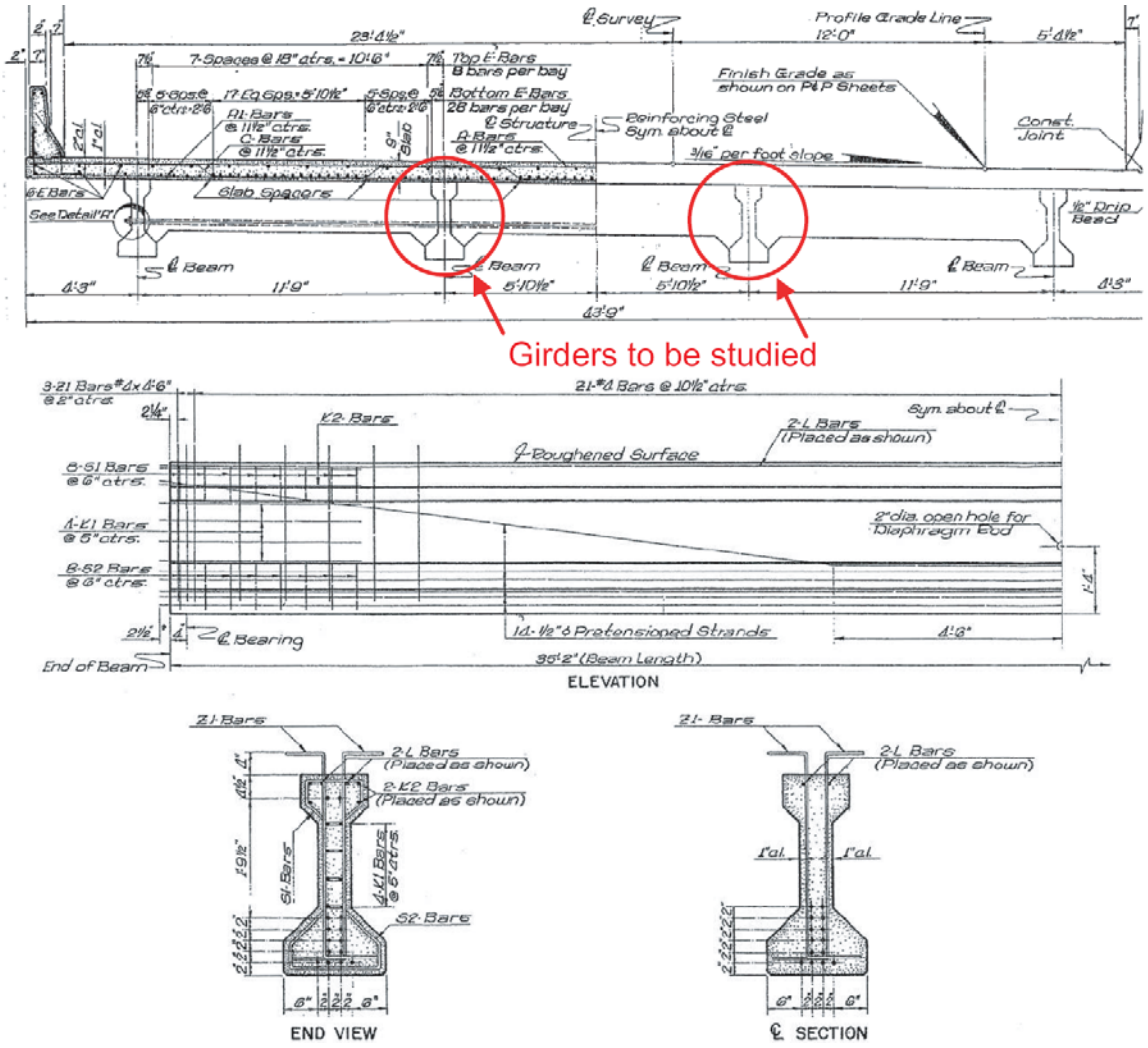

Figure 1: Elevation of the Little River Overflow Bridge ("Bridge C", NBI No. 19257) and the details of the selected girder (ODOT [1967]).

1.2 Technical Challenge and Proposed Solution

Physical experiments have been a powerful means in scientific research. With no exceptions, there is a large body of literature on experimental investigations of shear capacity of prestressed concrete girders. A non-exhaustive list includes Zwoyer [1953], Sozen [1957], Olesen et al. [1965], Russel and Burns [1993], Tawfiq [1995], Cumming et al. [1998], Ahlbom [1953]. Challenges in designing and conducting tests on girders in shear in this project come from these two major requirements/constraints:

1. The actual shear capacity of girders designed according to an out-of-date design code is in need.
2. We have to acquire and test full-scale girders in a cost-effective manner given the budget constraint and lab testing condition.

Given the loading capacity at Fears Structural Engineering Laboratory at the University of

Oklahoma, testing Type II AASHTO prestressed concrete girders is feasible. Two subsequent options are compared as shown in Table 1: Option 1 is to obtain girders from real-world bridges, which were designed according to the "quarter-point" rule, ship these girders to lab and test them to shear failure. Option 2 is to cast mock girders in a precast prestressed concrete production facility, ship them to lab for testing and test them to shear failure.

Option	Girder	Pros	Cons
1	Old	Fetched from real world. Time-dependent effect and aging condition built-in. Results convincing. Results directly related to other girders on the same bridge or even more.	Availability very limited. No severe damage hard to guarantee. Fatigue, corrosion and aging leading to unknown properties and making analysis challenging. Instrumentation limited. Costly shipping.
2	New	New design and casting leading to better controlled properties and making embedded instrumentation possible.	Aging effect hard to reproduce. Concrete strength hard to precisely match old design. Results hard to be convincing. Costly overall budget.

Table 1: Pros and cons of possible options in this study

Given the low chance to have any real-world Type II AASHTO girders available for testing, Option 2 was considered in the proposal of this project. The scope of work of the entire project was outlined accordingly as in Table 2. Fortunately, a rare opportunity presented itself to us and we were able to seize it with the support from ODOT engineers: A Type II AASHTO girder designed according to the "quarter-point rule" became available for this project after about forty years in service (Peters and Rusch [2006 - 2008]). To best utilize this precious first-hand information, the entire project was reshaped accordingly. See the actual scope of work in Table 2.

	Type II	Type III	Type IV
Web thickness	6"	7"	8"
Approximate typical span range (varying with beam spacing)	35'-50'	50'-75'	75'-100'
Proposed scope of work	Analytic study, experimental study, and finite element modeling	Analytic study	Analytic study
Accomplished scope of work	Analytic study, experimental study, and inverse problem†‡	Analytic study	Analytic study

Table 2: Scope of work of this study. †Limited preliminary work conducted on finite element modeling of a bridge girder. ‡(1) An additional experimental study conducted on the shear capacity of a Type II girder

reinforced with externally bonded glass fiber fabric. (2) another additional analytic study started on shear design using AASHTO-LRFR (AASHTO [2006]).

As will be introduced in detail in Section 2.2.1, there was a Type II AASHTO girder removed from the I-244 Bridge in Tulsa over the Arkansas River in August 2005. The challenge with this I-244 Bridge girder is that there are already some major damages that resulted in it being decommissioned from service. The bridge that the girder was removed from had corrosion issues from poor drainage. Girders with damages to a similar degree were removed and replaced, while those with minor damages were retrofitted with glass fiber reinforced polymer (GFRP), an externally bonded reinforcement. The retrofitted girders were first repaired with mortar and then glass fiber fabric (Sik [a]) which was attached using high strength impregnating resin Sik [b] to the girder. The selected I-244 Bridge girder had one severely corroded end. In this project, this very end was retrofitted using the same materials (Sik [a,b]) and procedure (Okl [2004]) by the same contractor (Peters and Rusch [2006]) as those girders strengthened and stayed in service on the bridge. The shear test result on the retrofitted end in Section 2.5.1 further provides the ODOT engineers with precious first-hand information on the performance of the GFRP reinforcement that ODOT engineers are interested.

The use of one single girder from the I-244 Bridge is fully exploited in the experimental study. First, independent and identical shear tests were performed on both ends (with one non-retrofitted and the other, retrofitted), respectively, to allow a comparison of the results on a light-to-light basis. These shear tests are referred to under the condition of the original I-244 Bridge girder hereafter. After these shear tests, the original I-244 Bridge girder was shortened by completely removing its two damage ends. Once again, independent and identical shear tests were designed for the shortened girder, referred to as the condition of the shortened I-244 Bridge girder hereafter. The advantage of this overall design was to maximize the gain from this precious and unique girder obtained from a real-world bridge. The disadvantage, however, was that the loading point was in a D- (i.e., disturbed or discontinuity) rather than B- (i.e., Beam or Bernoulli) region which complicated the subsequent analysis. To compensate for this limitation to some extent, the Wild Horse Creek Bridge girder, another bridge girder obtained from Coreslab Structures (Okla) Inc., was tested in shear on both ends, respectively, with one loading point in a B-region and the other, in a D-region. The girder was rejected at the precast facility due to its honeycombs near one of the supports. This girder was designed according to AASHTO [1999].

In order to better understand the status (after nearly forty years) and estimate the shear capacity of the selected I-244 Bridge girder, an inverse problem was formulated and attempts were made for this challenging problem. In short, other tests (not causing any permanent changes to the girder) and measurements were taken before the shear tests were conducted. All data measurements were analyzed in order to detect the actual values of flexural stiffness and prestressing stress of the girder. Although there are methods for determining long-term prestress losses, they apply to a wide variety of structural members and do not necessarily reflect the condition of the real-world girder and the uncertainties studied here. Nominal shear capacity is particularly sensitive to effective prestressing force under current design codes, so it's important to have accurate values when making calculations. The study on the inverse problem was thus

introduced in this project and played an important role.

Last but not least, the expenses under Options 1 and 2 can be compared. Excluding the shipping cost required for both options, Option 1 incurred $1,375.00 for removing topping slab residue and another $5,537.00 for retrofitting the corroded end with the GFRP, both by Concrete Services Corporation. Option 2 would lead to $9,924.83 to $18,905.78 for casting two to six Type II prestressed girders according to the quotation by Coreslab Structures (Okla) Inc. on March 1, 2006 (Quo [2006]). Recall the pros of Option 1 and additional first-hand information on the performance of GFRP, this comparison, once again, demonstrates the effectiveness of the solution put forth in this study.

1.3 Structure of Report

In summary, the experimental study is the centerpiece of this project. Testing two girders would not be adequate to draw a general conclusion on the "quarter-point rule". To overcome this limitation, a systematic analytic study is conducted for many cases of AASHTO prestressed concrete girder designs using different design codes. To better process the precious data obtained from the real-world girder, an inverse analysis is carried out. All these major research efforts are presented in this report. The structure of this report is shown in Table 3, while the project time lines are documented in Table 18 to 23 in Appendix A.

Section	Topic	Main contributor
1	Introduction	Jin-Song Pei, Randy D. Martin, Colby J. Sandburg and Thomas H.-K. Kang
2.2 - 2.5	**Experimental Study**: Testing of original I-244 Bridge Girder	Colby J. Sandburg, and Jin-Song Pei
2.7	**Experimental Study**: Testing of Shortened I-244 Bridge Girder	Randy D. Martin, and Jin-Song Pei
2.8	**Experimental Study**: Testing of Wild Horse Creek Bridge Girder	Randy D. Martin, Jin-Song Pei, and Thomas H.-K. Kang
3	**Analytic Study**: Shear Strength of Prestressed Concrete Girders	Randy D. Martin, Thomas H.-K. Kang, and Jin-Song Pei
4	**Inverse Problem**: Identification of EI Value and Prestressing Stress of I-244 Bridge Girder	Jin-Song Pei, Randy D. Martin, Thomas H.-K. Kang, and Colby J. Sandburg
5	Conclusion	Randy D. Martin, and Jin-Song Pei

Table 3: Structure of this report

2 EXPERIMENTAL STUDY: TESTING OF SELECTED I-244 AND WILD HORSE CREEK BRIDGE GIRDERS

2.1 Overview

This experimental study includes the following main types of tests:

Shear Tests - used to determine the shear capacity of the girders

Flexural Stiffness Tests - used to obtain the value of flexural stiffness in a nondestructive manner for improved analysis of shear capacity

Camber Measurements - used to estimate the prestressing stress as well as flexural stiffness of the girders

Material Property Tests - used to determine the strength of the concrete from destructive testing

Testing real-world bridge girders would offer first-hand information on the shear capacity resulting from use of the "quarter-point" rule, however testing one real-world girder from the I-244 Bridge would be insufficient. More experimental results would be desired. To meet this challenge, a total of 12 shear tests were conducted on two different girders under a total of three different conditions as outlined in Table 4.

	I-244 Bridge girder		Wild Horse Creek Bridge girder
	Original	Shortened	
Shear test	Two on non-retrofitted and retrofitted ends, respectively	Two on one end and one on the other	One on each end
Flexural stiffness test	24 tests with 12 configurations	Four tests with four configurations	Six tests with three configurations
Camber measurements	Ten sets	11 sets	Two sets
Material test	Three cylinders	Not applicable	To be done in a future study

Table 4: Summary of experiments in this project

Before the shear tests were performed, flexural stiffness tests were conducted and camber measurements were taken. Testing of material properties was done after the specimens were cored from the failed girder.

2.2 Introduction to I-244 Bridge Girder

2.2.1 Brief History

A real-world AASHTO Type II girder was located in the Becco facility near the airport in Tulsa, OK, for the use of this project. It was removed from the I-244 Bridge over the Arkansas River around August 2005 together with other girders when Dr. Jin-Song Pei had a chance to visit the site. These girders were meant to be abandoned, and the majority of them did disappear. This single girder was the only one that could be located in a decent condition later in the spring of 2006. Locating and obtaining this girder were made possible with a great deal of assistance by Mr. Richard Moon from ODOT. We were advised that this girder was designed according to a standard drawing shown in Figure 2. The girder started to be in service in the late 1960's (Peters and Rusch [2006]).

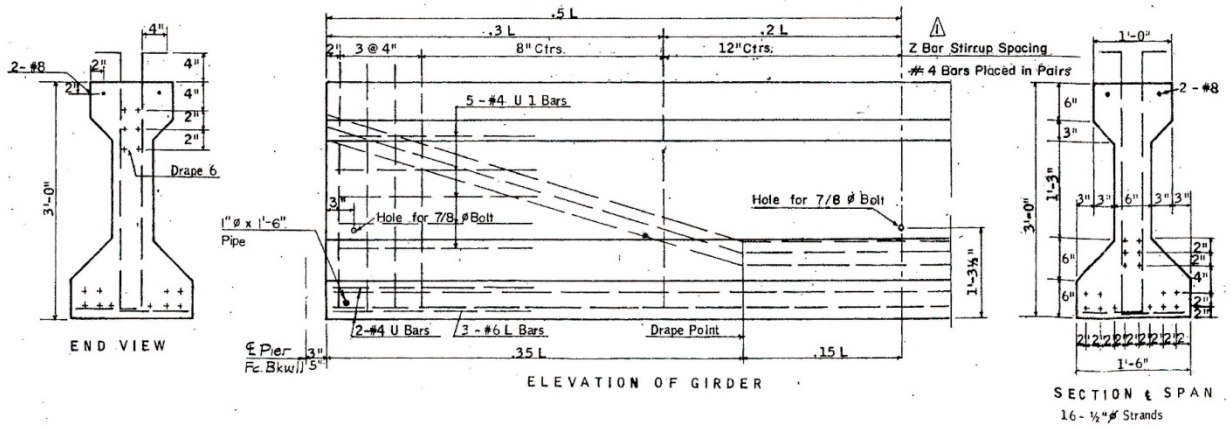

Figure 2: Elevation and details of the selected I-244 Bridge girder (ODOT [2006]).

Two field trips were made by this research team to Tulsa, OK for this girder during the project. Initially, the first trip to Tulsa was organized to view the condition of the girder and prepare the girder for transportation to the University of Oklahoma. During the first trip to Tulsa in April 2006, a local contractor, Concrete Services Corporation, was hired to remove the remaining slab from the top of the girder, the so-called "clean-up". See Figure 3 for the views before and after the clean-up. Once on site, major damages that had occurred to the girder were immediately noticed. These damages were resulted from the corrosion due to the lack of maintenance and perhaps, the removal process of the girder from the bridge. One end of the girder was severely corroded, therefore the girder was removed from the bridge. The track hoe used to demolish this and other girders from the bridge was documented in August 2005 and is shown in Figure 4. Given the original arrangement to abandon this girder, damages could easily occur in the demolition and shipping process. The clean-up process itself caused some visual damages, however they were not expected to be as severe as the above mentioned major damages as the personnel was supervised not to cause additional damage to the girder. A composite picture documenting the clean-up is presented in Figure 5.

(a) (b)

Figure 3: The I-244 Bridge girder (a) before (taken by Mr. Richard Moon) and (b) after the slab was removed by Concrete Services Corporation.

Figure 4: Track hoe used to demolish the girder from the I-244 Bridge.

In light of the existing damages the girder had had, a proposal was made to ODOT to (1) retrofit the corroded end with the same materials and method that were used to retrofit the other girders on the I-244 Bridge, (2) test the retrofitted end, and (3) compare the result with of the non-retrofitted end to study the contribution of the retrofitting material. For all visible damages, proper documentations would be required to ensure the accuracy of theoretical and numerical studies of this girder. The second field trip took place in June 2006 spanning about a week so that Concrete Services Corporation could retrofit the corroded end following what they had done to the other girders on the I-244 Bridge. Before the retrofitting started, a depth gage developed by Dr. Jin-Song Pei and Mr. Colby Sandburg, shown in Figure 6, was used to document some damage details to be covered by the external reinforcement in a cost effective manner on site. In short, the depth gage allowed the distance from the concrete to be known. From this information the amount of concrete that spalled off could be determined.

Figure 5: Augustine, a Concrete Services Corporation employee, removing remaining slab on April 21, 2006

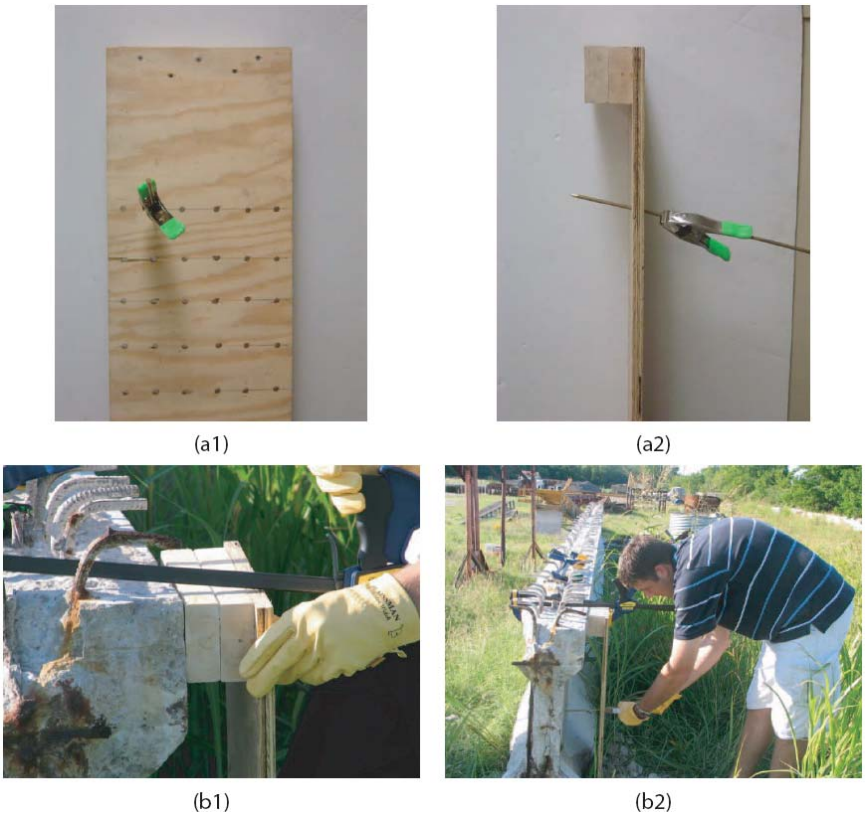

Figure 6: (a1) Front view, and (a2) side view of the depth gage. (b1) The depth gage being installed, and (b2) the depth gage being used.

The retrofitting process was documented in detail (Sandburg [2007]). Figure 7 shows a step-by-step view of the retrofitting process carried out by Concrete Services Corporation. The material was cured for 24 hours before the burlap was removed. To protect the retrofitted girder a UV coating was applied. When the contractor had finally finished the retrofitting the girder, transportation of the girder was organized.

Figure 7: Retrofitting process documented by Mr. Christopher Davis: (a1) using a pneumatic drill to remove unsound concrete; (a2) using a standard hammer to remove unsound concrete so that more damage was not done; (a3) original view of damage to the bottom of the girder; (b1) sandblasting the surface; (b2) using a pressure injection epoxy to repair existing cracks; (c1) applying the initial coat of the wet mortar; (c2) applying the second coat of the intermediate mortar; (c3) the final mortar being the thickest and the repaired end finally shaped; (c4) the burlap sack that was used during curing; (d1) rolling on the epoxy to the girder prior to install the FRP wrap; (d2) impregnating the three-layer FRP wrap prior to installing it, and (d3) rolling the FRP wrap onto the girder to avoid air voids in the finished product.

American Transfer was hired to transport the girder. The girder was placed on a flat bed truck using a lift. It was later confirmed that the lift picked the girder from the mid-point when being loaded on the truck. This was not advised but happened due to the limitations of the equipment. Once the girder was loaded and secured to the truck, the girder was transported to Fears Structural Engineering Lab at the University of Oklahoma. The unloading process was challenging caused by the limitation of the crane capacity of the lab as documented in Sandburg [2007]. All difficulties were successfully overcome under the close supervision of Mr. Michael

Schmitz, the lab manager. See Figure 8 for the snapshots of the process.

After of a series of testing of the I-244 Bridge girder at Fears lab, the procedures and results of which are presented in Sections 2.3 to 2.5, Chuck's Concrete Cutting Company was hired to core cylinder specimens and cut the two damaged ends off. Material testing was then performed on some concrete specimens cored. Continued testing on the shortened girder is presented in Section 2.7.

(a1)

(a2)

(a3)

(b1)

(b2)

(b3)

(c1)

(c2)

Figure 8: Girder unloading at Fears Lab: (a1) The girder on the delivery truck; (a2) the delivery truck backing into Fears lab; (a3) the cribbing built to support the girder while the truck left; (b1) the roller the girder was rolled on; (b2) the girder supported by the crane and the cribbing; (b3) the steel support the girder rested on after the truck left; (c1) the girder being lowered to the ground, and (c2) the girder being placed into the final location.

2.2.2 Existing Damages and Reference System

The I-244 Bridge girder had been in service and demolished prior to being selected for testing in this project so the existing damages of the girder in addition to the severe corrosion were inevitable. Visible damages were documented. Figure 9 summarizes the damages documented during the first and second field trips.

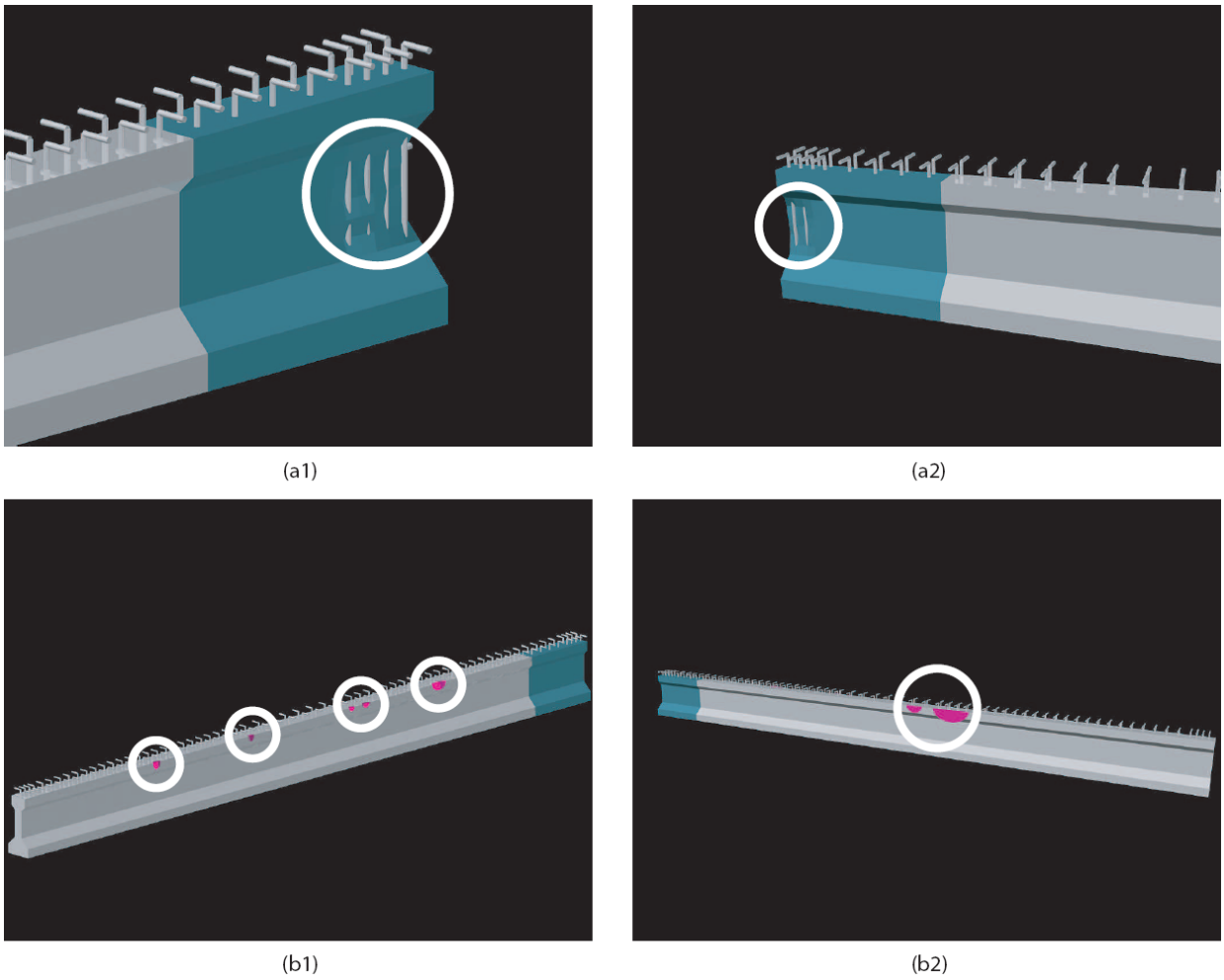

Figure 9: AutoCAD rendering with damages documented and highlighted. (a1) and (a2) Damages due to corrosion, and (b1) and (b2) damages caused when the girder was removed from the I-244 Bridge and perhaps, during the clean-up process.

As shown in Figure 10, numerous locations along the girder were visibly damaged once the girder was unloaded at Fears lab. Some damages are assumed to be from the removal of the girder from service. The slab was removed using a track hoe (see Figure 4) so the girder was more mobile. Some longitudinal cracks that propagate from the area of missing concrete suggest a large shear force similar to the hydraulic ram on the track hoe that removed the concrete. An inverse analysis in Chapter 4 will explore the effect of visible and invisible damages caused to the flexural stiffness of the girder for a more accurate estimation of the

prestressing stress and shear capacity.

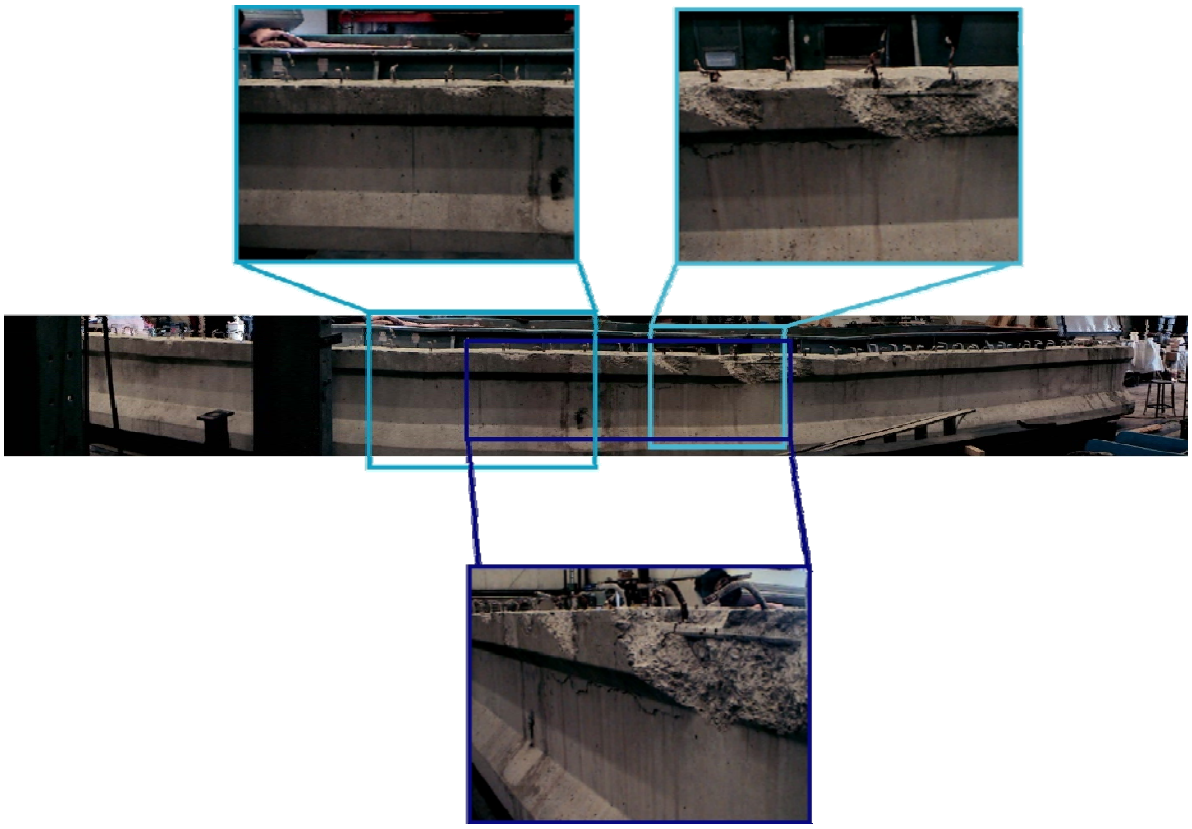

Figure 10: Location and extent of some of damages of the I-244 Bridge girder. These damages include both caused by removing the girder from the bridge and clean-up process.

When the girder arrived at Fears Lab, the girder ends were very rough and thus not a good option for the origin of a reference system. Also, talks of cutting the girder ends after shear tests had initiated, so the origin of the girder needed to remain after these ends were removed. Three methods were considered to define the origin. The first method was based on the diaphragm hole at mid-span of the girder. The second method was based on nails cast in the concrete at the ends and in the middle of the girder. The third and final method was based on the second to last steel stirrup at each end. The distance was split to determine the middle. All three methods defined the middle of the girder in a similar location, so the first method was used. Figure 11 shows where the girder was relative to Fears Lab and a zoom-in view of the origin. The north and south were defined as the plus and minus directions, respectively.

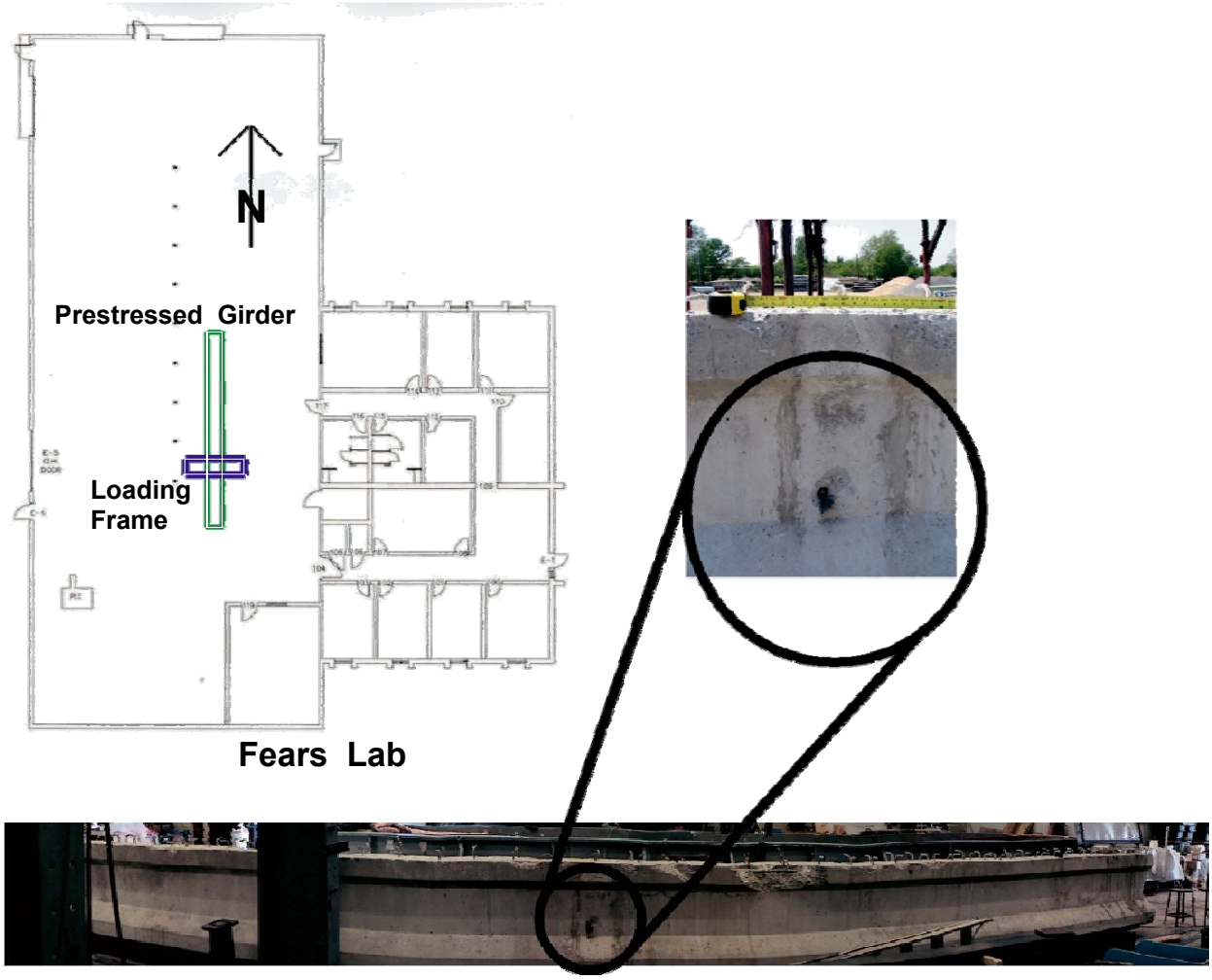

Figure 11: A schematic plan view of Fears Lab shows where the I-244 Bridge girder and loading frame are located as well as two photos to show where the diaphragm hole is located.

Once the girder was under the loading frame and out of the main traffic areas at Fears lab, visible damages on the girder, shown in Figure 10, were patched with a commercial repair concrete. When the repairs were complete and dry, the girder was painted white for further testing. Following the decision of the origin, other testing preparations include drawing grid lines of 3" by 3" onto the two sides of the girder throughout the span by Mr. Aaron Landrum using Sharpie markers and using a pacometer borrowed from the ODOT to scan the location of some stirrups and bend-up locations of the draped strands by Mr. Krisda Piyawat. Figure 12 contains photos of the grid system placed on the girder, which enables an efficient documentation of cracks in further testing.

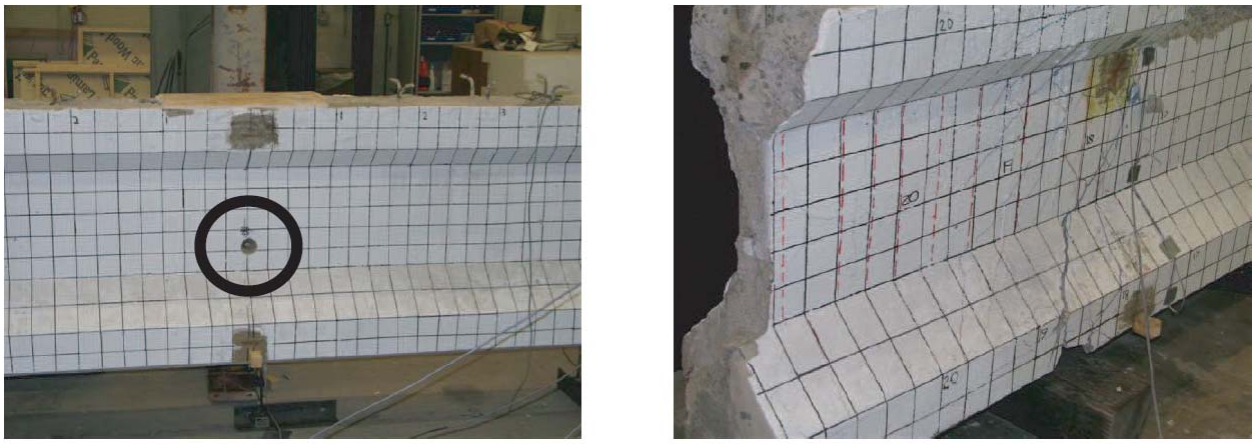

(a) (b)

Figure 12: Grid system placed on the I-244 Bridge girder, where (a) shows the origin, i.e., the hole pointing to the diaphragm's location (circled), and (b) shows the grid system drawn by Mr. Aaron Landrum using Sharpie markers and the stirrups located by Mr. Krisda Piyawat using a pacometer borrowed from ODOT.

2.3 Camber Measurements of Original I-244 Bridge Girder

Camber measurements were taken to calculate the prestressing stress in the girder (See Chapter 4). To determine the shear capacity prior to testing, it was found through a parametric study that the prestressing stress has significant influence on the shear carrying capacity (Sandburg [2007]). The parametric study looked at the shear capacity of different prestressing stresses according to both the ACI and LRFD design codes. Both show an increase in shearing capacity as the prestressing stress increases.

To measure the camber along the entire span, the distance from the floor to the soffit of the girder was used first. It was quickly noticed by Mr. Michael Schmitz that the floor was not level and thus the camber measurements were not accurate. To counter the unlevel floor, a string was used and hung from support to support. This string was pulled tight so that it was level to the eye. The second camber reading was made from the string to the soffit to the girder. Because the string was attached to the support, the camber measurements needed no adjustments like the first camber reading. The only adjustments that need to be made were because of the uneven soffit of the girder. Raw camber measurements taken from the original I-244 Bridge girder are plotted in Figures 13 and 14.

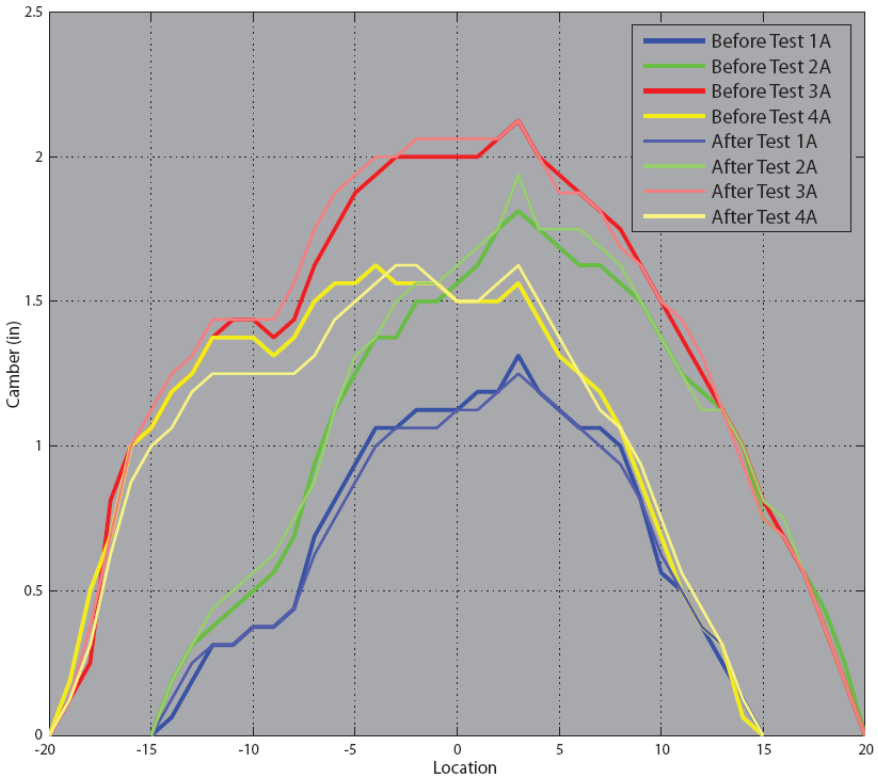

Figure 13: Summary of all measured camber profiles of the original I-244 Bridge girder before and after flexural stiffness tests.

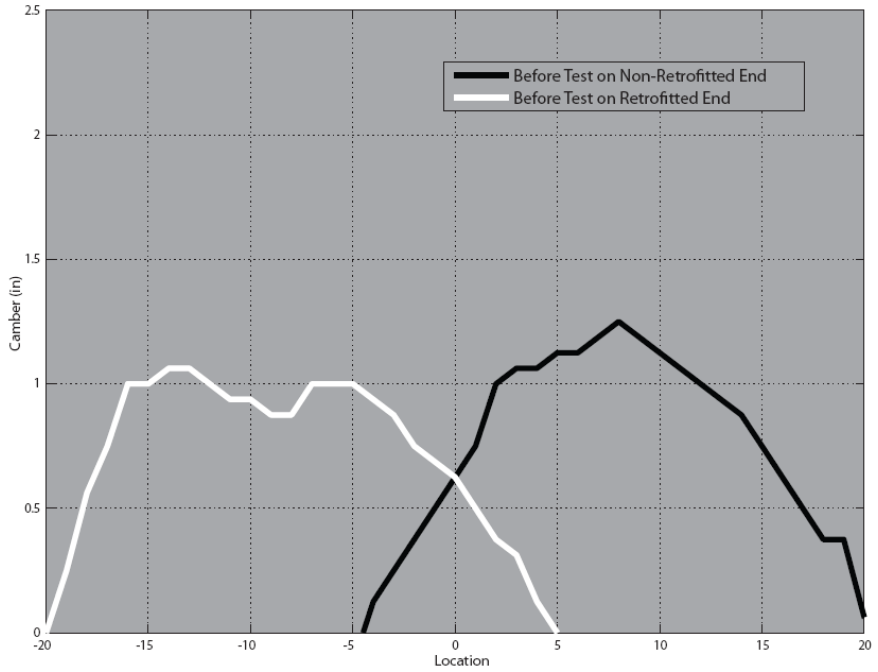

Figure 14: Summary of all measured camber profiles of the original I-244 Bridge girder before shear tests.

2.4 Flexural Stiffness Tests of Original I-244 Bridge Girder

2.4.1 Test Configurations

Lin and Burns [1981] show that the overall prestressing loss over time can be approximated by 45 ksi for pre-tensioned prestressed concrete. Further considering the prestressing steel had a strength of 270 ksi and was originally prestressed to 70% of its ultimate strength, the current prestressing stress was estimated as 144 ksi. This value was used to estimate the possible failure load of the girder for the sake of testing preparation.

In order to determine the actual prestressing stress using camber measurements, the flexural stiffness, *EI*, of the girder needs to be estimated. To do so, 24 flexural stiffness tests were conducted with 12 configurations shown in Table 5, each being tested up to 10 and 15 kips. Using multiple locations of the girder in all these tests allows a thorough examination of the flexural stiffness along the span and avoids ill-conditioning of the inverse problem (Santamarina and Fratta [2005]). Testing at two different maximum loads (10 and 15 kips) was to verify whether the girder's behavior was still in its linear range. 15 kips of load was approximately 8% of the girder's flexural capacity (Sandburg [2007]), based on which we assumed that all flexural stiffness tests did not cause damages to the girder and thus did not alter the shear capacity (which was to be tested after all flexural stiffness tests). The identification numbers used in Table 5 are explained as follows. First, the serial numbers were assigned according to support conditions:

- Tests involving the non-retrofitted end are labeled with 1 or 2. Tests 1 were conducted with a thirty foot simply supported span. The thirty feet was in the middle of the girder, and the cantilevers of five feet on each side were left. Tests 2 were conducted with a thirty-five foot span and only a five foot cantilever existed on the retrofitted end of the girder.

1. Tests involving the retrofitted end are labeled with 3 or 4. Tests 3 were conducted with a forty foot simply supported span. Tests 4 were conducted with a thirty-five foot span and only a five foot cantilever existed on the end without retrofitting.

Once the support conditions were determined, the loading points were selected out of the following three options:

- A - Loaded at the mid-span of the girder
- B - Loaded at ten feet closer to the retrofitted end
- C - Loaded at ten feet closer to the non-retrofitted end

	A	B	C
1	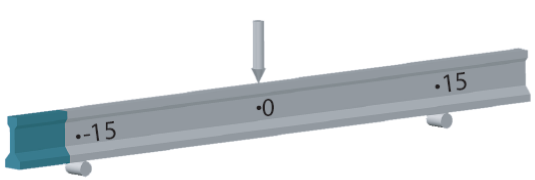	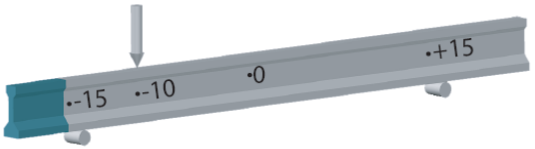	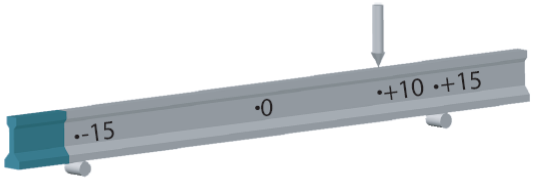
2	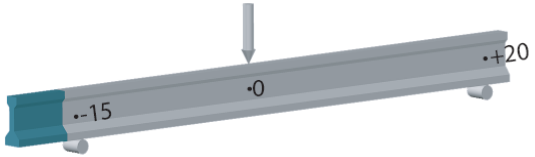	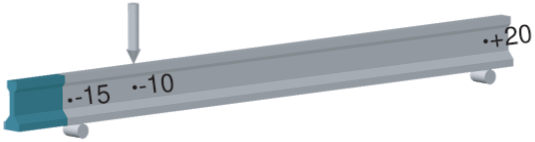	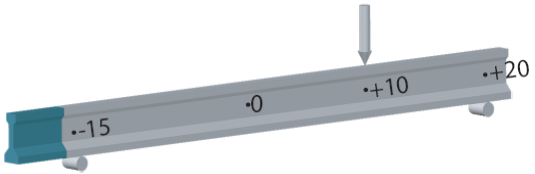
3	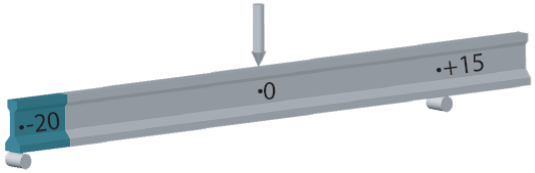	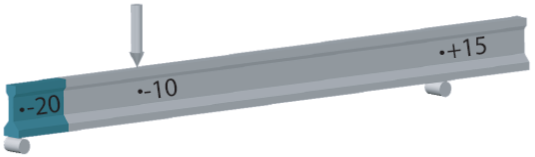	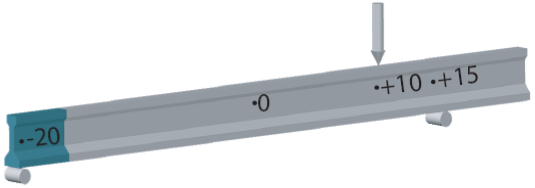
4	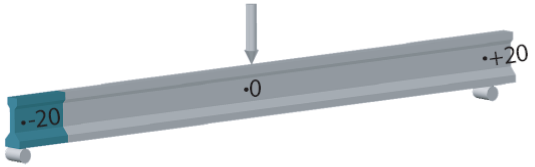	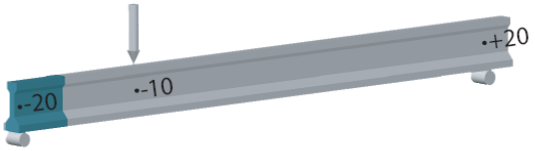	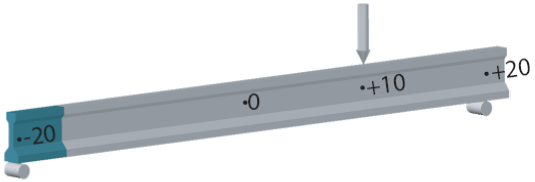

Table 5: All test configurations of flexural stiffness tests on the original I-244 Bridge girder.

2.4.2 Test Procedure

To gain accurate results, a reference system and grid lines were prepared beforehand (see Section 2.2.2). In addition, a series of details were taken care of under the guidance of Mr. Michael Schmitz. These include creating a smoothing loading surface using a 1' by 1' steel plate setting on Hydro-Stone (see Figure 15(a1)). The same method was applied to all flexural stiffness and shear tests. Two load cells (see Fig. 15(a2)), six linear variable displacement transducers (LVDTs, see Fig. 15(c1) and (c2)), and several strain gauges were used in flexural stiffness tests. Troubleshooting strain gauges was carried out separately, while the calibration was documented in Sandburg [2007]. In all tests, the difference in the readings of the two load cells were within 1%; the readings of the two load cells were thus averaged in the results (Sandburg [2007]). The data acquisition system (DAQ) used throughout the experimental study in this project (see Fig. 15(b1)) was developed by Dr. Christopher Ramseyer. The LabVIEW program files used in this project were prepared by utilizing the template files provided by Dr. Ramseyer.

The first test was Test 2C at 10 kips. After setting up the test, but before the test began, a camber measurement was taken. Next, the LabVIEW program was started. When the DAQ system was running, the load was applied. Because these tests were static tests and flexural stiffness was the end result, load was applied in small increments to increase the number of data points. A typical increment was 1000 pounds, but it was found that as low as 250 pounds could be added at a time. These load steps were applied, and the loading rate was about 1000 pounds per minute. Once the peak load was applied, a visual inspection of the girder was conducted to ensure that cracking or other damage had not occurred before the load was removed. Due to a limitation of the hydraulic system used, the load was removed at a rate of 3000 pounds per minute. Once the 10 kip test was completed, the 15 kip test was conducted immediately in the same fashion. When the 15 kip test had been completed, another camber measurement was taken so that it could be compared with the camber measurement taken previously.

Upon the completion of the 15 kip test, the supports needed to be moved. With the help of the crane, the girder was raised. The supports were moved to the new location, and the girder was subsequently lowered onto the new location. A plumb-bob was used to ensure that the load would be applied at the center of the girder at the correct location. Once the setup was done properly, the test was resumed. After a required four moves of the supports and retesting, it was time to move the girder so that the load could be applied to another location. In order to move the girder, a technique similar to unloading the girder (Sandburg [2007]) was used where one end was lifted and then the girder was rolled using the other support as a roller. Testing was resumed similar to the previous testing after the girder had been centered under the loading frame.

Figure 15: Instrumentation used in testing the original I-244 Bridge girder: (a1) Loading plate; (a2) one of the load cells used to determine the load applied to the girder; (a3) hydraulic pump to apply the load; (b1) front panel of the DAQ system; (b2) bracing used for stability; (b3) loading frame used for flexural stiffness and shear tests; (c1) and (c 2) LVDTs, and (c3) wire potentiometers.

2.4.3 Results

Processing data to obtain pertinent information of the structure or structural component is the ultimate goal of any experimental study in structural engineering. While collecting data at Fears Lab the DAQ system was programmed to write two files. The first file was copied to the "original" folder and had the initial voltage readings from the devices that were used. The

second file was placed in the "modified" folder and contained the relative voltages (i.e., real voltage - original voltage) multiplied by the calibration factor of the device used. This calibration allowed the LVDTs to be reported in inches and load cells in pounds. When this modified data was graphed into a load-displacement curve (see Figure 16(a)), there were points on the plot that are erroneous because of the way the DAQ system wrote to the files. The devices were read in order, but not at the same time. To correct these errors, steps taken are illustrated in Figure 16(b). Sandburg [2007] documents the strategy, process and verification of the MATL AB files used for this step of data cleansing. At a later stage of the project, the way to use the same DAQ system was improved to benefit this data cleansing step (see Section 4.4.1).

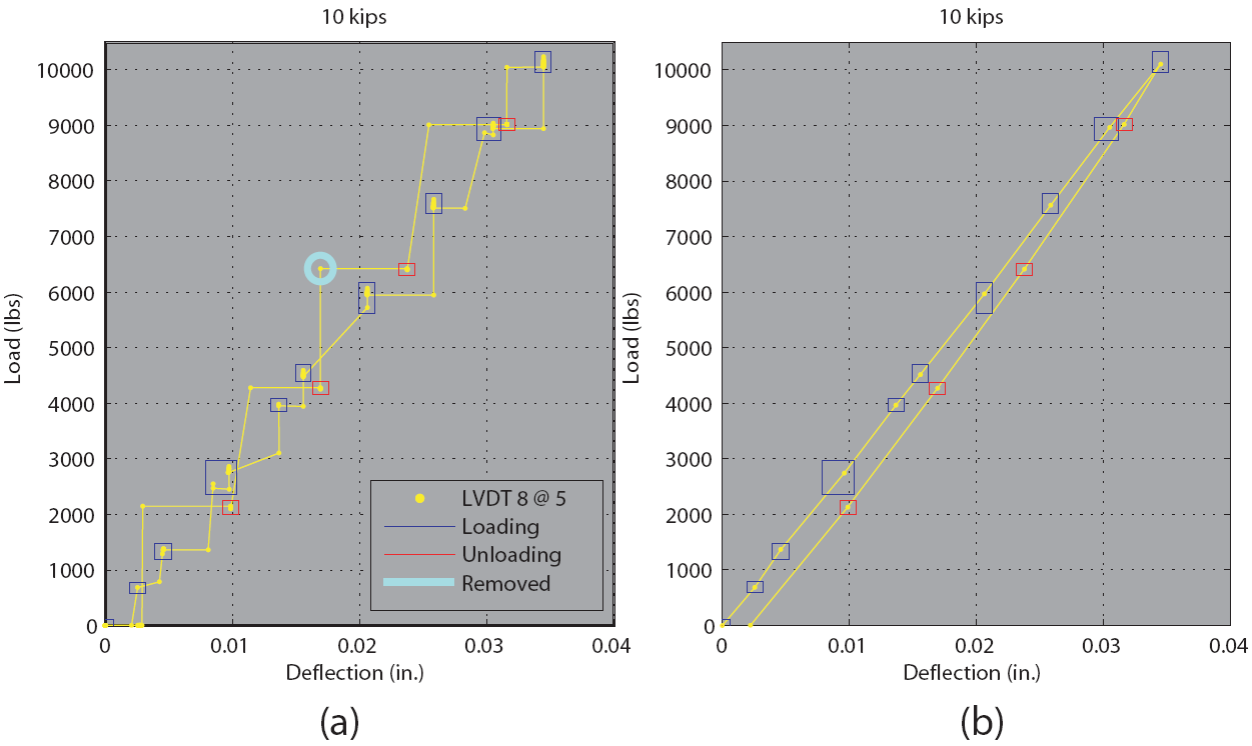

Figure 16: Illustration of data cleansing. (a) An original plot that shows the erroneous points, and (b) a modified plot that has the erroneous points removed and other data points averaged.

While all results of the flexural stiffness tests are presented in Sandburg [2007], Figure 17 shows a typical plot. After the above-mentioned steps of data cleansing, all of the channels were plotted for both 10 kip and 15 kip tests. The $\frac{P}{\Delta}$ curves based on the linear regressions from the two tests are superimposed to confirm the linearity of the flexural stiffness tests. In addition, a plot of two LVDT's readings that read the deflection at the same cross section of the girder was used to create a torsion check for both loading cases. This torsion plot shows if the girder rolled to one side or the other during the tests. Overall, 18 out of 24 tests were not affected by poor performance of the LVDTs. It can be seen that the stiffness of the retrofitted end from Tests 3A to 4C is higher than that from Tests 1A to 2C (see Sandburg [2007]), which is consistent with the finding in the relevant literature (ACI [2002]).

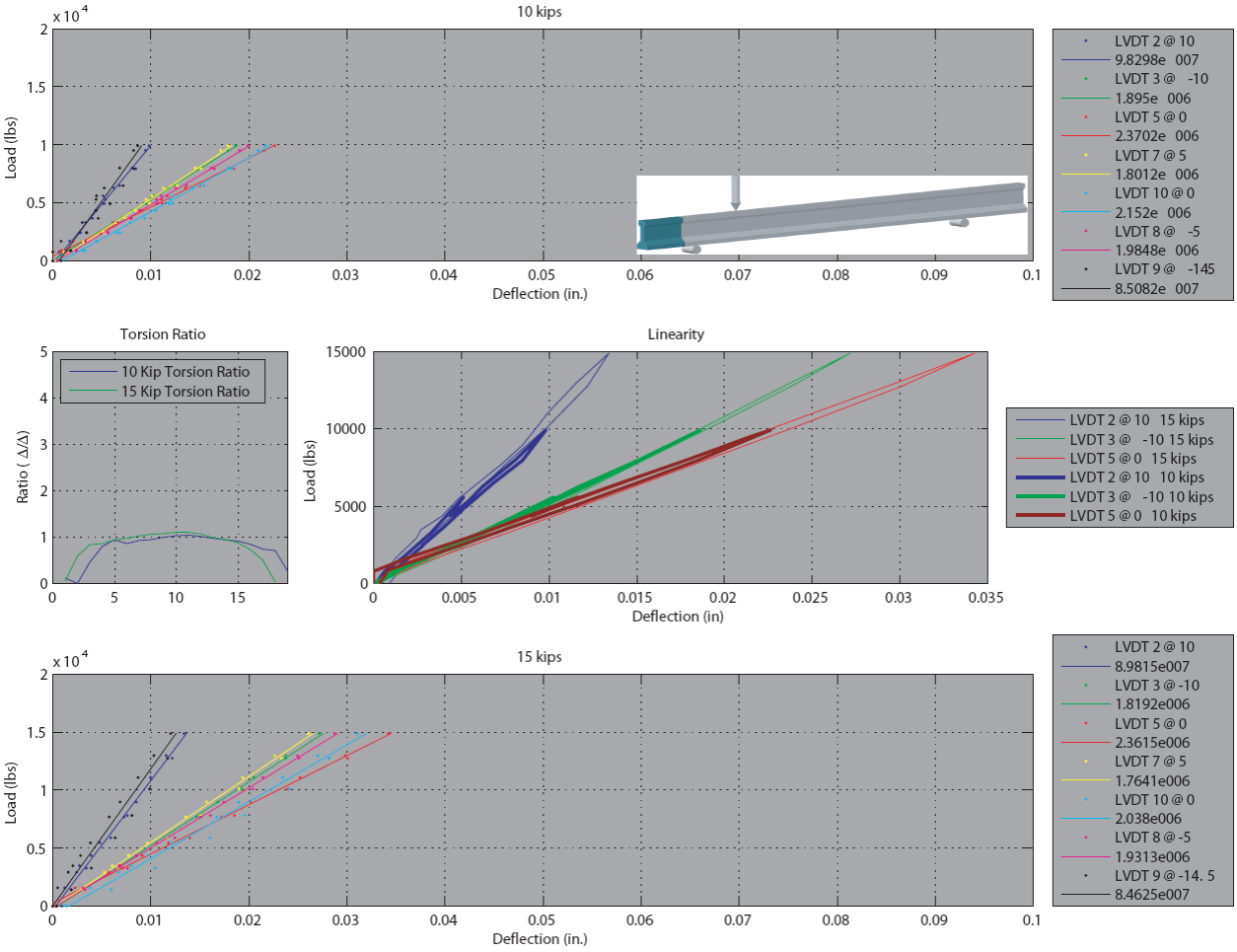

Figure 17: Results of flexural stiffness test 1B.

2.5 Shear Tests of Original I-244 Bridge Girder

2.5.1 Test Configurations and Procedure

There were a total of two sets of shear tests, with a point load applied close to one end of the original I-244 Bridge girder while the other end left cantilevering. See Figure 18(a) and (b) for the setup and the locations of all instrumentation used when the point load was applied to the non-retrofitted and retrofitted ends, respectively. This overall design of tests allowed the shear capacities of the non-retrofitted and retrofitted ends to be evaluated uninterruptedly and then compared on a light-to-light basis. The advantage of this overall design was to enable multiple independent, identical shear tests on this unique girder obtained from a real-world bridge. The disadvantage, however, was that the loading point was in a D- rather than B-region which complicated the subsequent analysis. In each set, the shear test was repeated using the same setup. The repetition was made because of the limitation of the lab loading capacity. The girder did not show a complete failure in the first shear test in each set, therefore the second shear test was designed to explore the remaining shear capacity.

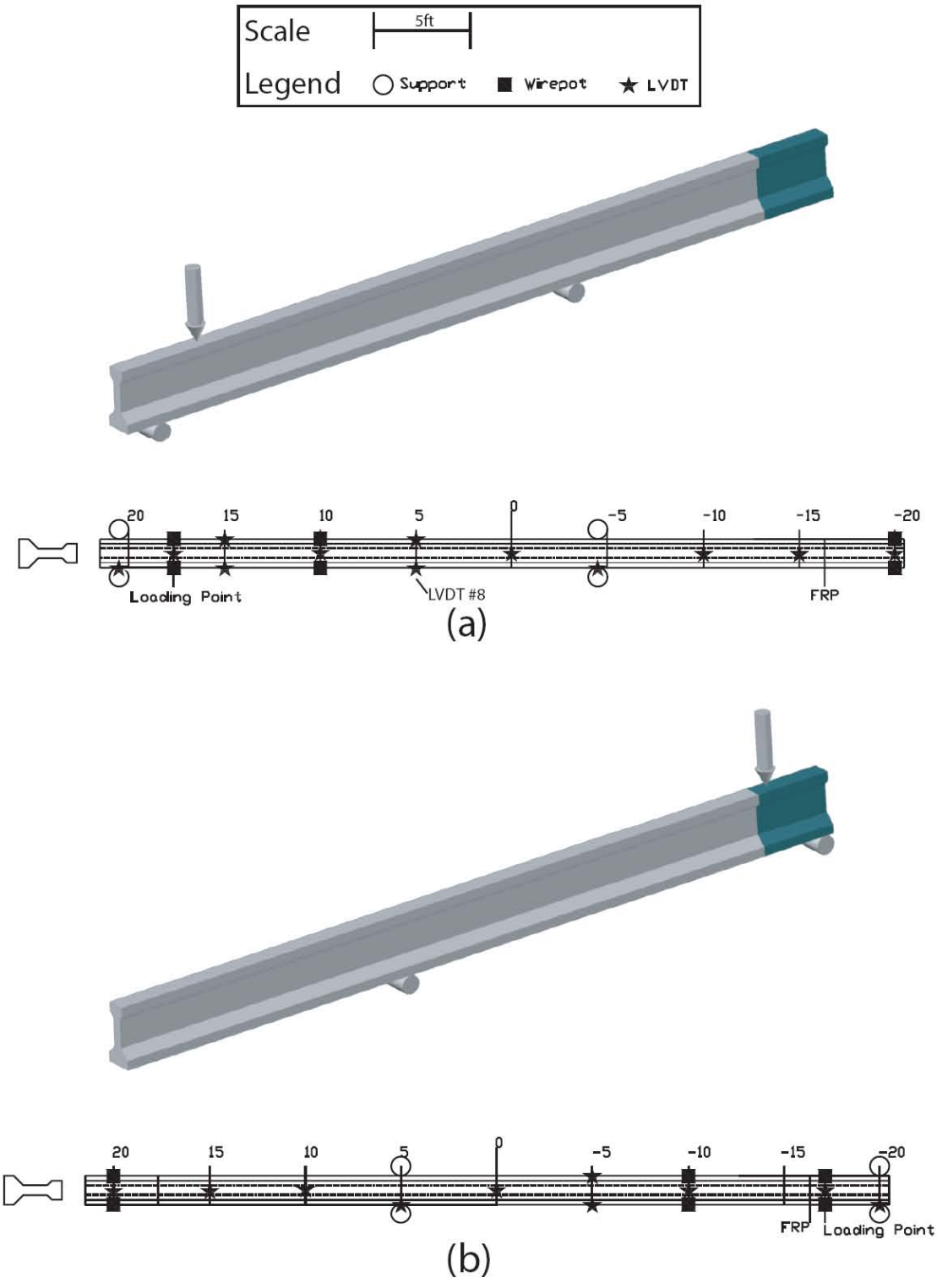

Figure 18: Illustrations of the setup and instrumentation for (a) the first set of shear tests on the non-retrofitted end of the girder, and (b) the second set of shear tests on the retrofitted end.

For the shear tests on the non-retrofitted end, the loading frame was moved and positioned so that the load would be applied at 34" (which was approximately equal to the effective depth, *d*) away from the support. The support was defined at 20.5' on the grid system after a careful examination of the stirrup locations on both ends of the girder to allow for a future light-to-light comparison of the results. The other support was defined at - 4.5' to make a span of 25' for the simply-supported portion of the girder. After the girder and loading frame were in position, bracing elements were needed on each side of the girder. These braces shown in Figure 15(b2) were made of steel W sections and were bolted to the floor so that they were not touching the girder but could support the girder if it were to roll accidently. In order to capture the entire girder deflection both LVDTs (see Figure 15(c1) and (c2)) and wire potentiometers (see Figure 15(c3)) were used during the shear tests. These devices were placed along the girder (see Figure 18) so that the spacing of the LVDTs and wire potentiometers were evenly spread throughout the girder.

When the instrumentation was set up and had been wired to the DAQ system, a camber measurement was taken. This camber measurement was taken from support to support. After the camber measurement was taken, the DAQ system was started and the load was applied. A loading rate much higher than that for flexural stiffness tests was adopted for two reasons: (1) The goal was to capture the failure load rather than the loading process, and (2) the failure load would be much higher than the maximum loads in flexural stiffness tests. A loading rate of about 5000 pounds per minute was planned so that the loading would take about one hour. The actual loading took about two hours first because the failure load exceeded the prediction. Cracks and other issues occurred during the test were dealt with immediately further slowed down the duration of the loading phrase. Manually keeping the loading rate as the test progressed was not easy. The first shear test was run with two load cells. When the load applied reached the capacity of the smaller load cell, the hydraulic pump used to apply the load (see Figure 15(a3)) began leaking. The load was then removed and the pump fixed. When unloading, the load was removed almost instantly given the limitation of the available loading system; no unloading curve was able to be documented (Sandburg [2007]). A second shear test was done to confirm that the maximum load reached in the first shear test was indeed the failure load. The second shear test never reached the maximum load of the first shear test, so the maximum load obtained from the first shear test was considered the actual failure load.

As the loading was taking place, the data was saved in another location at 50 kip intervals in order to protect the data from a computer crash. Meanwhile, cracks were documented by photos and a hand sketch. At some locations along the span, the readings of the LVDTs were expected to be out of their short ranges towards the end of the test. These LVDTs were removed in the middle of the testing and the corresponding load value was noted for data processing purpose. To be cautious with the safety of instrumentation threatened by the debris during the testing, one more LVDT was disconnected from the test once the load exceeded the expected value. As another means to overcome the short range of the LVDTs, wire potentiometers were adopted in the shear tests. A sacrifice was made in the resolution of the measurements because the stroke of the wire potentiometers is twenty times that of the LVDTs (10 inches versus 0.5 inch). The wire potentiometers were easier to instrument than the LVDTs as well as being more reliable during the tests when compared to problems with getting LVDTs to work properly.

When both shear tests on the non-retrofitted end were completed, the setup began for the shear tests on the retrofitted end. The setup included moving the braces and the loading frame to new locations as well as setting up the DAQ system again. The procedures for loading and documentation were also similar to the shear tests on the non-retrofitted end. A test took approximately two hours. This first shear test was halted due to a visual inspection of the bolts on the loading frame to the cross member that supports the hydraulic ram. Once the capacity of the frame was confirmed, a second test was preformed to check if anymore load could be applied to the girder. Similar to the second shear test on the non-retrofitted end, no more load than the first test could be applied.

2.5.2 Results

Table 6 summarizes the maximum loads reached in all four shear tests conducted on the original I-244 Bridge girder. Failure patterns documented by drawings and photos are presented in Figures 19 and 20 for the shear tests on the non-retrofitted and retrofitted ends, respectively.

In addition to an increase in the maximum load in the shear tests caused by the externally bonded glass fiber reinforcement, it should be noted that, during the first shear test on the retrofitted end, cracking sounds were heard. Visible damage in the retrofitted area, however, could not be identified. The failure patterns of the retrofitted end differed significantly from those of the non- retrofitted end.

Loading point	Test ID	Maximum load (kip)	Loading point	Test ID	Maximum load (kip)
Non-retrofitted end	1st	300	Retrofitted end	1st	370
Non-retrofitted end	2nd	270	Retrofitted end	2nd	355

Table 6: Summary of shear test results of the original I-244 Bridge girder.

Data cleansing steps are similar to those for flexural stiffness test results (see Section 2.4.3). As mentioned previously, wire potentiometers were used in addition to LVDTs to capture deflection in the shear tests. The readings of those LVDT disconnected from a test in the middle of the testing were discarded after the recorded load value marking the disconnection (see Section 2.5.1). All results from wire potentiometers and LVDTs were used independently to plot load-displacement curves obtained from all shear tests and presented in Sandburg [2007]. Even with a lower resolution, the wire potentiometers were found to produce reliable results compared with their LVDT counterparts.

Figure 21 illustrates the softening trend shown in the second as compared with the first shear test. This trend further indicates that the first shear test did cause severe irreversible damage to the girder.

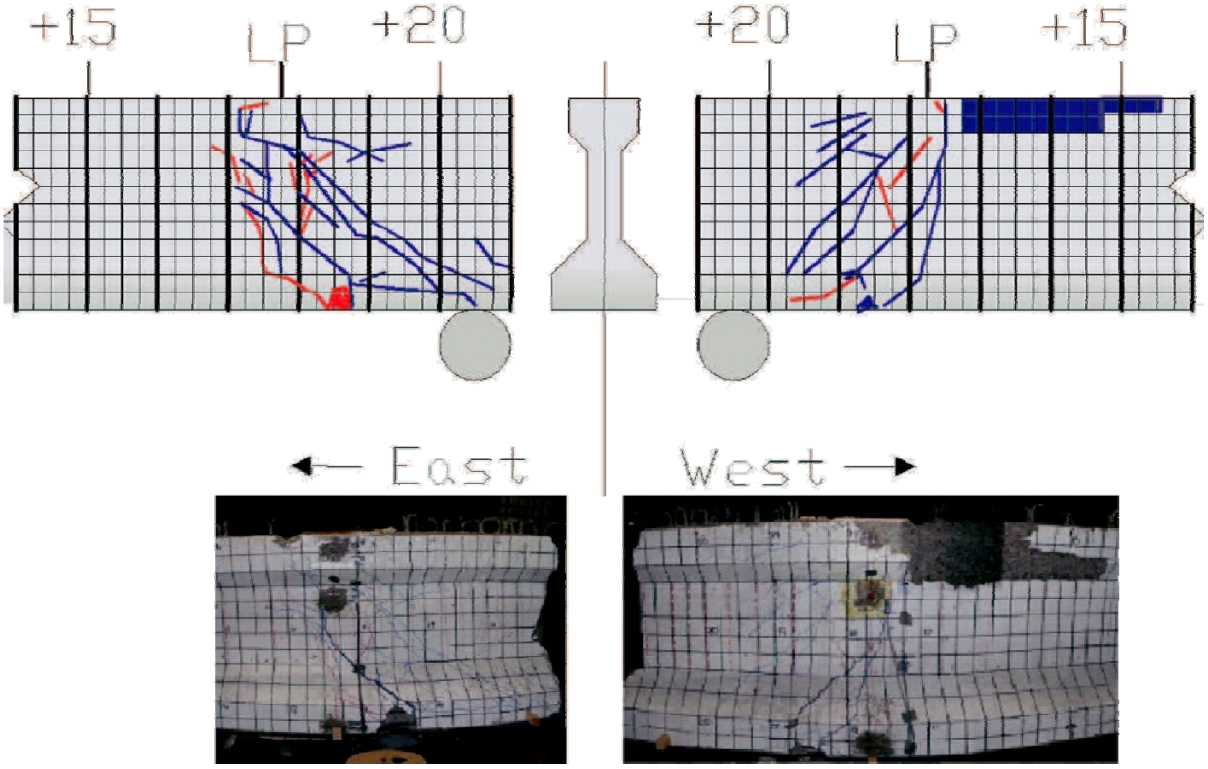

Figure 19: Crack pattern on the girder as a result of the two shear tests on the non-retrofitted end.

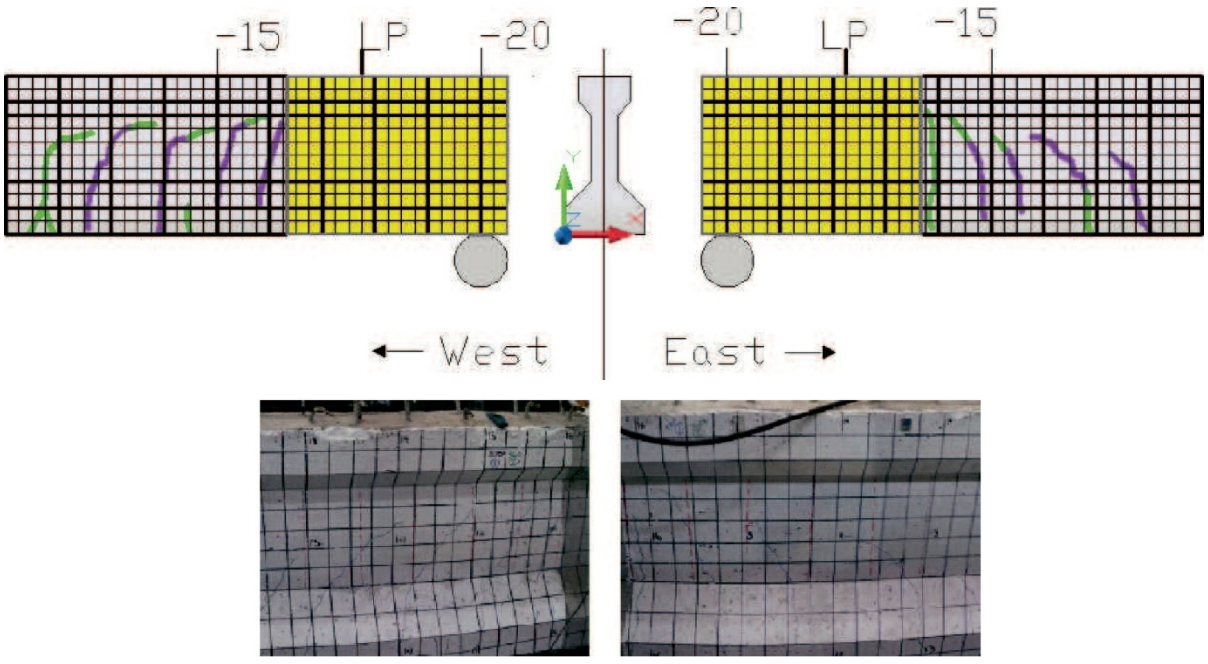

Figure 20: Crack pattern on the girder as a result of the two shear tests on the retrofitted end.

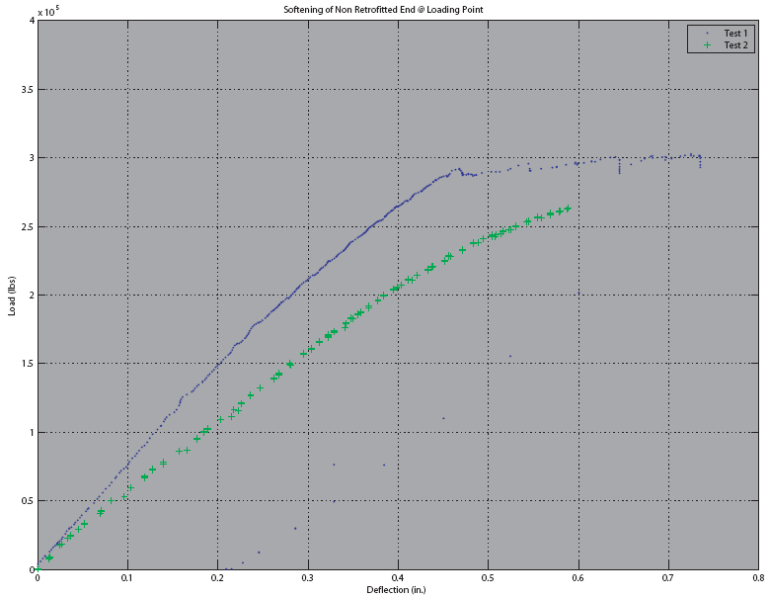

Figure 21: An illustration of softening trend from the first to second shear tests performed on the non-retrofitted end.

2.6 Material Properties of Original I-244 Bridge Girder

When the I-244 Bridge girder was cut after the completion of the above-mentioned four shear tests, cylindrical specimens were cored from the cut-off non-retrofitted end. These cores were 6" deep and 2.7" in diameter. The former followed the web thickness, while latter was dictated by the blade used. Three specimens were tested in compression using a Forney LC-1 testing machine (For [2005]) following ASTM [2001]. See Figure 22 for the test setup, while other details can be found in Sandburg [2007].

Figure 22: (a) Forney LC-1 testing machine (For [2005]) used for material testing, and (b) a view into the Forney machine with a concrete cylinder.

The material testing could have been done earlier if the cylindrical specimens were cored from the mid-span of the girder. This arrangement was not adopted in order to perform all shear tests on the girder in its prime condition. Coring the specimens during the cutting of the girder was also a cost-effective arrangement.

Table 7 shows the test results, calculated and adjusted strength values. Photos showing the failure patterns are included in Sandburg [2007].

Specimen	Load (lbs)	Calculated strength (psi)	Adjusted strength (psi)
1	36.260	6280	6462
2	36.720	6364	6548
3	25.580	4433	4561

Table 7: Failure loads, strengths, and adjusted strengths (according to Mindess et al. [2003]) of three 2.7" x 6" cylindrical concrete specimens cored during the cutting of the original I-244 Bridge girder and tested in compression according to ASTM [2001].

Given the dimensions of cored specimens, the calculated strength needed to be adjusted to obtain the strength following the standard cylinder. Mindess et al. [2003] was referred to as a quick guide, while a future improvement of this analysis could be achieved following other references specifically for the range of concrete strength and considering the time-dependent effect. Two adjustments were needed; empirical charts in Mindess et al. [2003] were followed. First, a reduction in strength of 98% was found since $\frac{l}{d}$ was 2.2, greater than the standard of 2.0. The size effect was considered next. An increase of 105% was found since the diameter of the specimen was 2.7", less than the standard of 6.0".

Given the normal design strength $f_c^{'}$ = 5000 psi, two out of three adjusted strength values are about 6500 psi. This is expected since concrete strength does continue to increase with time. More quantitative evaluation of these values could be conducted in a future work. More importantly, more specimens need to be tested. The dimensions and weights of each specimen need to be measured. The new results could be utilized to explore the reason behind the only low strength obtained from this study.

2.7 Shortened I-244 Bridge Girder

2.7.1 Procedure

This section describes the procedure for flexural stiffness tests, camber measurements and shear capacity tests that were performed on the shortened I-244 Bridge girder. The tests took place from June through July 2007 at Fears Structural Engineering Laboratory on the University of Oklahoma campus.

The flexural stiffness tests were designed with the intention of using deflection data from three locations (-10, 0 and +10) to estimate span-constant flexural stiffness as had been done on the original girder. The test configurations including locations of load, LVDTs and supports are shown in Figure 23. The procedure for carrying out the flexure tests was the same as that used

for the original I-244 Bridge girder; however, the sampling rate was changed on the data acquisition system. The system was set to scan once every ten seconds. The load was applied every six cycles while the system was waiting to avoid collecting data that spanned two load steps.

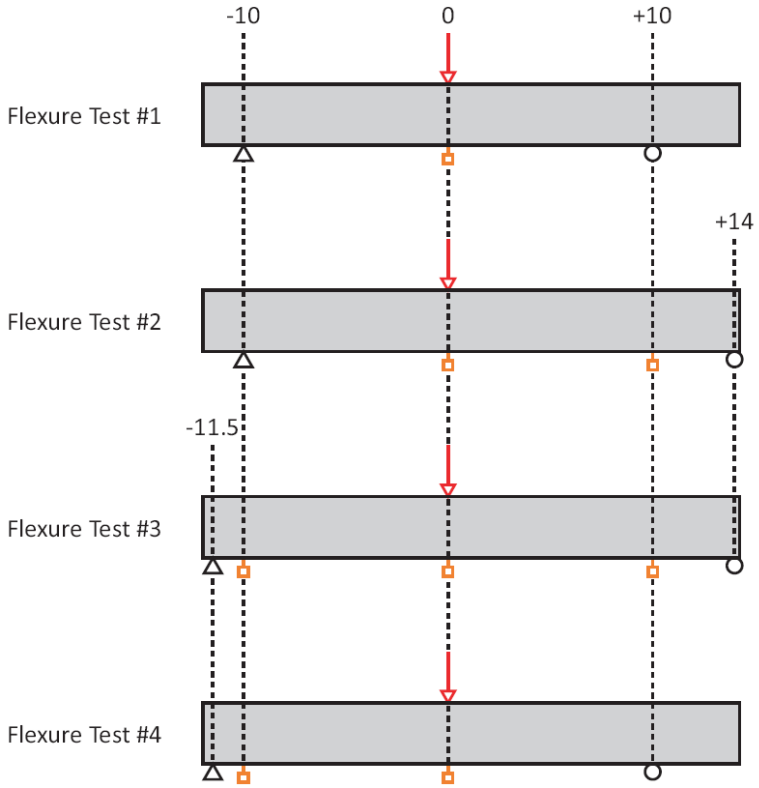

Figure 23: Flexure test configurations for shortened I-244 Bridge girder.

Camber measurements were taken immediately before and after each flexural stiffness test was conducted. The same tools and methods were used as what had been done for the original I-244 Bridge girder.

Shear capacity tests configurations were designed for the shortened I-244 Bridge girder so that results could be compared with the original I-244 Bridge girder. The same shear and supported spans were used. The locations of loading, LVDTs and supports are shown in Figure 24. The same procedure was used for the shear tests as for the original I-244 Bridge girder. Strain measurements were taken during these tests, but the readings were unreliable and omitted from the report.

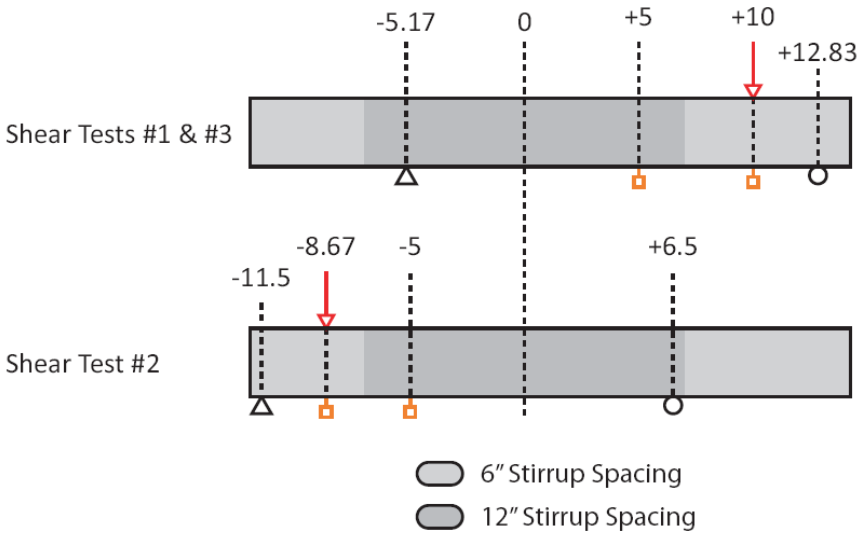

Figure 24: Shear test configurations for shortened I-244 Bridge girder.

2.7.2 Results

The results for the flexural stiffness tests I-244 Bridge girder is presented in Martin [2009]. The results show a linear relationship for the deflection as it was measured at each location. The maximum load and measured deflection are very small, which could cause the measurement error to have more of an impact on the analysis.

A sample camber profile for the same flexure test configuration is shown in Figure 25. The unevenness of the soffit shows for the shortened I-244 Bridge girder as well around locations -5 and +3. Despite the sharp changes in slope, the overall shape is fairly symmetric, which is expected. An intuitive understanding is that the distribution of the flexural stiffness is fairly uniform for the shortened girder. The point of maximum camber is very near one of the discontinuities, so it's somewhat difficult to say for sure where the maximum camber occurs. More quantitative analysis of these results will be carried out in a future study.

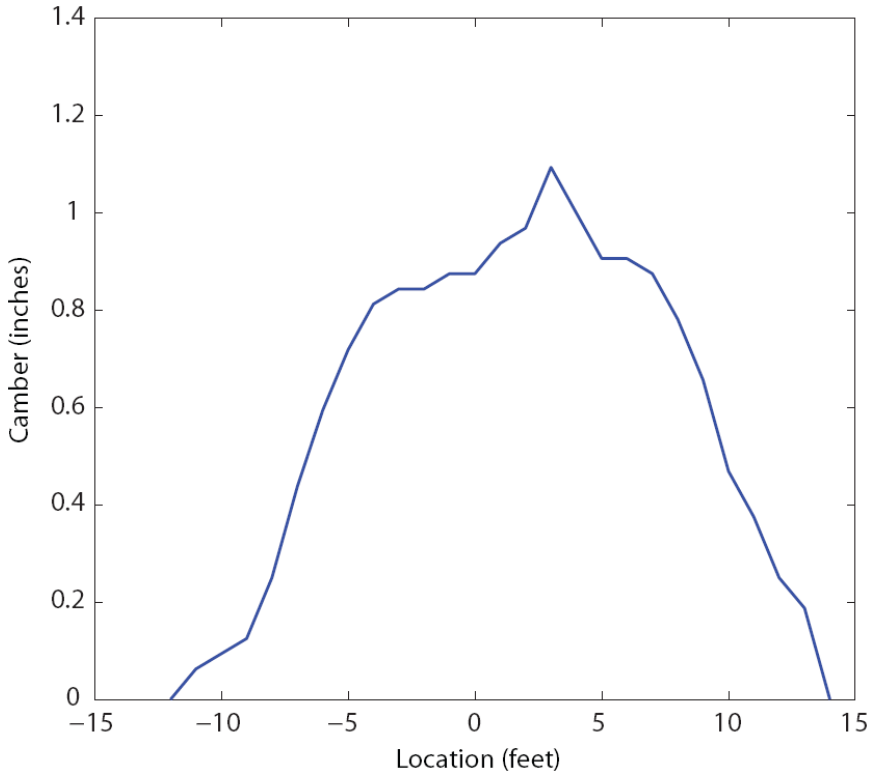

Figure 25: A sample camber profile of the shortened I-244 Bridge girder measured before flexure test configuration #3.

The results of the shear capacity tests are shown in Table 8. Shear test configuration #3 was a repeat of test #1 due to issues with the hydraulic pump. Even in the second test, the capacity of the pump limited the test. It is expected that the shear capacity is similar to that of the original I-244 Bridge girder because the stirrup spacing was the same over the shear spans. Test #2 resulted in bond failure of the prestressing strands. Since the girder was cut to remove the damaged portions from testing of the original girder, the strands were flush with the ends of the girder. After shear test #2, however, the prestressing strands were pulled into the girder. Longitudinal cracks were noticeable on the end of the girder and along its soffit.

Loading point	Test ID	Maximum load (kips)
Close to previous non-retrofitted end	#1	294
Close to previous retrofitted end	#2	226
Close to previous non-retrofitted end	#3	304

Table 8: Results of shear tests of the shortened I-244 Bridge girder.

2.8 Wild Horse Creek Bridge Girder

2.8.1 Introduction

The Wild Horse Creek Bridge girder was designed according to AASHTO Standard Specifications (1999) and was cast on July 18, 2006. The length and weight are 34 feet and about 13,100 lbs, respectively. The girder was not to be used for any structural purpose due to honeycombing at one of the supports. Elevation and details of the selected Wild Horse Creek Bridge girder are presented in Figure 26.

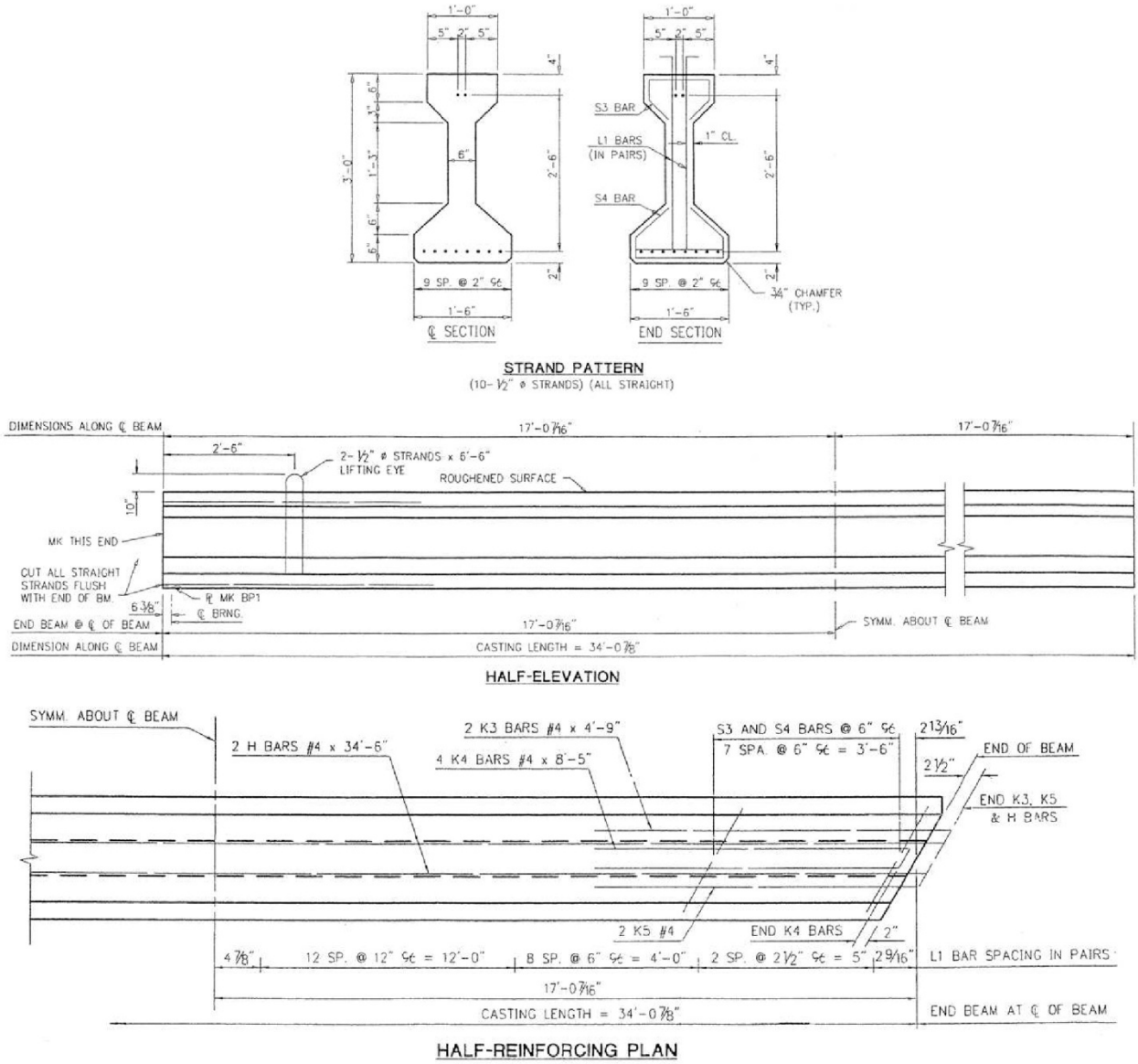

Figure 26: Elevation and details of the selected Wild Horse Creek Bridge girder (Coreslab [2007]).

2.8.2 Procedure

This section describes the procedure for flexural stiffness tests, camber measurements and shear capacity tests that were performed on the Wild Horse Creek Bridge girder. The tests took place from June through August 2008 at Fears Structural Engineering Laboratory on the University of Oklahoma campus.

Flexural stiffness test configurations were designed with piecewise constant flexural stiffness in mind. In order to create a well-behaved system of equations, the coefficient matrix, which is based solely on the test configurations, must not be singular. Another consideration for the test configurations was to try and distribute the sensitivity to the solution of each section's *EI* (see Section 4.4). The resulting test configurations including locations of load, LVDTs and supports are shown in Figure 27.

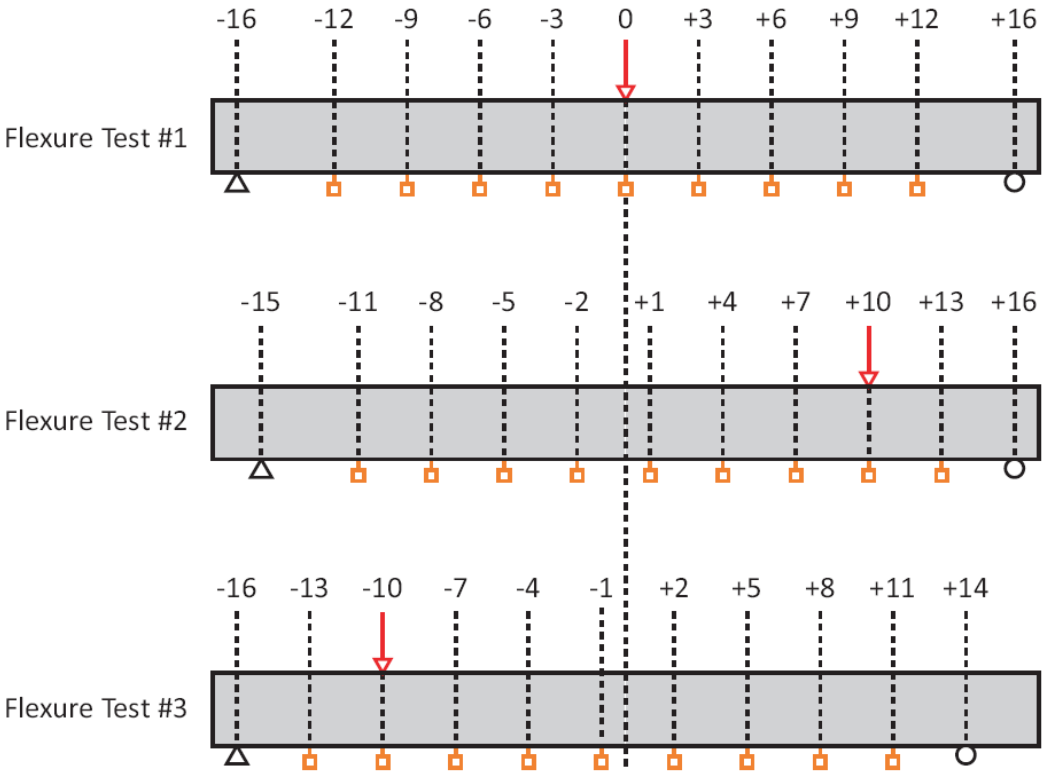

Figure 27: Flexural stiffness test configurations for the Wild Horse Creek Bridge girder

The flexural stiffness test procedures were largely unchanged from previous tests; however there were some improvements that will be discussed here. The maximum load was increased to approximately 30 kips. The benefit included a larger range of collected data. This is still well under the cracking load for the girder, so the subsequent tests should be unaffected. Tests were repeated at the same load level to ensure consistency between tests. In most cases, the first test showed a small amount of residual deflection due to settling of the supports; initially, a third test run confirmed that the residual deflection was not due to nonlinear behavior. The loading rate was increased to approximately two kips for every ten cycles of the data acquisition system, which was paused while load was being applied. This ensures that the data does not

contain points that are from a combination of load steps. The reduced preprocessing effort and shortened test helped the overall efficiency without sacrificing quality.

Camber measurements were taken after each shear capacity test. The girder was nearly fully supported for these measurements as shown in Figure 28.

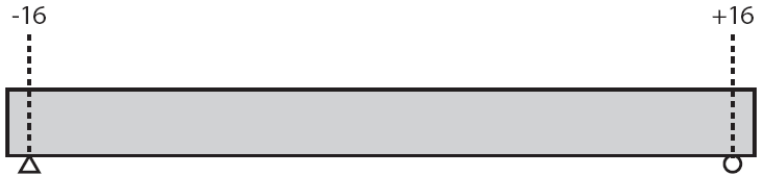

Figure 28: Configuration for measuring camber of the Wild Horse Creek Bridge girder.

The procedure for taking camber measurements improved from earlier tests by pinning the masonry string at the center of each support. Previously, no particular attention was made to the location of zero measured camber as long as it was touching the support. This should increase the quality of the data because rotation is greatest near the supports. Measurements were taken from the top of the string to the girder soffit at each foot along the supported span with a ruler accurate to one hundredth of an inch.

Shear tests were performed to determine the actual shear capacity of the Wild Horse Creek Bridge Girder. Figure 29 shows the locations of load, LVDTs and supports for the shear tests as they were performed.

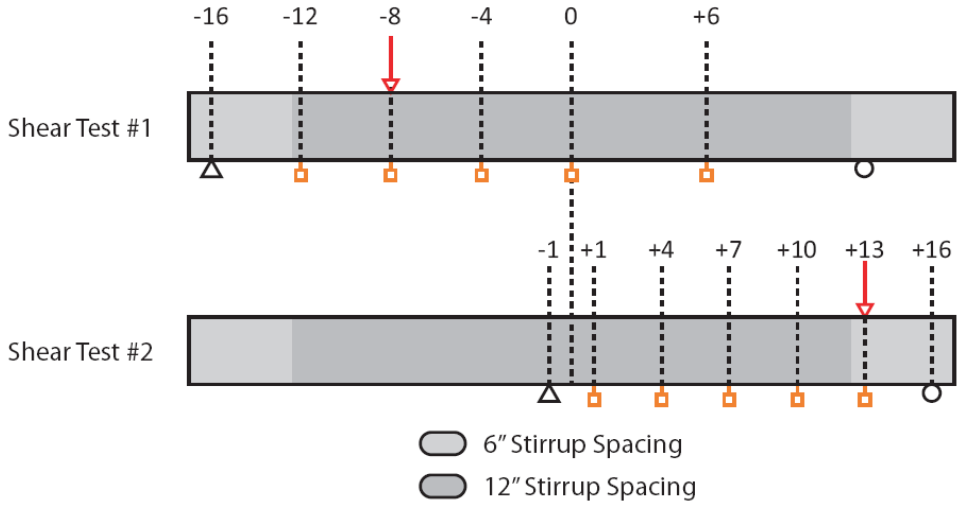

Figure 29: Shear test configurations of the Wild Horse Creek Bridge girder performed July 2008.

The two tests differ rather significantly in the location of the applied load. The purpose was to check the capacity at the quarter span and to see which failure mechanism controlled. Even though this girder was designed by modern standards, this was important because it gives some indication on how AASHTO Type II girders would fail. For Test #1, a rugged BDI strain transducer (Bri [2007]) with a two foot extension was placed on the soffit of the girder spanning the loading area in order to accurately collect the cracking load.

The procedure for conducting the shear capacity tests was generally the same as previous tests except for some relatively minor differences. The improved method of loading and collecting data (same as for the flexural stiffness tests conducted on this girder) was used for the shear tests. The loading rate was approximately ten kips per minute until reaching one hundred kips, followed by five kips per minute for the remainder of the tests.

2.8.3 Results

The results of the two shear tests for the Wild Horse Creek Bridge girder are presented in Table 9.

Test	Maximum load (kip)	Failure mode
#1	145	Flexure
#2	320	Shear

Table 9: Results from shear capacity tests conducted in summer 2008.

It should be noted that Shear Test #1 resulted in flexural failure. The camber profile of the Wild Horse Creek Bridge girder after the first shear test is shown in Figure 30.

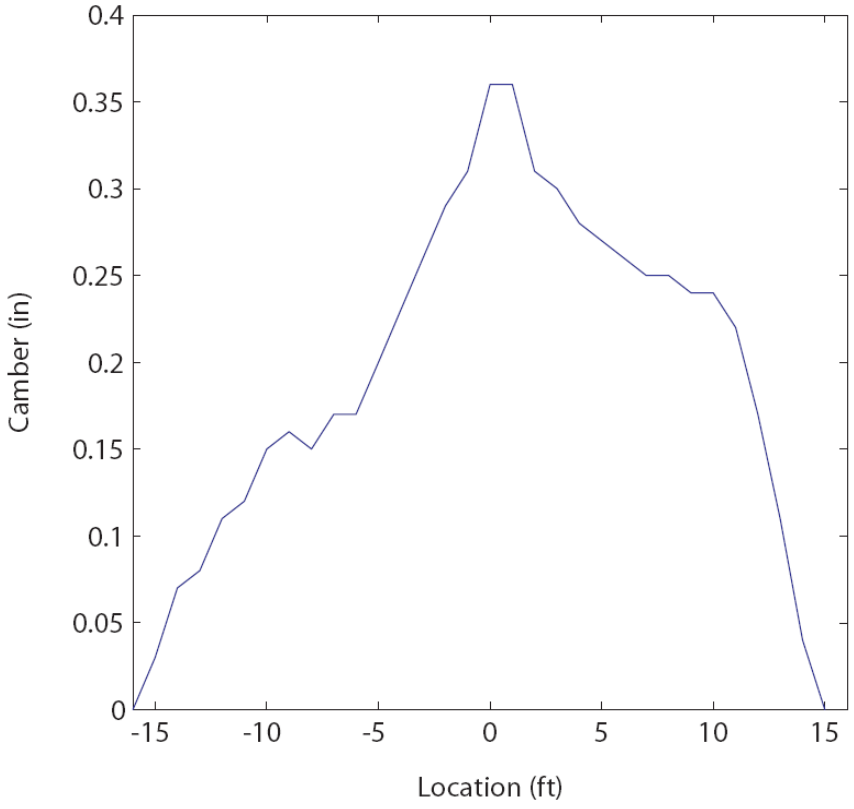

Figure 30: Camber profile of the Wild Horse Creek Bridge girder after Shear Test #1 failure

Theoretically, the curve should be a combination of quadratic and quartic curves, both centered about midspan. There is, however, a shallower slope on the south side of the girder, which indicates increased stiffness. One would think the flexural cracks would have reduced the flexural stiffness on the south end of the girder, but it isn't apparent from Figure 30. Most likely this is a cause of the prestressing force. Once the load is released, the girder soffit goes back into compression and cracks don't affect how forces are distributed through the girder. Another intuitive explanation is that the failure under the loading point at −8 caused cracks in the surrounding area leading to a weakened flexural stiffness in the area. Comparatively, the flexural stiffness on the untested end is higher. A steeper slope on the untested end can be observed. This trend is consistent with the camber measurements from both the original and shortened I-244 Bridge girder and can be further explored in a future study.

Although there were no ridges on the soffit of the Wild Horse Creek Bridge girder like those that were found on the I-244 Bridge girder, there still seems to be some degree of unevenness particularly around -7.5’ and +5’. The assumption is that the girder's soffit was perfectly flat prior to the application of prestressing force and self-weight, which may be questionable. This unevenness may also be used to examine the measurement error.

Local debonding of the prestressing strands from the flexural failure should not affect the moment diagram too much. According to Lin and Burns [1981] only external shear forces create bond stress between the tendon and concrete. The flexural capacity of the girder was so low that the shear forces likely were not able to produce enough bond stress so as to cause any slippage. The load deflection data from the flexural failure does indicate that the prestressing steel was yielding, so that may cause some localized moment reduction. According to Equation (7-19) (Lin and Burns [1981]), the transfer length is 13”. Flexural yielding should only occur at one point on the prestressing steel, meaning that the total affected area is just over two feet of the total span.

3 ANALYTIC STUDY: SHEAR STRENGTH OF PRESTRESSED CONCRETE GIRDERS

3.1 Introduction

The actual shear strength of the girders determined in Chapter 2 is only a number unless it is compared with some standard for expected performance. Granted, this expectation has not been constant throughout the years. Codes evaluate structural members usually become less conservative as more information becomes available through research. Assuming that codes are able to predict capacity more accurately as knowledge increases, some concerns arises when a new code is more conservative than an old one. The point of this analysis is to determine whether or not this is the case with the 1973 11th Edition of AASHTO Standard Specifications for Highway Bridges (ASSTHO [1973], shorthanded as AASHTO-STD hereafter) because of its adoption of the quarter point rule.

The quarter-point rule raises speculation that there is a deficiency on the demand side of the design equation. AASHTO-STD states, "for the design of web shear reinforcement, it is recommended that shear be investigated only in the middle half of the span length." This means that only half the shear from distributed loads and a maximum of three-quarters the shear from point loads will be considered for design. Since AASHTO-STD calculates nominal shear strength differently than newer codes like AASHTO LRFD Bridge Design Specifications, 2004 3rd Edition (ASSTHO [2004], shorthanded as AASHTO-LRFD hereafter) and ACI 318-08 Building Code Requirements for Structural Concrete (ACI [2002], shorthanded as ACI-318 hereafter), it's not obvious whether or not there is a problem. However, a detailed analysis can provide some insight about the circumstances where this problem might exist. This analysis focuses on AASHTO prestressed concrete girders because they are a popular choice in Oklahoma.

While it is useful to know when bridges designed using AASHTO-STD fail to meet current codes, the tested shear capacity of real-world prestressed concrete girders gives direct evidence of the actual condition of structures. The challenge with shear testing real-world girders (old or new) is that the ratio of applied shear at nominal moment capacity to nominal shear capacity is less than one, so the girder may not experience shear failure when one-point loading is applied. In order to cause shear failure and to experimentally assess the shear capacity, the load must be placed close to the support where applied shear is largest and applied moment is smallest, within the D-region (a distance twice the member depth from the face of the support according to ACI-318 Appendix A). Once point loads are applied inside D-regions the mechanism for distributing loads does not follow girder theory, so it is harder to predict the failure mode. Strut and tie models (STM, hereafter) are one method for dealing with loading in D-regions and will be examined.

In this chapter, overviews of nominal shear capacity for AASHTO-STD, AASHTO-LRFD and ACI-318 are presented first, followed by a code to code comparison. A bridge of particular interest to the Oklahoma Department of Transportation (ODOT) in McCurtain County, Oklahoma (NBI #19257) because of the large girder and transverse reinforcement spacing is analyzed according to each of the specifications for nominal shear capacity to determine if there is cause for concern. STM are also discussed and applied to both girders from the experimental

study. Finally, the nominal capacities for the tested girders are compared with the STM and experimental results. This chapter attempts to draw conclusions based on code to code and code to experimental results comparisons to provide some guidance on which actions, if any, need be taken to ensure the safety of bridges in Oklahoma.

Table 10 shows an overview of the accomplished work in this chapter as well as topics in a future study:

		Shear Capacity and Demands				Strut and Tie Models		
	Girder	AASHTO-STD	AASHTO-LRFD	ACI-318	AASHTO-LRFR	AASHTO-LRFD	ACI-318	Failure Mode
Real	I-244	Figure 44	Figure 44	Figure 44	Figure 44	Figure 44 Table 12	Figure 44 Table 12	Figure 43
	I-244 w/ FRP	NA	TBD	TBD	Table 13	TBD	TBD	TBD
	WHC	TBD	TBD	TBD	TBD	TBD	TBD	TBD
	LRO	Figure 40	Figure 40	Figure 40	Table 13	NA	NA	TBD
Imaginary	Type II	Figures 35-39	Figures 35-39	Figures 35-39	NA	NA	NA	NA
	Type III	Figures 35-39	Figures 35-39	Figures 35-39	NA	NA	NA	NA
	Type IV	Figures 35-39	Figures 35-39	Figures 35-39	NA	NA	NA	NA

Table 10: Overview of accomplished analysis in this project and some identified future work. I- 244: the selected I-244 Bridge girder tested at the non-retrofitted end; I-244 w/ FRP: the selected I-244 Bridge girder tested at the non-retrofitted end; WHC: the selected Wild Horse Creek Bridge girder, and LRO: the Little River Overflow Bridge girder. TBD: future work to be done; NA: not applicable.

3.2 Overview of Codes

This section provides an overview of shear design for AASHTO-STD, AASHTO-LRFD and ACI-318. The pertinent loading, method for determining nominal shear capacity and minimum shear reinforcement is presented here.

3.2.1 AASHTO Standard Specifications (1973)

AASHTO-STD uses a load factor design (LFD) philosophy for prestressed concrete. A brief comparison between allowable stress design (ASD), LFD and load and resistance factor design (LRFD) is presented in Section 3.3.1. A source of concern for this old design specification is its use of the quarter point rule, which states that design shear need only be considered for the middle half of the girder. As a result, design shear is smaller which can cause strength deficiencies in the outer quarters of the span, where shear is largest.

The shear critical section for AASHTO-STD, where maximum design shear exists, is located at the quarter point of the simply-supported girder. The code specifies a distributed lane load in addition to a point load located to cause maximum stress at the section being analyzed (see Figure 31); however, engineers have also been known to apply the actual design truck loads (see Figure 32) when they exceed the standard design stresses (Peters and Rusch [2006 - 2008]). This study follows the methods outlined in the code including the quarter-point rule. As such, the point load must be placed at the quarter-span of the girder to get maximum stress near the supports (Figure 33).

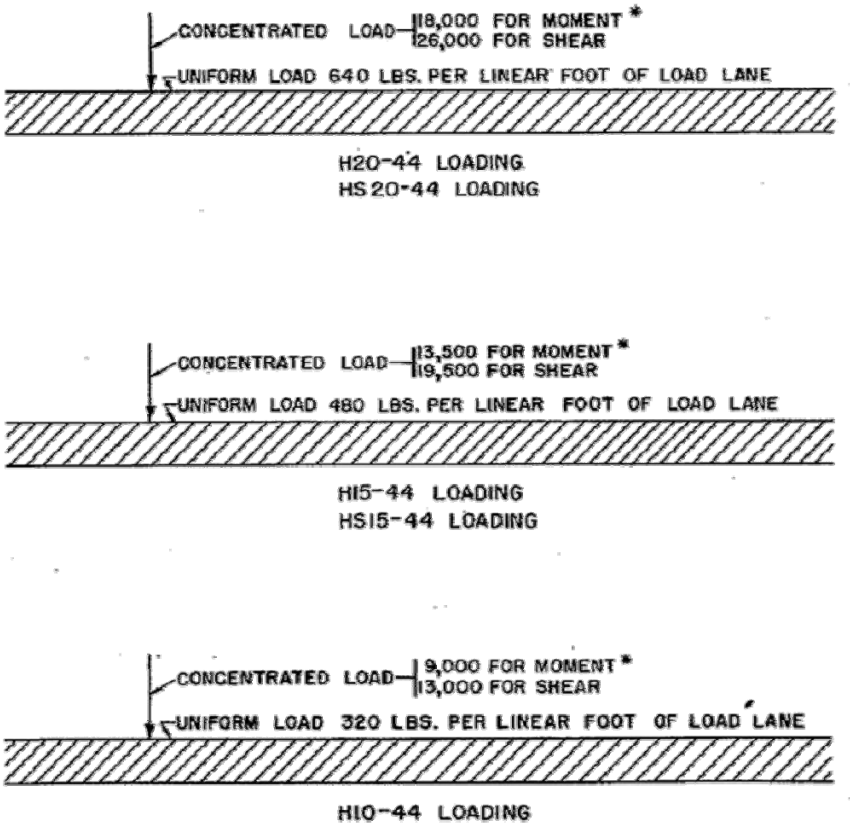

Figure 31: Lane loading for AASHTO-STD based on desired truck loading (AASHTO, 1973).

AASHTO-STD considers three load combinations: Group I, Group II and Group III. For Group I, a proper choice must be made for the design truck based on the expected loading which includes H10, H15, HS15, H20 and HS20 (see Fig. 32). For truck loading less than H20, Group IA load combination is used instead of Group I to consider the possibility of overloading.

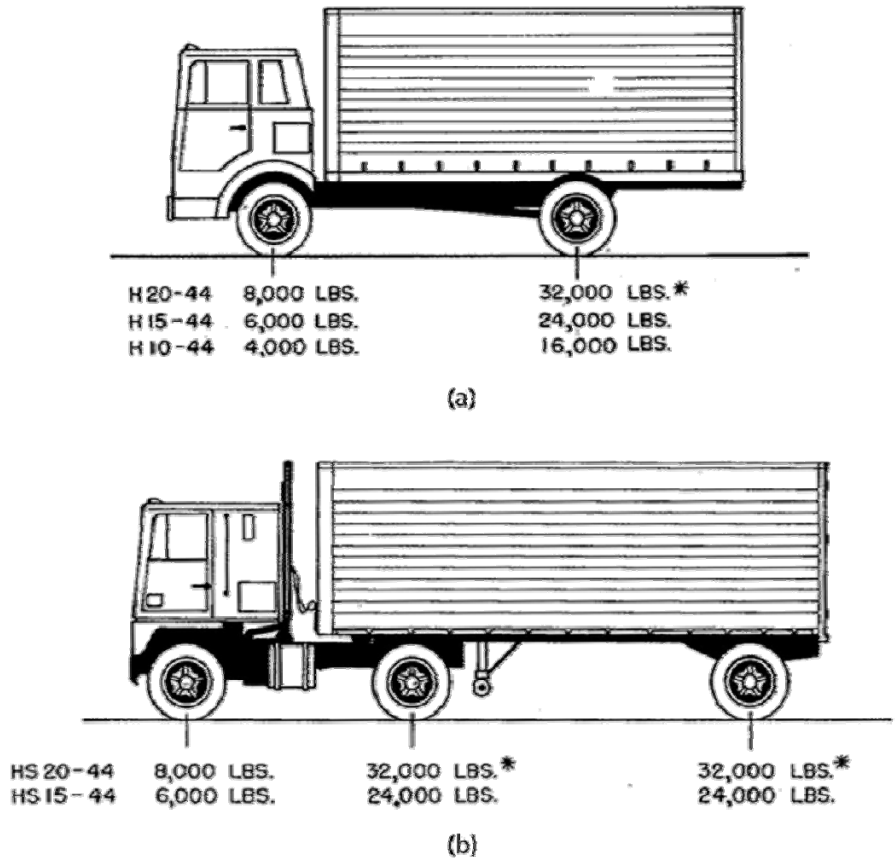

Figure 32: (a) H and (b) HS design trucks (AASHTO, 1973).

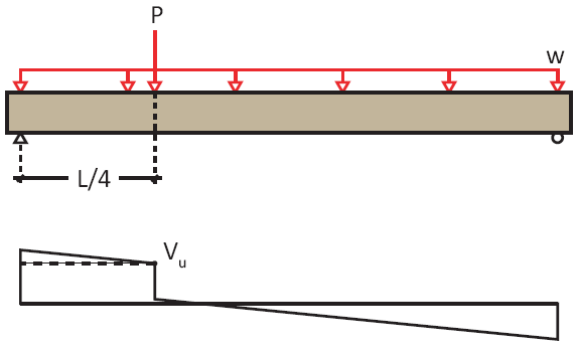

Figure 33: Shear diagrams for distributed and point loads under AASHTO-STD.

Figure 31 also shows another area where AASHTO-STD may lead to under-designed members. The point loads that are applied for shear are less than the loads that would be produced from each of the design trucks. The presence of the distributed lane load, however, could possibly make up for the reduction in point loads. For truck loading less than H20, the Group IA load combination is used instead of Group I for the strength limit state because overloading is more likely to occur.

Nominal shear strength under AASHTO-STD is found by summing the shear resistance of concrete and steel web reinforcement. Equations (1) and (2) are used to compute these values.

$$V_c = 0.06 f_c' b' jd \quad \textbf{(1)}$$

$$V_s = \frac{2A_v f_{sy} jd}{s} \quad \textbf{(2)}$$

where:

V_c = Shear resistance of concrete not to exceed $180 b' d$

V_s = Shear resistance of steel web reinforcement

b' = Width of web

j = Ratio of distance between centroid of compression and centroid of tension and d

d = Distance between extreme compression fiber and centroid of prestressing steel

A_v = Area of web reinforcement

f_{sy} = Tensile stress capacity of web reinforcement

s = Spacing of web reinforcement

Although the effect of prestressing force on the nominal shear capacity is not explicitly included, the calculation of V_c is not the same as for reinforced concrete. Interestingly, V_c is 25% larger for reinforced concrete considering the same section. On the other hand, V_s for prestressed concrete is twice that of reinforced concrete. This significantly changes the constitution of V_n, giving more weight to reinforcing steel. With no limit on V_s or V_n a girder could theoretically get nearly all of its shear resistance from reinforcing steel, which could inhibit the distribution of internal stresses.

Minimum shear reinforcement is defined by Equation (3) for AASHTO-STD:

$$A_v = \frac{100 b' s}{f_y} \quad \textbf{(3)}$$

Minimum shear reinforcement is based on the geometry of the girder and strength of the reinforcing steel.

The quarter-point rule causes shear demands to be relatively low, but it isn't the only concern about shear design for AASHTO-STD. The reduced loads that are applied to the girder could be another cause for girders to not meet current codes requirements' for shear capacity. The contribution to shear capacity from concrete seems conservative due to it being limited by a maximum concrete compressive strength of 3 ksi. As a result, the shear capacity from steel makes up a large portion of the total nominal shear capacity, which may be conservative. In

order to draw some conclusion about girders designed under this code, code to code comparisons will be examined in Section 3.3.

3.2.2 AASHTO LRFD (2004)

The AASHTO-LRFD specification differs from AASHTO-STD in that the critical section is d_v from the face of the support ($0.72h$ or $0.9d$ as defined by AASHTO-LRFD). This approach may be more conservative than AASHTO-STD because there is potential for increased shear demands when loads are present on the outer quarters of the span. Conversely, AASHTO-LRFD allows a STM be used as an alternative to the general method when a load causing greater than one half the design shear at the support lies within a distance of $2d$ from the face of the support. This should give less conservative shear capacities than the standard method and will be discussed later in Section 3.5.

Design live loads are defined by the HL-93 loading specification which includes a distributed lane load (equal in intensity to AASHTO-STD HS20 truck loading), a design tandem and an HS20 design truck which is shown in Figure 32 in the previous section. The greater stress caused by the design tandem or HS20 truck loads is used for design. Typically, the design tandem will control on shorter spans where loads on the design truck may fall off the span or add little to design shear.

AASHTO-LRFD includes twelve limit states which are broken down into four basic categories: strength, extreme event, service and fatigue. Some load factors have a range ensuring that the extreme stress is found for each limit state.

AASHTO-LRFD is based on Modified Compression Field Theory (MCFT) for shear design. Compression Field Theory uses strain in the web of a girder to determine the inclination of diagonal compressive stresses (Bentz et al. [2006]). MCFT extends this by accounting for the mean principal tensile stresses. Since the angle of tensile stresses in the web can vary, so too can the contribution to nominal shear resistance of the web reinforcement; as this angle decreases with respect to the member axis, the shear resistance of reinforcement increases. A table is required to determine the angle of tensile stress in the web, which complicates the process and makes it impossible to perform so-called "back of the envelope" calculations. AASHTO_N.xls is a spreadsheet written by Bentz [2000] that is used for all calculations in this analysis.

For completeness, the design procedure for AASHTO-LRFD will be summarized. As in AASHTO-STD, the nominal shear strength is divided into components as shown in Equation (4); however, the effect of vertical prestressing force is included directly.

$$V_n = V_c + V_s + V_p \tag{4}$$

where:

V_c = Shear resistance of concrete
V_s = Shear resistance of steel web reinforcement
V_p = Vertical component of effective prestressing force

The concrete and shear components of nominal shear strength can be found using Equations (5) and (6):

$$V_c = 0.0316\beta\sqrt{f_c'}\,b_v d_v \quad \textbf{(5)}$$

$$V_s = \frac{A_v f_y d_v \cot\theta}{s} \quad \textbf{(6)}$$

where:

β	=	Softening parameter of concrete (unitless)
f_c'	=	Compressive strength of concrete (ksi)
b_v	=	Width of web adjusted for ducts (in)
d_v	=	Effective shear depth (in)
A_v	=	Total area of shear stirrups (in^2)
f_y	=	Ultimate stress of shear stirrups (ksi)
θ	=	Angle of inclination of shear stress
s	=	Spacing of shear stirrups (in)

Values for β and θ must be found through an iterative process that is based on longitudinal strain at middepth and the ratio between the applied shear stress and the compressive strength of the concrete. These values are calculated using Equations (7) and (8). Note that Equation (8) assumes that the minimum reinforcement requirement is met (which is discussed later in this section). If it is not met, then a slightly different equation must be used.

$$\grave{o}_x = \frac{\frac{M_u}{d_v} + 0.5N_u + 0.5(V_u - V_p)\cot\theta - A_{ps} f_{po}}{2\left(E_s A_s + E_{ps} A_{ps}\right)} \quad \textbf{(7)}$$

$$\nu = \frac{V_u - \phi V_p}{\phi b_v d_v} \quad \textbf{(8)}$$

where:

ε_x	=	Largest longitudinal strain at middepth of the member when subjected to M_u, V_u and N_u
M_u	=	Factored moment at section
d_v	=	Effective shear depth
N_u	=	Factored axial force
V_u	=	Factored shear at section
θ	=	Angle of inclination of shear stress
f_{po}	=	Jacking stress of prestressing tendons ≃ 0.7 f_{pu}
f_{pu}	=	Ultimate stress of prestressing tendons ≃ 0.9 f_{pu}
ν	=	Applied shear stress of concrete
ϕ	=	Reduction factor = 0.9

The first step is to assume a value of θ so that an initial calculation can be made for ε_x. The initial value of ε_x should not be taken as greater than 10^{-3}. If the strain is positive then the values can be input directly into Table 5.8.3.4.2-1 from AASHTO-LRFD. If the calculated strain is negative, it must be recalculated using Equation 9. The assumed value for θ is then checked against that which is given in the table. If they match then the iteration may stop. If not, ε_x must be recalculated with the given value from the table. Once θ converges, the table values for β and θ may be interpolated to provide more accurate results before inputting into Equations (5) and (6) to calculate the nominal shear resistance.

$$\grave{o}_x = \frac{\frac{M_u}{d_v} + 0.5N_u + 0.5(V_u - V_p)\cot\theta - A_{ps}f_{po}}{2\left(E_cA_c + E_sA_s + E_{ps}A_{ps}\right)} \tag{9}$$

where:

E_s = Modulus of reinforcing steel
A_s = Area of reinforcing steel
E_{ps} = Modulus of prestressing steel
A_{ps} = Area of prestressing steel
E_c = Modulus of concrete
A_c = Area of concrete

Minimum shear reinforcement under AASHTO-LRFD is required to minimize the perpetuation of diagonal cracks and increase ductility (AASHTO 2004). The amount of steel required is proportional to the root of concrete compressive strength as is shown in Equation (10).

$$A_v \geq \frac{\sqrt{f_c'}b_v s}{f_y} \tag{10}$$

This relationship between minimum reinforcement and concrete compressive strength shows that cracking and ductility are greater concerns for high strength concrete.

3.2.3 ACI 318-08

ACI-318 is also based on load and resistance factor design. The calculation for nominal shear capacity is similar to late revisions (1980 to present) of the AASHTO Standard Specifications for Highway Bridges which has recently been replaced by AASHTO LRFD. ACI-318 does not include provisions for loading, instead relying on other codes such as IBC. Since AASHTO-LRFD is the most current design code for bridge design, those loads will be used in this report for ACI-318.

Like the other codes, ACI-318 divides the nominal shear strength into contributions from concrete and steel transverse reinforcement. They are computed using the following equations:

$$V_{ci} = 0.6\sqrt{f_c'}b_w d_p + V_d + \frac{V_i M_{cre}}{M_{max}} \tag{11}$$

$$V_{cw} = \left(3.5\sqrt{f_c^{'}} + 0.3 f_{pc}\right) b_w d_p + V_p \quad \textbf{(12)}$$

$$V_s = \frac{A_v f_y d_v}{s} \quad \textbf{(13)}$$

where:

V_{ci} = Concrete shear capacity when cracking results from combined shear and moment (lb)

V_{cw} = Concrete shear capacity when cracking results from high principal tensile stress (lb)

V_s = Shear capacity of steel web reinforcement (lb)

M_{cre} = Moment causing flexural cracking at section due to externally applied loads (lb-in)

V_d = Unfactored shear due to dead load (lb)

V_i = Factored shear at section due to externally applied loads (lb)

M_{max} = Factored moment at section due to externally applied loads (lb-in)

f_{pc} = Compressive stress in concrete at centroid of gross section resisting externally applied loads including effective prestressing force (psi)

b_w = Width of web adjusted for ducts (in)

d_v = Effective shear depth (in)

A_v = Total area of shear stirrups (in^2)

f_y = Yield stress of web reinforcement (psi)

s = Spacing of shear stirrups (in)

V_p = Vertical component of prestressing force (lb)

The nominal shear resistance of concrete is taken as the lesser of V_{ci} and V_{cw}. Typically, V_{cw} will control near the supports and V_{ci} will control closer to midspan. The effective prestressing force is included directly in the equation for V_{cw} as the vertical contribution of prestressing force and in the term f_{pc} which includes only the uniform axial compression due to effective prestressing force. It is important to note that, although not shown explicitly in the equations above, the effective prestressing force is used in V_{ci} as it must be considered when determining M_{cre}.

Minimum shear reinforcement is presented in Equation (14).

$$A_v \geq \frac{0.75\sqrt{f_c^{'}} b_w s}{f_{yt}} \quad \textbf{(14)}$$

where:

$f_c^{'}$ = Compressive strength of concrete (psi)

b_w = Effective width of web (in)

s = Spacing of shear reinforcement (in)

f_{yt} Tensile strength of shear reinforcement (psi)

Another equation is presented for minimum shear reinforcement for girders that exceed a

certain amount of prestressing force that's related to the flexural reinforcement which produces lower results. The smaller of the two is taken as the minimum shear reinforcement so Equation 14 may be applied to any girder.

ACI-318 relies on other codes for determining the appropriate design loads; in this case AASHTO-LRFD is be used. This does not, however, indicate that the design shear will be identical because the critical sections for AASHTO-LRFD and ACI-318 are different. The nominal shear capacity estimation is based on equations that are still used in some areas where AASHTO-LRFD has not yet been adopted. The code to code comparisons in Section 3.3 will help show the implications of the change.

3.3 Code Comparison

This section will discuss some of the differences between AASHTO-STD, AASHTO-LRFD and ACI-318. First, a brief comparison of the different design philosophies (ASD, LFD and LRFD) is presented. A quantitative comparison begins with computing the minimum transverse reinforcement for a Type II AASHTO PRESTRESSED CONCRETE girder. Next, the design shear for three typical AASHTO girders (Types II, III and IV) is compared. To complete the code comparison, the nominal shear capacities are analyzed alone and in conjunction with the shear demands.

3.3.1 Design Philosophies

The method in which concrete structures are designed has evolved over the years. Allowable Stress Design (ASD) was used up until the early 1970s; the I-244 girder obtained from Tulsa was designed using this method in 1970. ASD only considers the service limit state, meaning that only service loads are analyzed. In order to overcome instances of overloading and fatigue, factors of safety are applied to the design loads. This had been the method of choice for decades and it proved to be safe.

Load Factor Design (LFD) replaced ASD as the predominant method for concrete design in the early 1970s. LFD has a couple advantages over ASD. First, dead and live loads are treated differently. Since dead loads are much easier to estimate, the load factor for dead loads is less than that for live loads. In instances where there is high ratio of dead to live load, ASD would require a larger section because the same load factor is applied to all loads. LFD takes advantage of our knowledge of the structure and gives a more efficient design. Additional limit states are also incorporated into LFD. Where ASD only looks at the service loads, LFD adds strength and extreme event limit states. This ensures the safety of the structure during events that the structure is not likely to see on a regular basis.

In 1994, AASHTO introduced the LRFD design code and has been transitioning ever since. LRFD expands on what started with LFD, adding more limit states and even more load factors. There is little that is fundamentally different between the two methods. Perhaps the biggest difference is in how the load factors are determined. A statistical model was used to determine load factors for LRFD, which made the margin of safety more uniform across members in a structural system (Grubb [1997]).

The progression of design philosophies for concrete structures has focused on improving the efficiency of design in addition to adding a safeguard against extreme events. It's easy to see

how LRFD has accomplished the efficiency part of the equation. It will be some time before most structures designed under LRFD have reached the end of their design life, so it may be premature to say that LRFD is safer.

3.3.2 Minimum Shear Reinforcement

The minimum shear reinforcement requirements vary between each of the codes analyzed in this study based on the concrete compressive strength. The values of minimum shear reinforcement for a Type II girder with Grade 60 transverse reinforcement are shown in Figure 34.

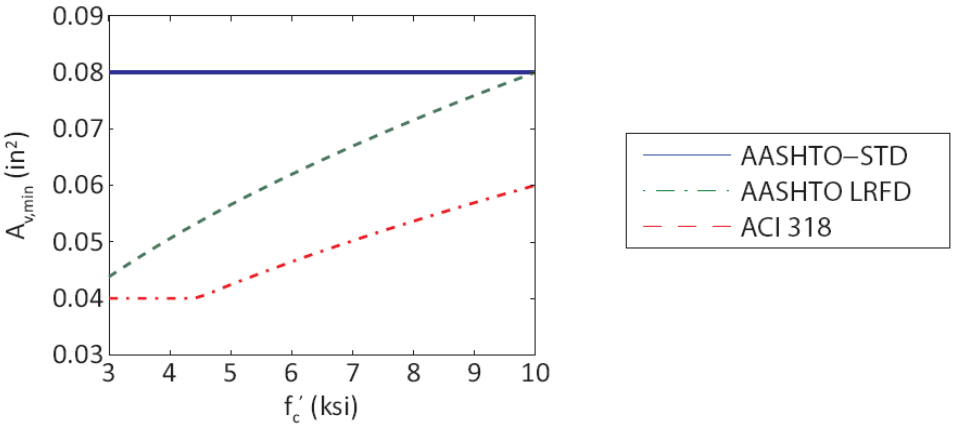

Figure 34: Minimum shear reinforcement with varying concrete compressive strength.

AASHTO-STD has a constant value for the minimum shear reinforcement for a given section. The other two codes are a function of the concrete compressive strength. The only differences between AASHTO-LRFD and ACI-318 are that ACI-318 adopts a multiplier of 0.75 and specifies a lower limit, which is reached when $f_c^{'}$ is less than 4444 psi. The values for minimum shear reinforcement are very small for AASHTO girders because the web width is quite small. Thus, minimum shear requirements are always satisfied for AASHTO Type II girders with at least one leg of #3 rebar ($A_v = 0.11$ in^2).

3.3.3 Shear Demands

Shear demands are quite different among the codes; therefore there is a need to identify shear demands separately for each code. In this study, shear demands are determined by applying the loads as they are presented in the code. Calculations are made for model AASHTO Type II, III and IV prestressed concrete girders with spans of 30, 60 and 90 feet, respectively. ACI-318 provides load factors but no design loads, stating that all applicable loads must be considered. Since AASHTO-LRFD represents the current practice for bridge design, those loads will be input to the load factors of ACI-318 to determine those shear demands. It should be noted that the shear demands calculated in this section are used in the margin of safety analysis in Section 3.3.5. The following are the basic assumptions for determining shear demands:

- Only dead, live and impact loads are considered

- Live loads are distributed according to applicable factors
- Dead loads consist of the weight of the girder, slab, parapet and overlay (if present)
- HS20 truck loading is used

For this analysis, AASHTO-STD is controlled by the Group I load combination, as opposed to Group IA, because HS20 truck loading is applied. The Group I load combination is shown in Equation (15).

$$\text{Group I} = \frac{1.3}{\phi}\left[\text{D} + \frac{5}{3}(\text{L} + \text{I})\right] \quad \textbf{(15)}$$

where:

D = Dead load
L = Live load
I = Impact load
ϕ = Shear reduction factor = 0.90

The impact load is taken as a fraction of the live load and is defined by Equation (16).

$$\text{I} = \frac{50}{L + 125} \quad \textbf{(16)}$$

where:

L = Length of span that is loaded to produce maximum stress

The value for *L* is somewhat ambiguous from its description. Fortunately, the code provides direction under several scenarios. When shear is analyzed with truck loading, as in this case, *L* should be taken as the distance from the point load to the far reaction.

The live loads consist of a distributed lane load and a point load as discussed in Section 3.2.1. The intensity of the lane load is defined by the code as 0.64 kips per linear foot. For HS20 loading, the point load is taken as 26 k and placed at the point causing maximum stress, which, following the quarter point rule is at the quarter span. Since the point load is placed at the quarter span for each type of girder, its contribution to the applied shear remains constant. The only changes in shear demand come from the uniformly distributed dead and lane loads, which vary with span. For the model Type II, III and IV girders, the calculated shear demands for AASHTO-STD are 114, 149 and 190 kips, respectively.

For AASHTO-LRFD, several more load combinations are available to cover more limit states and combinations within those limit states. Strength I controls for this analysis because of its emphasis on live loads. This load combination is shown in Equation (17) not including terms that are neglected or not applicable.

$$\text{Strength I} = 1.25\text{DC} + 1.50(\text{DW}) + 1.75(\text{LL} + \text{IM}) \quad \textbf{(17)}$$

where:

DC = Dead load due to structural components
DW = Dead load due to wearing surface
LL = Live load
IM = Impact load equal to 33% of the truck or tandem loading

The load factor for dead loads varies between 0.9 and 1.25. The factor of 1.25 is chosen to produce the extreme scenario. Whereas impact loading for AASHTO-STD is applied to all live loads, LRFD specifies that it need only include loads from the design tandem or truck.

Applying the design loads for AASHTO-LRFD is somewhat more complicated than AASHTO- STD. The procedure (in this analysis, at least) is based on disallowing the use of the strut and tie method. This way, maximum shear demands can be found that require the general method for analysis. With this in mind, it is not only imperative to change the location of the tandem and truck loads to comply with the critical section for each type of girder, but the point loads within 2d of the face of the support may not cause more than one half the total design shear requirements at the face of the support. It seems that the design tandem may control for shorter spans but the design truck controls for each of the model girders studied in this analysis. The factored shear demands for HL-93 loading are 130.18, 213.32 and 285.90 kips for the model girders in ascending order.

The same procedure for AASHTO-LRFD is used for ACI-318 to determine the unfactored demands. The only difference being that the critical section for ACI-318 is $h/2$ instead of d_v as it is for AASHTO-LRFD. The controlling load combination is shown in Equation 18.

$$U = 1.2D + 1.6L \quad \textbf{(18)}$$

where:

D = Dead load
L = Live load (includes impact load)

The shear demands for Types II, III and IV girders are 129.91, 206.85 and 275.89 kips, respectively. A comparison between the shear requirements of the codes is shown in Figure 35.

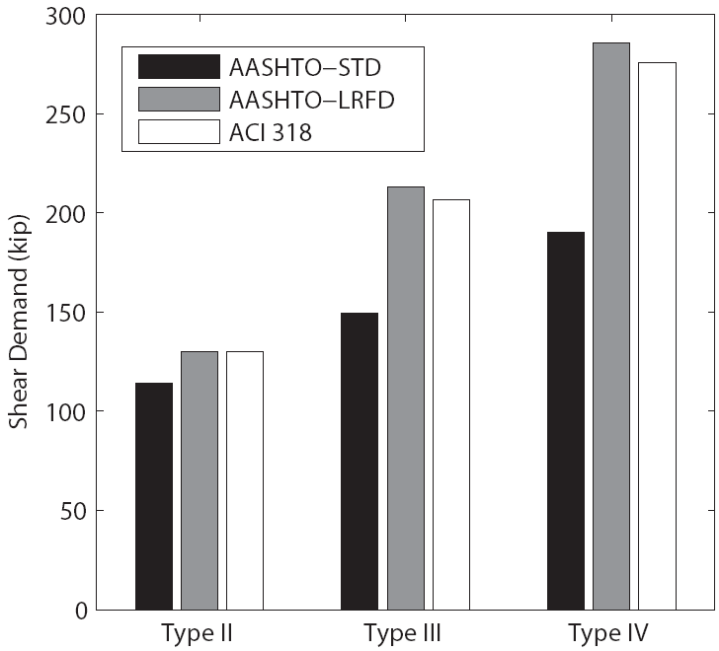

Figure 35: Comparison of ultimate shear demands between codes.

Notice that as the girder sections (and their spans) get larger, the AASHSTO Standard Specifications fall progressively behind the requirements of the other codes. As mentioned before, this is largely due to the fact that the location of the critical section lies at the quarter span for AASHTO- STD. Since it is at a relative location, the shear demands for truck and tandem loading have a maximum of 75% their value. Newer codes' critical sections are based on the geometry of the cross section. Having nothing to do with the span, the shear demands can reach higher proportions of the applied loads. For short spanned girders, such as a Type II, the difference in shear demands is noticeable, but within a small relative range. For a Type IV girder, the current shear demands are approximately 50% larger. Shear demands vary between the codes analyzed in this study. This is due to the variations in critical section, live loads and load factors. The significance of the differences in shear demands will be examined in more detail in Sections 3.3.4 and 3.3.5.

3.3.4 Nominal Shear Strength

To directly compare the nominal shear strength between the codes, three AASHTO prestressed concrete model girders (Types II, III and IV) are selected as described in Section 3.3.3. Each of the girders are designed with straight-profile prestressing steel to support the maximum moment produced by loads according to AASHTO-LRFD. The moment capacity of the girders is calculated with Equation (19).

$$M_n = A_{ps} f_{ps} \left(d - \frac{a}{2} \right) \quad \textbf{(19)}$$

The term f_{ps} is estimated from Equation 18-3 in the ACI code. The properties used for design and analysis of these model girders are listed in Table 11 unless specified otherwise.

$f'_{c,girder}$ (ksi)	$f'_{c,deck}$ (ksi)	f_{pu} (ksi)	f_{se} (ksi)	s (in)
8	4	270	180	8

Table 11: Properties of model girders used in this section, unless specified otherwise.

The nominal shear capacities are calculated for each of the model girders with $f_c^{'}$ ranging from 4 to 10 ksi according to AASHTO-STD, AASHTO-LRFD and ACI-318. The results are shown in Figure 36.

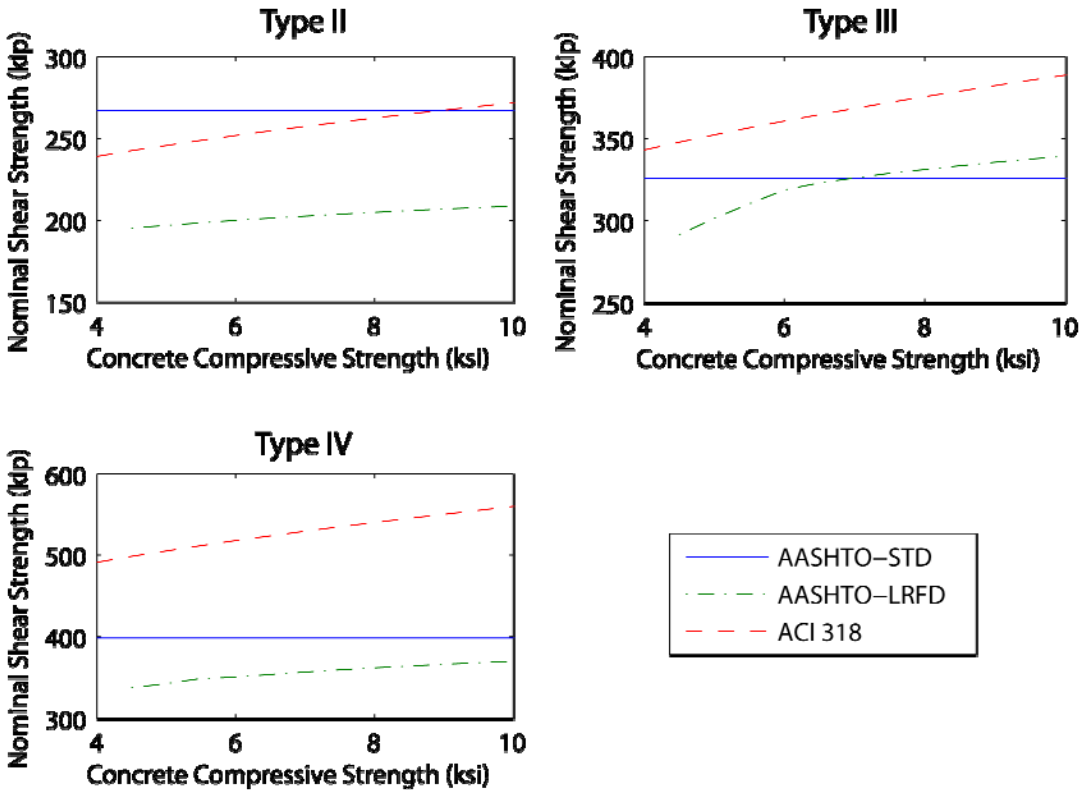

Figure 36: Nominal shear strength as affected by concrete compressive strength for AASHTO Types II, III and IV prestressed concrete girders, respectively.

The most important point to take from Figure 36 is that the newer codes are more conservative when calculating nominal shear resistance. Common sense says that shear resistance should increase with $f_c^{'}$, but this doesn't happen with AASHTO-STD. The concrete compressive strength is implicitly limited to 3 ksi because of the limit on V_c, $180\,b^{'}jd$. The newer codes have limits on V_n and/or V_s, but they are not reached for the sections analyzed here.

Another useful comparison is to look at nominal shear capacity with varying transverse reinforcement spacing. These calculations are only made for a Type II girder where transverse

reinforcement provides the largest portion of shear resistance. The results are shown in Figure 37.

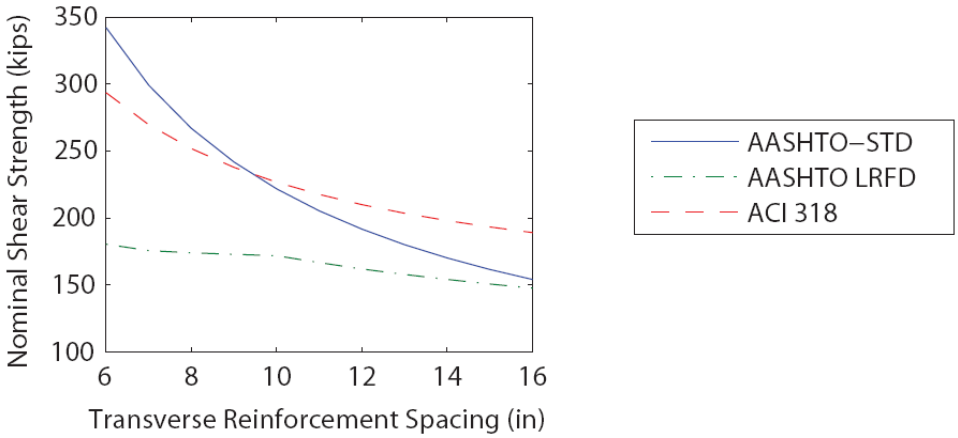

Figure 37: Nominal shear strength of a Type II girder with varying stirrup spacing.

AASHTO-STD is affected the most by changes in transverse reinforcement spacing because of the relatively large ratio of V_s/V_n. This results in AASHTO being conservative for large transverse reinforcement spacing and unconservative for small transverse reinforcement spacing. For transverse reinforcement spacing from approximately 9.5 to 14 inches, AASHTO-STD falls between AASHTO-LRFD on the low end and ACI-318 on the high end. Since ODOT is transitioning to AASHTO-LRFD, this range is also unconservative, although there is less concern about the safety as discussed in the following section.

3.3.5 Margin of Safety

While the comparison accounting for only the absolute nominal shear capacity is helpful in identifying different evaluations of the shear capacity of the same girder, this method may not be appropriate in assessing whether the old girder designed according to AASHTO-STD is safe and meets all current codes. In other words, the shear capacity to shear capacity comparison does not reflect the whole design process of each code. In the codes, load and strength reduction factors are different, as is also the magnitude of design dead and live loads. Also, the location of shear critical section is not the same for each code. Therefore, all these design considerations should be compared and analyzed together.

In order to provide a sense of how the codes in this analysis compare, the margin of safety is calculated. In this report, the margin of safety is defined as the ratio of the factored nominal shear capacity to design shear demand considering all load and reduction factors as expressed in Equation (20).

$$\text{Margin of Safety} = \frac{\text{Factored nominal shear capacity}}{\text{Design shear demand}} = \frac{\phi V_n}{V_u} \text{ or F.S.} \times \left(\frac{V_n}{V_u} \right) \qquad \textbf{(20)}$$

where ϕ is the load reduction factor, V_n is the nominal shear capacity, V_u is the design shear demand obtained from that accounting for all load or safety factors, and F.S. is the factor of safety.

Comparing the margins of safety from different codes is a good way to see how the performance expectations have changed. The design shear requirements used here are detailed in Section 3.3.3. Figure 38 show results of margin of safety calculations of the model girders with varying concrete strength.

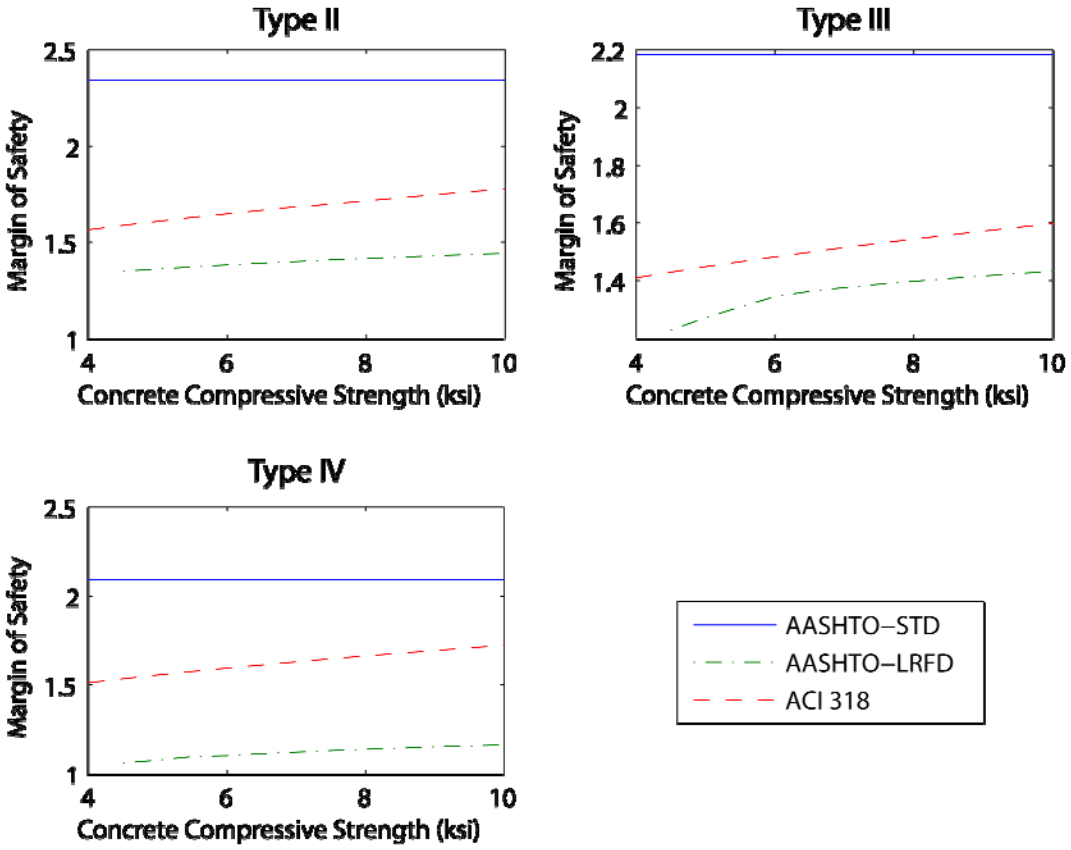

Figure 38: Margin of safety as affected by concrete compressive strength for AASHTO Types II, III and IV prestressed concrete girders, respectively.

While the shape of the curves is the same as those from nominal shear strength analysis, their relative positions are different. For each type of girder, the tendency is nearly the same. The margin of safety according to AASHTO-STD is around one point greater than AASHTO-LRFD. It's possible that a girder may have looked safe at the time it was designed, but the margin of safety could fall below 1.0 when analyzed under a current code and therefore be considered unsafe.

The margins of safety are also calculated for a Type II girder with varying transverse reinforcement spacing. The results are shown in Figure 39.

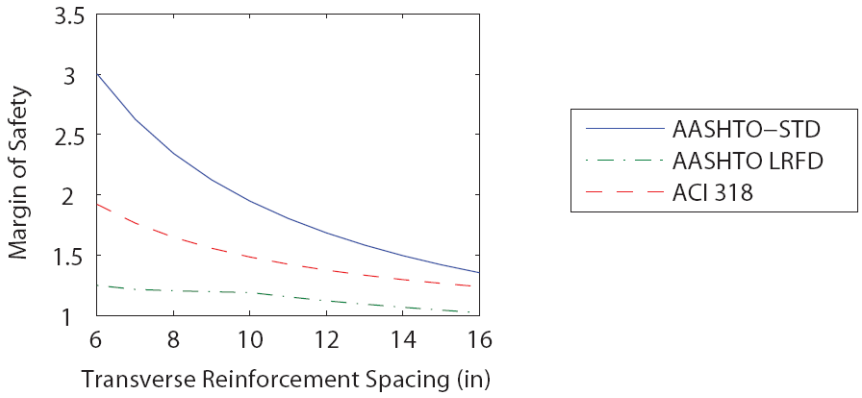

Figure 39: Margin of safety of a Type II girder with varying stirrup spacing

From an analytical standpoint, this analysis shows that as transverse reinforcement spacing increases, the disparity of margin of safety between AASHTO-STD and current codes decreases. It's hard to expect girders designed under AASHTO-STD to meet the requirements of the newer codes given the larger design shear requirements and this analysis reinforces that.

As mentioned earlier, comparing the nominal capacity for a given member from different codes may not give the best indication of how older girders will perform because other factors in the code, the quarter point rule and design loads, for instance, should be taken into consideration when deriving formulas that estimate V_c, V_s, etc. The margin of safety includes both aspects of the code, and thus all these considerations are included in the analysis. For each type of girder, the comparison of margins of safety indicate that girders designed under AASHTO-STD may be in danger of being structurally deficient, but this problem is less dire for girders with large transverse reinforcement spacing. Although each of the model girders analyzed in this section maintained a margin of safety greater than one for the newer codes, it's doubtful that all girders designed during the 1960s and 1970s will fall into this category. For example, old girders that might have been designed with a margin of safety approximately 1.5 based on AASHTO-STD may lie below 1.0.

3.4 McCurtain County Bridge NBI #19257

A bridge crossing the Little River Overflow in McCurtain County, Oklahoma is of concern because of some of its design features. The bridge was designed according to the 11th Edition of The AASHTO Standard Specifications for Highway Bridges which uses the quarter point rule to determine shear demands. This section will follow the methods used in Section 3.3.4 for analyzing nominal shear capacity.

The bridge features a 40’9” clear roadway with 1’4” parapets. Four Type II AASHTO prestressed concrete girders support the roadway spaced at 11’9”. Each of the girders has 14-1/2” prestressing two of which are harped at an angle of 7.8°. Shear reinforcement is provided by two #4 Grade 40 Z-bars spaced at 10.5”. The concrete compressive strength of the girder is assumed to be the same as the I-244 girder, 5 ksi, because both girders were manufactured around the same period. The relatively large spacing between girders and transverse reinforcement spacing cause increased shear demands and reduced shear capacity, respectively. The interior girders are of greater concern because they are subjected to larger loads and are thus the focus of this analysis. Figure 40(a) shows the shear demands for the interior girders of the Little River Overflow Bridge. Figure 40 compares the nominal shear capacities and margins

of safety, respectively, for AASHTO-STD, AASHTO-LRFD and ACI-318.

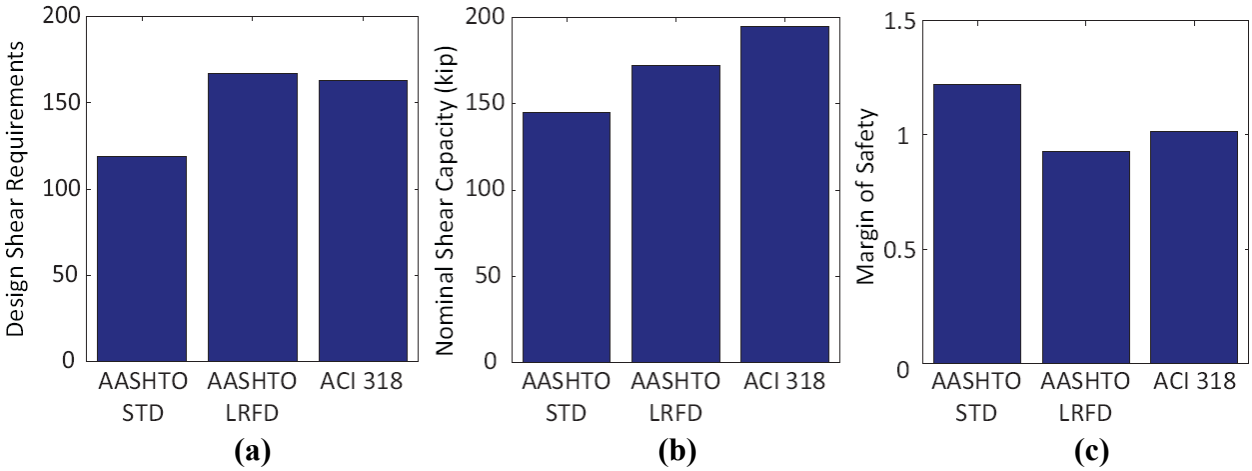

Figure 40: (a) Design shear requirements, (b) nominal shear capacities, and (c) margins of safety for the Little River Overflow Bridge in McCurtain County, Oklahoma

The shear demands of AASHTO-LRFD are roughly 40% larger than that of AASHTO-STD. AASHTO-STD has a lower nominal capacity than the newer codes because most of the shear resistance comes from the transverse reinforcement. On the Little River Overflow bridge, the transverse reinforcement has a yield stress of 40 ksi and its spacing is relatively large at 10.5", so it is somewhat marginalized. Even though the nominal capacity is smaller for AASHTO-STD, the margin of safety is still significantly larger than that of the newer codes because of the increased shear demands.

This analysis shows that the interior girders on the Little River Overflow Bridge in McCurtain County, Oklahoma do not satisfy the requirements as laid out by AASHTO-LRFD and they barely meet the requirements for ACI-318. This is true even though the nominal capacity is higher when evaluated with the newer codes. This bridge requires professional attention to ensure that the interior girders will not be damaged by overloading (e.g., load posting).

3.5 Strut and Tie Models

Strut and tie models (STM) can be used when girder theory is not applicable, such as D-regions. The girder is modeled as a truss where concrete struts take the compressive loads and steel ties take the tension loads (Kuchma et al. [2008a]). Since the shear tests conducted in this study were performed within D-regions, strut and tie models are used to estimate shear capacity. Provisions from both AASHTO-LRFD and ACI-318 are considered in this section. Detailed calculations are available in Martin [2009].

A proper truss model should show how forces are distributed throughout the girder. Schlaich [1987] states that the model producing the least strain energy is the most appropriate. In almost all cases where a point load is applied with a shear span to depth ratio less than 2.0, the least strain energy occurs when a compressive strut connects the load and support (Brown and Bayrak [2008]). Since the experimental tests were done with a shear span to depth ratio of approximately 1.0 to promote shear failure rather than flexure failure, a STM was chosen. Example 6 *Prestressed Beam* by Matamoros A. and Ramirez J. in Reineck [2007] was made a close reference to in this study. The STM is shown in Figure 41 where dashed lines indicate struts and solid lines indicate ties.

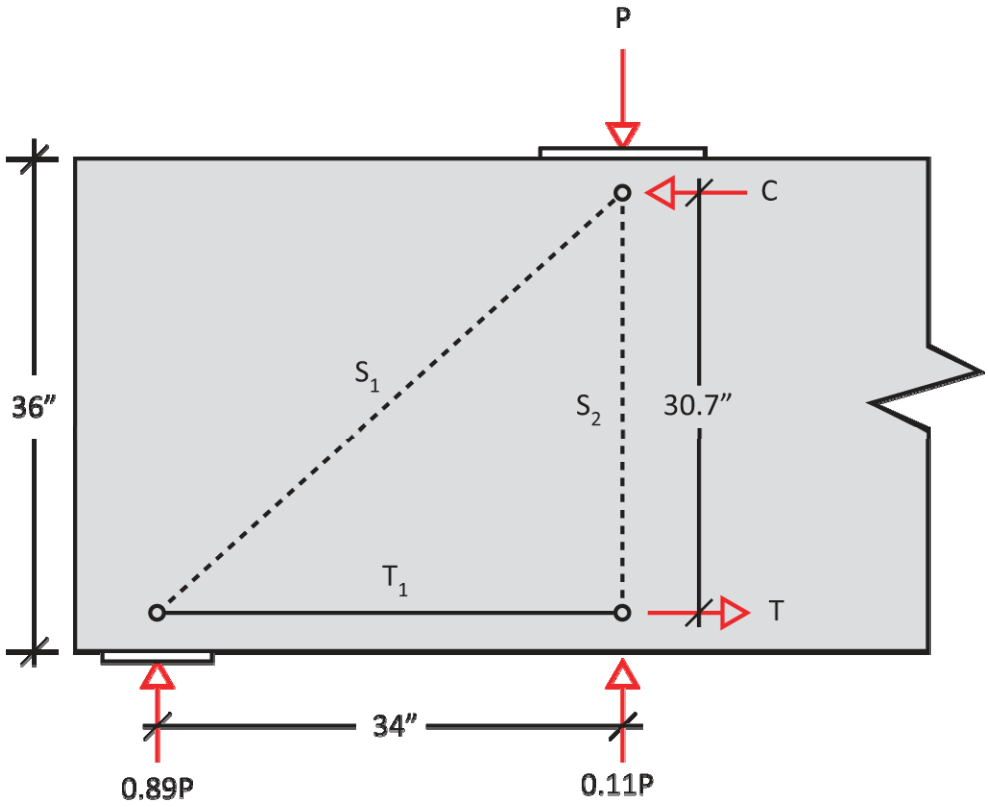

Figure 41: Truss model used for analysis.

An attempt was made to include the harped strands in the model but the design was inefficient. Multiple nodes included struts and ties intersecting at small angles (less than 25°). This increases strain energy because most of the force that is transferred by one member is transferred back to the region where it originally came from. In a sense, little was done to move the force through the girder. ACI-318 strictly prohibits these types of nodes. AASHTO-LRFD allows them, but the stress capacity of the struts is reduced. As such, the model shown in Figure 41 applies to both AASHTO-LRFD and ACI-318 and is the only model analyzed in this study.

The width of tie T_1 is taken as twice the distance from the soffit of the girder to the center of gravity of the steel. The node connecting tie T_1 and strut S_1 is considered to be non-hydrostatic

to prevent unrealistic node geometry. Under these circumstances, the width of strut S_1 is based on the length of the bearing plate and the width of tie T_1. The available concrete for strut S_1 is controlled by the web, because it is the thinnest part of the member. The location of the horizontal compressive force is taken as a distance approximately half the stress block at that location, assuming concrete crushing.

Nominal strut and tie capacities for AASHTO-LRFD are shown in Equations (21) and (22), respectively.

$$P_n = f_{cu} A_{cs} \tag{21}$$

$$P_n = f_y A_{st} + A_{ps}\left[f_{pe} + f_y \right] \tag{22}$$

Nominal strut and tie capacities for ACI-318 shown are in Equations (23) and (24), respectively.

$$F_{ns} = f_{ce} A_{cs} \tag{23}$$

$$F_{nt} = A_{ts} f_y + A_{tp}\left(f_{se} + \Delta f_p \right) \tag{24}$$

These equations are basically the same. Both codes use a limiting stress for the concrete strut capacity and include both conventional steel reinforcement and prestressing strands in calculation of tie capacity. The development of stress in steel ties must be considered in evaluating the tie capacity. The main difference is in how the limiting stress of the concrete struts is calculated. These are shown in Equations (25) and (26).

$$f_{cu} = \frac{f_c'}{0.8 + 170\grave{o}_1} \le 0.85 f_c' \tag{25}$$

$$f_{ce} = 0.85 \beta_s f_c' \tag{26}$$

where

$$\grave{o}_1 = \grave{o}_s + \left(\grave{o}_s + 0.002\right)\cot^2 \alpha \tag{27}$$

The value for ε_1 is based on the tensile strain in the strut due to the adjoining tie and the angle between the strut and tie. The β_S factor is determined by the type of strut. When the width of a strut is allowed to increase at its midsection, as is the case in this analysis, it is called bottle shaped. For a bottle shaped strut the β_S factor is taken as 0.6 or 0.75 depending on whether the minimum transverse reinforcement requirement is met.

Strength of nodal regions is also considered. AASHTO-LRFD applies a factor of 0.85, 0.75 and 0.65 to f_c' for nodes containing no ties, ties in one direction and ties in more than one direction, respectively. ACI-318 uses a similar equation to Equation 23 substituting β_n for β_S. The value of β_n is based on the number of ties intersecting the node; 1.0 for no ties, 0.8 for one tie and 0.6 for two or more ties.

Strut S_1 and tie T_1 from Figure 41 are of the most interest because failure was observed at these locations during the shear capacity tests. Table 12 lists the results of the calculations for applied shear capacities for the strut S_1 and tie T_1.

	$\phi V_{n,S_1}$	$\phi V_{n,T_1}$
AASHTO-LRFD	145 kip	36.5 kip
ACI-318	121 kip	62 kip

Table 12: Nominal shear capacity based on capacity of strut S_1 and tie T_1.

The analysis reveals that the failure load is governed by the tie. With only 10 inches of anchorage length, the stress in the steel is a small fraction of its potential. AASHTO-LRFD specifies a linear relationship for developing the prestressing strands totaling 88 inches. ACI-318 specifies a bilinear relationship for the development of prestressing strands; 25 inches for f_{se} and 30 inches for Δf_p. These results will be compared with the experimental results in Section 3.7.

3.6 Failure Modes

Brittle failure can come from either concrete crushing in flexure or tensile stresses due to applied shear. Concrete crushing is avoided in flexural design by ensuring that reinforcing steel yields first. As there is no connection between shear and flexural design, shear capacity is merely checked for compliance with shear demands. This leaves a vulnerability to brittle shear failure when flexural resistance is large near the supports. For example, shear demand due to unexpected extreme loading may exceed the nominal shear capacity if the flexural capacity of the girder is not exhausted. As evidenced the girder in this study, this is atypical and perhaps unlikely, but it is possible. By making sure the applied shear at nominal moment capacity is always less than the nominal shear capacity, similar to seismic design for RC, the design can be considered safe from brittle failure.

A nominal moment envelope is constructed from support to midspan for the I-244 girder based on flexural capacity. The applied shear for the corresponding nominal moment envelope is found by applying a point load at each point along the span. In this way, it is possible to find the maximum possible shear force that can be applied to the girder before it fails in flexure. Both the nominal moment envelope and the nominal shear envelope are based on equations from ACI-318 and are shown in Figures 42 and 43.

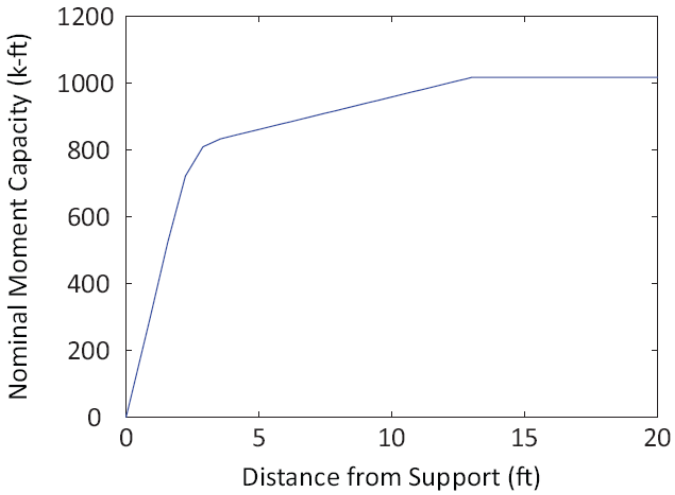

Figure 42: Nominal moment capacity for I-244 girder based on ACI-318.

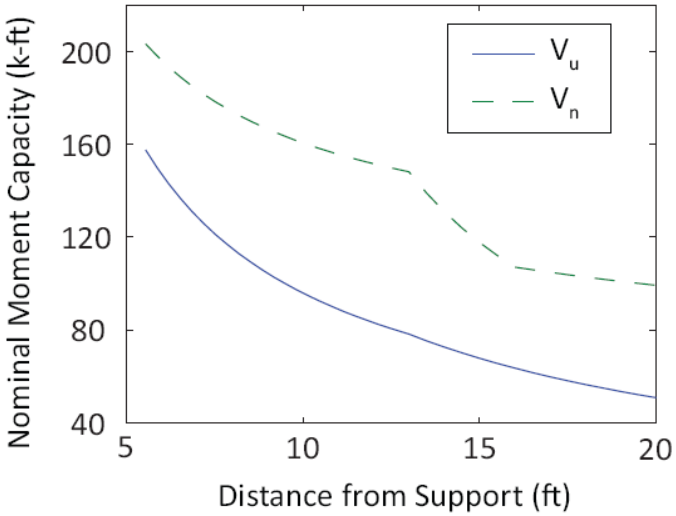

Figure 43: Shear envelope based on nominal moment resistance (see Figure 42).

According to Figure 43 this girder is not likely to suffer shear failure prior to flexural failure. The nominal shear capacity always exceeds the maximum possible shear capacity that can be applied before flexural failure occurs. This type of design is safe because it ensures ductile failure.

3.7 Comparison between Nominal and Experimental Shear Capacity

A comparison between nominal capacities estimated by codes and actual tested capacity gives an indication of the condition of girders in use. Nominal shear capacity is analyzed using properties of the girder at the section that was tested: $f_c^{'}$ = 5 ksi and s = 8 in. The effective

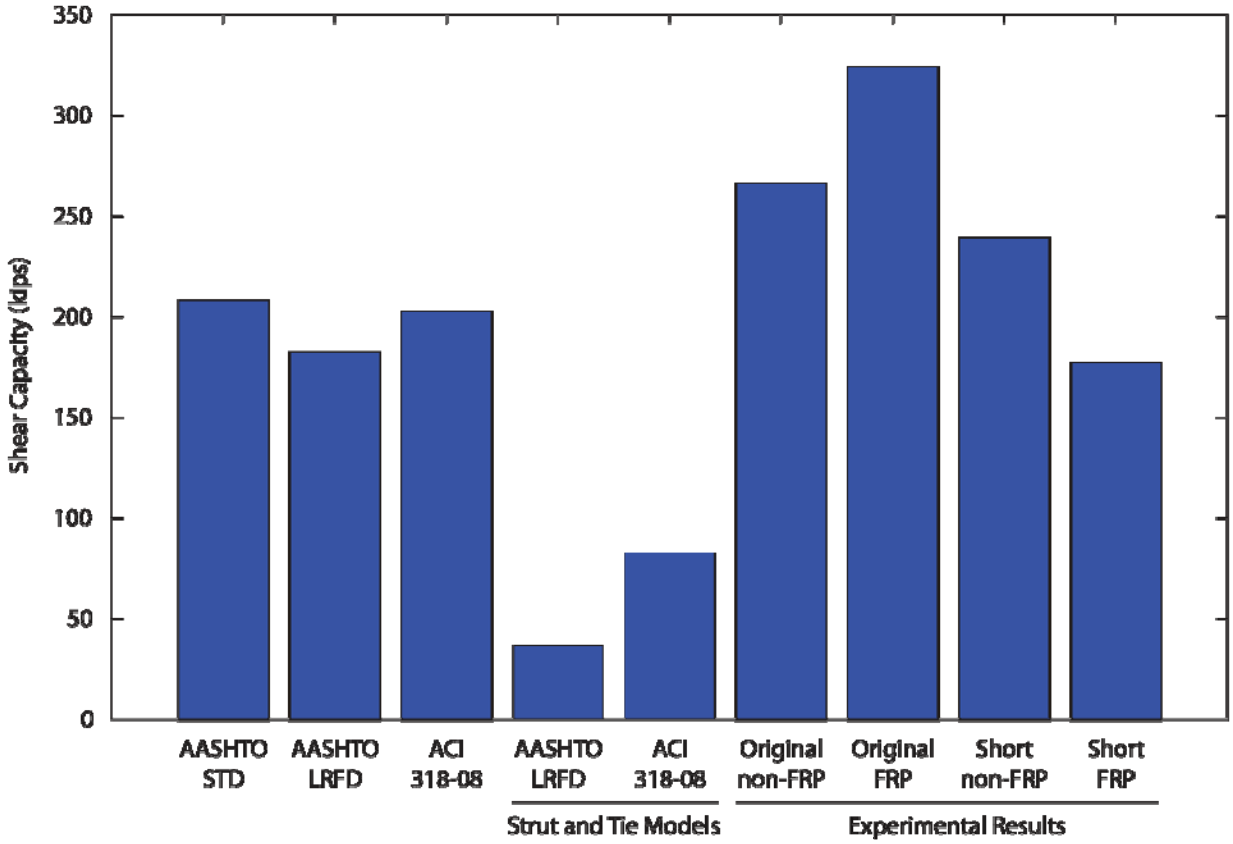

prestressing force is assumed to be 150 ksi. Strut and tie capacity is also included to reflect the configuration in which the girder was tested. The results are shown Figure 44.

Figure 44: Comparison between the nominal shear strength and measured shear capacity of the selected I-244 Bridge girder.

The actual tested capacity of the Type II I-244 Bridge girder exceeds the nominal capacity of each codes including strut and tie provisions by a wide margin. This indicates that, although the girder may be of concern from an analytical standpoint, there is enough capacity to satisfy current demands. Strut and tie capacity is extremely conservative, however, this is due to the lack of sufficient anchorage length for the prestressing strands. Assuming that anchorage length is sufficient to fully develop the strands, the compressive strut controls. However, the nominal applied shear under this circumstance is still less than the nominal capacity estimated using the general methods for analysis.

3.8 Load Posting based on LRFR

Load posting schemes based on Guide Manual for Condition Evaluation and Load and Resistance Factor Rating of Highway Bridges, 2005 (LRFR; hereafter) are briefly discussed, along with determination of the rating factor for the actual girders studied. LRFR is the current system to determine safe live loads for bridges, although LFR may still be used and is included in the LRFR specification. A rating factor is calculated, shown in Eqs. (28) and (29), to compare the applied live load with the nominal capacity less the permanent loads.

$$RF = \frac{C - \gamma_{DC} DC - \gamma_{DW} DW \pm \gamma_P P}{\gamma_{LL} LL(1 + IM)} \quad \textbf{(28)}$$

$$C = \phi \phi_C \phi_S R_n \quad \textbf{(29)}$$

where

RF	=	rating factor
C	=	structural capacity
γ_{DC}	=	LRFD load factor for structural components and attachments
DC	=	dead-load effect of structural components and attachments
γ_{DW}	=	LRFD load factor for wearing surfaces and utilities
γ_P	=	LRFD load factor for permanent loads other than dead loads
P	=	permanent loading other than dead loads
γ_L	=	evaluation live-load factor
LL	=	live-load effect
IM	=	dynamic load allowance
ϕ	=	Strength reduction factor (= 0.75 per AASHTO-LRFD for shear)
ϕ_C	=	condition factor (= 0.85 for poor condition, 0.95 for fair condition, and 1.0 for good condition
ϕ_S	=	system factor that accounts for the level of redundancy
$\phi_C \phi_S$	$\geq$	0.85
R_n	=	nominal member resistance (as inspected)

For a rating factor greater than one, the loading condition is considered safe. In cases where a rate factor is less than one, load postings or bridge strengthening may be required to prevent damage to the structure. LRFR also considers the past performance of a bridge; when there are no signs of distress after years of service, such action may not be justified and is not required.

The rating factor is calculated for three types of loading: inventory, legal, and permit. HL-93 loading, which is equivalent to HS20 truck loading plus uniform lane loading, is used for inventory as a means to see if the bridge can withstand all legal loads. In the event that the rating factor is less than one for HL-93 loading, the bridge can be rated with legal loads based on either state, local or AASHTO specifications or by loads determined by the owner to be applicable to the individual bridge. Permit load rating may be performed on bridges that satisfy the requirements for inventory or legal loads. Permit loads may come from state, local or AASHTO guidelines. Detailed LRFR procedures are provided in the paper by Jaramilla and Huo [2005].

The I-244 and Little River Overflow bridges were rated for shear using inventory and AASHTO legal loads according to LRFR to determine their level of performance. The bridge rating is represented by its weakest member or, as is the case in this study with the interior girders, the member(s) with the largest loads. AASHTO legal loads consist of three typical trucks that control for short (Type 3), medium (Type 3S2) and long (Type 3-3) spans. State legal loads may be different than what are used for this study, however, AASHTO [2005] explains that their legal loads are representative of legal loads across the country. Nominal capacities were calculated for each loading condition because the values vary slightly due to differences in the ratio of applied shear to moment at the critical section. Table 4 shows the RFs for each type of loading along with condition ratings of poor, fair and good.

Table 13: Rating factors of I-244 and LRO bridges for inventory and AASHTO legal loads

	Inventory			Legal								
	HL-93			Type 3			Type 3S2			Type 3-3		
Bridge	Poor	Fair	Good	Poor	Fair	Good	Poor	Fair	Good	Poor	Fair	Good
I-244	0.81	0.95	1.01	1.47	1.70	1.82	1.59	1.84	1.97	1.64	1.90	2.03
LRO	0.67	0.78	0.83	1.03	1.19	1.28	1.18	1.37	1.46	1.22	1.42	1.52

Although neither bridge passes the inventory check for all condition ratings, they both do for the AASHTO legal loads. As such, either of these bridges could be rated for permit loads assuming that the legal loads used in this study are representative.

4 INVERSE PROBLEM: PRELIMINARY RESULTS OF IDENTIFICATION OF EI VALUE AND PRESTRESSING STRESS OF I-244 BRIDGE GIRDER

4.1 Motivations

Failures or potential failures of aging infrastructures have started to draw tremendous attention from the public. Using proper real-world measurements from the infrastructure and applying inverse problem approaches, critical properties of aging infrastructures can be estimated and possible damages can be detected before failures occur. This entails the motivation of the preliminary study presented in this chapter. There is an actively growing multidisciplinary area called *structural health monitoring* to address the pressing research needs related to aging civil infrastructures. Our study benefits from and will make a contribution to structural health monitoring.

In this project, it is necessary to estimate remaining prestressing stress, f_{se}, for the sake of an accurate prediction of shear capacity of the aging real-world girder. To achieve this goal by using camber measurements, it is essential to estimate the real value of flexural stiffness, *EI*, rather than making a gross assumption of it (e.g., a consistent *EI* value throughout the span as commonly seen). Tests are designed to estimate these unknown properties as reported in Chapter 2; this preliminary study explores the subsequent data processing and result interpretation. Results and remaining issues are presented; future work is identified.

4.2 Overview

4.2.1 Identification of Piecewise Constant EI Values

1. This is an inverse problem where we formulate a problem based on mechanics and then solve it mathematically. There are always nonunique solutions (the so-called *nonuniqueness*) associated with inverse problems. This means that a specified experimental result would be fit equally well when totally different problem formulation s (e.g., using different models and/or parameters and/or parameter values) are adopted. This is one of the fundamental challenges in inverse problem and structural health monitoring.

2. As illustrated in Figure 45, we make a basic assumption of having five piecewise constant *EI* values throughout the span (with Section 1 assigned to the girder end strengthened with GFRP); the length of each section with a constant *EI* value measures one-fifth of the entire span. Like any assumption, there are pros and cons associated with this one. The pros include (1) avoid making a gross assumption of a constant EI value, (2) a piecewise constant *EI* is a good compromise between the complexity of the unknown condition and properties of the real-world girder and the idealization for the purpose of theoretical studies. The cons are mainly from the only five piecewise constant *EI* values considered in this study. If the actual *EI* value is a drastically varying function of the span, then this assumption will not work well.

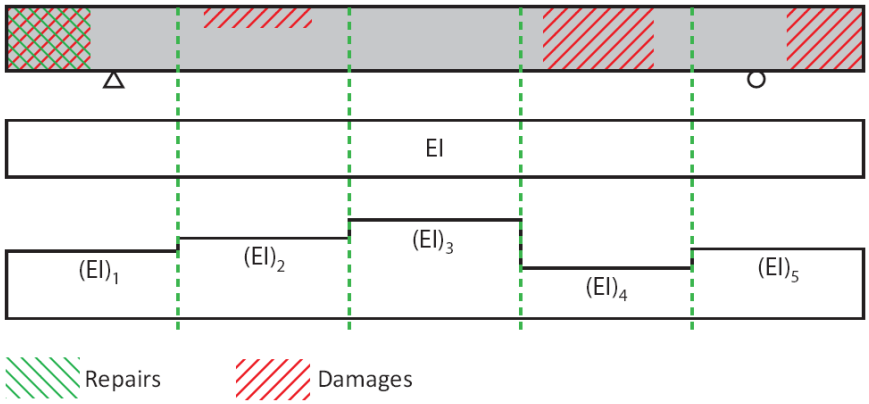

Figure 45: Illustration of constant *EI* value vs. five piecewise constant *EI* values for a generic case.

3. We utilize two types of experiments in our study for this inverse problem. On one hand, we conduct flexural stiffness tests. On the other hand, we measure the camber along the entire span. These two types of experiments are selected based on their efficiency, and our lab testing and instrumentation conditions. Other options, such as modal testing, would be proper but not explored thoroughly in this study. A detailed discussion on each type of the tests and available measurements is discussed in Sections 4.3.2 and 4.3.3.

4. In terms of numerical methods, a standard linear least-squares method is adopted to minimize the approximation errors to obtain the five piecewise constant *EI* values. We propose a method to assign proper initial values to the quantities to be identified, which is found efficient. The key in this novel work is to utilize the understanding (i.e., *a priori* knowledge) of the physical properties to be identified. We carry out our result interpretation in the same fashion by taking full advantage of the knowledge in prestressed concrete.

5. Our initial results are very promising. Future work mainly includes extensive validations of the identified results.

4.2.2 Identification of Prestressing Stress

1. The nonuniqueness challenge remains as for the identification of five piecewise constant *EI* values.

2. We make a basic assumption of having one constant prestressing stress throughout span.

3. Camber measurements are utilized in this inverse problem with the application of principle of supposition. The system to be identified can be treated as a linear system given the understanding of prestressed concrete under the loading conditions considered in this inverse problem.

4. Nonlinear least-squares methods are used in the numerical procedure.

5. Our preliminary analysis shows a significant influence from the time-dependent behavior of prestressed concrete including creep of concrete and relaxation of steel tendon. To obtain more rational results of prestressing stress, more analytical work to improve the inverse problem formulation and additional measurements are essential in future expansions of this study.

4.3 Technical Challenges

4.3.1 Justification of Basic Assumption

To justify the aforementioned basic assumption made in this research, several hard questions are specified and addressed as follow:

What would cause the Young's modulus, *E*, to vary over the span? f_c' should increase with time. How the creep of concrete affects *E* needs to be further studied.

What would cause the second moment of inertia, *I*, to vary over the span? First, the unknown or uncertain existing damages that could potentially contribute to I_{cr} or I_{eff}. Second, the varying location of the harping strands, which is estimated to affect the value of *I* by about two percent.

Why five *EI* values for our girder? It is more rational to identify the product as in flexural stiffness *EI* rather than *E* and *I* individually based on the available test results. An ideal option would be to identify ***EI*(*x*)**, where *x* is the longitudinal coordinate of the girder. In practice, however, it would be more feasible to identify *EI* as a piece-wise constant function of *x*. Five equally divided sections are adopted in this study, which is based on the following considerations:

1. The *EI* value at the mid-span of the girder would be required as the most representative value for the entire span, therefore an odd number of sections would be the option.
2. The effect of GFRP to the value of *EI* needs to be explored. Note that the girder end strengthened with GFRP covers 4' from the very end of the girder. This indicates the need of having each section wider than 4' over a total of about 40'.
3. Having five sections in total seems a good compromise between having too many or too few number of sections. The more sections the girder is divided into, the more accurate the identification results would be. This, however, would only be feasible when there were a sufficient amount of proper data.

4.3.2. Available Tests

The pros and cons of utilizing flexural stiffness tests for the inverse problem are listed as follows: Pros: (1) The effect and complicated (and even unknown) causes for the large camber of the girder are bypassed, and (2) displacement measurements alone are used to make the instrumentation easy. Cons: (1) Small load and displacement readings (collected at a handful number of sparse locations along the span) can cause large errors in numerical analysis,

and (2) measurements of rotation angles and strain would help but are not available in this study.

The pros and cons of utilizing camber measurements for the inverse problem are listed as follows:

Pros: (1) Large camber readings are measured with various spans under a simply supported condition, and (2) dense data points per data set (one data point per foot along the span) makes it possible for spline fitting of the raw data measurements. Cons: (1) The complexity is involved in the estimation of time-dependent properties of the real-world girder, which is required for the formulation and result interpretation of the inverse problem, and (2) the unknown/uncertain span- varying properties are involved in the inverse problem. To elaborate more, there are several major challenges that must be overcome to produce a good analysis of the camber measurements:

- One challenge is the limited amount and varying quality of the camber data as a whole. The data was collected following a processing of (1) figuring out how camber measurements throughout the entire span can be taken accurately and efficiently and (2) gaining an in-depth understanding of the complexity of the inverse problem at hand. Even though correct judgments and decisions were made when the camber measurements of the original I-244 girder were first taken in 2006, more camber measurements by using different support locations would have been taken to better help the inverse analysis.

- More challenging than the above-mentioned one, we do not have any quantitative record of the loading histories and environmental factors that for sure play a significant role in the final camber of this real-world girder (Branson [1977], ACI [1997]).

- Perhaps the greatest challenge in this study is to explain why the camber of the I-244 girder got out of control to begin with. To control the camber, a high density overlay had to be placed before the bridge could be opened (Peters and Rusch [2006 - 2008]). Predicting time-dependent behaviors of prestressed concrete girders in a real-world environment is always full of uncertainties and thus challenging, the topic of which still calls for tremendous research ACI [1997] - Let alone its inverse problem counterpart.

Note that sometimes, the two types of tests could complement each other. Table 13 gives an example of fitting the results using polynomials.

Type of Tests	Pros	Cons
Flexural stiffness	Lower-order polynomial fitting	Too few points to fit per test
Camber	Higher-order polynomial fitting	A good amount of data points to fit

Table 14: Contrast between analyzing flexural stiffness test data and camber measurements

4.3.3 Comparison of Various Types of Measurements

Available and unavailable types of measurements are discussed as follows:

Strain Strain measurements are directly related to $\frac{M(x)}{EI(x)}$, while $M(x)$ can be calculated conveniently from the known value of the applied load. The pros and cons of collecting and processing strain measurements are listed as follows:

Pros: (1) It is very direct to offer the value of $EI(x)$ right at the location where a strain gauge is placed, and (2) it is widely adopted in structural health monitoring, i.e., relevant literature is available. Cons: (1) Small reading may lead to large numerical errors, and (2) we have not developed a robust data acquisition system for multiple channels of strain gauges.

Rotation angle Rotation angles are directly related to the first integral of $\frac{M(x)}{EI(x)}$. The challenge is how this quantity can be measured effectively and efficiently using the existing instrumentations at our lab. Some initial thoughts were discussed during the project, however we did not pursue them further.

Deflection Deflections are directly related to the second integral of $\frac{M(x)}{EI(x)}$. The pros and cons of collecting and processing deflection measurements are listed as follows:

Pros: (1) They are easy to measure. (2) $\frac{P}{\Delta}$ can be obtained conveniently. Consequently, the stiffness or flexibility of each $\frac{P}{\Delta}$ curve can be derived efficiently. Cons: (1) Zero deflections are expected at supports, and very small deflections are expected close to supports. These cause difficulty to estimate the *EI* value of the girder end area strengthened with GFRP. (2) Configurations involving an overhang was hard to implement as experienced in this project. This further prevents us from getting a reliable estimation of the *EI* value of the girder end area strengthened with GFRP.

4.4 Estimating Flexural Stiffness

4.4.1 Data Cleansing

It has been a learning process for the team to get familiar with the data acquisition system offered by Dr. Christopher Ramseyer and use it properly.

The flexural stiffness test data collected from the original I-244 bridge girder in 2006 and reported in Section 2.4 was scanned constantly. The load was applied in steps while the data acquisition system was scanning. The load steps were inconsistent in terms of both time and load because of an inherent limitation with the test rig. This leads to problems when processing the data. Since the system was constantly scanning, one or more lines of data will be present where the deflections do not correspond to the load. Additionally, some load steps will have more data points which will skew the regression.

The flexure stiffness tests performed on the shortened I-244 Bridge girder in 2007 and reported in Section 2.7 were conducted at a much lower scanning rate, pausing ten seconds between each scan. This helps with the abundance of data, and possibly with the load being

applied during a scan; however, a new problem arises from this change. Data may need to be eliminated because of the load being applied mid-scan when there are too few data points for that load step.

To ensure that enough data would be available for processing, the scanner run constantly and paused in between load steps for flexure tests conducted on the Wild Horse Creek Bridge girder in 2008 and reported in Section 2.8. This ensures that the data from the load cell and deflection measuring devices is part of the same load step. One problem that arises from this is that the load is harder to control because it must be read from a dial gauge connected to the hydraulics instead of the reading from the load cell. The preprocessing effort is handled in two ways. Lines of data will be eliminated where the change in load does not correspond to the change in deflection. The data points for each load step will then be averaged so that each load step has equal weight. This doesn't address the variation in size of the load step, but should still improve the quality of the regression. Programs were written in MATLAB to carry out the necessary action for preprocessing.

4.4.2 Problem Formulation

Following Section 4.2 especially Figure 45, the traditional method has been to make the assumption that flexural stiffness remains constant throughout the span. While this is very likely a good assumption to make for a new girder, old girders may have reduced *EI* over some or all of the span. For example, cracking can cause reductions in the moment of inertia that are sometimes hard to detect. By assuming that the girder is divided into five sections with equal length, each with its own constant *EI*, a more realistic picture of the flexural stiffness of the girder could be reached.

Equation (30) shows the basis of the analysis for identifying the assumed five piecewise constant *EI* values from one typical flexural stiffness test:

$$\frac{\Delta}{P} = \frac{k_1}{(EI)_1} + \frac{k_2}{(EI)_2} + \frac{k_3}{(EI)_3} + \frac{k_4}{(EI)_4} + \frac{k_5}{(EI)_5} \tag{30}$$

where $\frac{P}{\Delta}$ can be determined from one test based on the measured load and displacement. The coefficients k_1 to k_5 are theoretical values that can be estimated by using, say, the principle of virtual force. See Figure 46 for an illustration where k_1 equals the integral of Mm over the interval of $(EI)_1$, k_2 equals the integral of Mm over the interval of $(EI)_2$, and so on. The values of $(EI)_1$ through $(EI)_5$ are the unknowns to be identified.

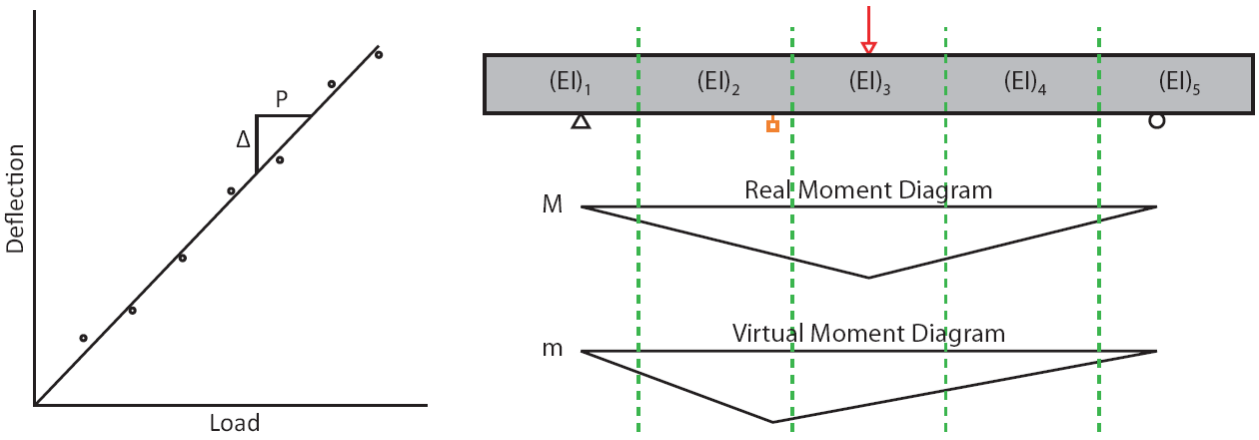

Figure 46: An illustration of the quantities involved in Equation (28).

Note that there are five unknowns to be identified in one equation as shown in Equation (30). To solve them all, more independent equations are needed from different flexural stiffness tests as illustrated in Figure 47.

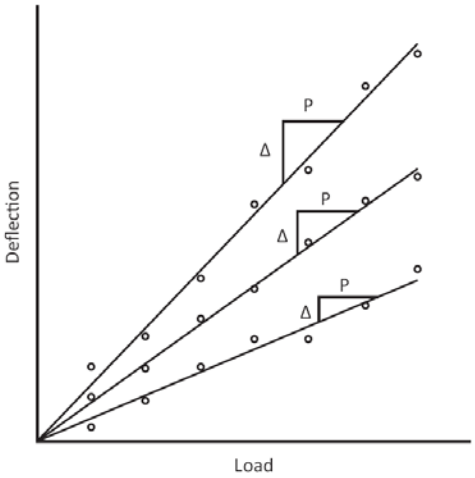

Figure 47: An illustration of multiple load-displacement relationships obtained from multiple flexural stiffness tests.

Basically, these five unknowns can be solved from an over-determined system of equations presented in a matrix product as in Equation (31):

$$Ax = b \tag{31}$$

where $x = \left[\frac{1}{(EI)_1}, \frac{1}{(EI)_2}, \frac{1}{(EI)_3}, \frac{1}{(EI)_4}, \frac{1}{(EI)_5} \right]$ contains the reciprocals of the five piecewise constant flexural stiffness *EI* values (i.e., five piecewise constant flexural flexibility values) to be identified. The matrix A is concatenated from the coefficients *k*'s as in Equation (28),

while the vector b has the measured $\frac{\Delta}{P}$ from all selected flexural stiffness tests. Directly solving for the flexibility values $\frac{1}{EI}$'s rather than stiffness values *EI*'s avoids the use of nonlinear least-squares solvers. Standard linear least-squares solvers can be effectively used to solve for the unknown vector *x* in Equation (29) Mat [2008]), after which the reciprocal of each components of *x* is calculated to obtain the five *EI* values.

4.4.3 Programming Effort

A set of general-purpose MATLAB codes is developed to make all the calculations necessary to obtain five piecewise constant *EI* values for a simply supported beam given an input of load-deflection and test configuration data. While the functions and their descriptions are show in Table 14, the flowchart in Figure 48 shows the order of how the functions are called.

File	Description
'piecewise_ei_input.m	use configuration data to create an input array for 'piecewise_ei_coefficients.m'
'piecewise_ei_coefficients.m'	take input array from 'piecewise_ei_input.m' to calculate each row of matrix *A*
'piecewise_ei_coefficient_check.m'	verify that the coefficients calculated in 'piecewise_ei_coefficients.m' are correct by comparing their sum with the value obtained from the standard deflection equation where *EI* is considered constant

Table 15: Programs called by "piecewise_ei.m" to assist in calculating five *EI* values.

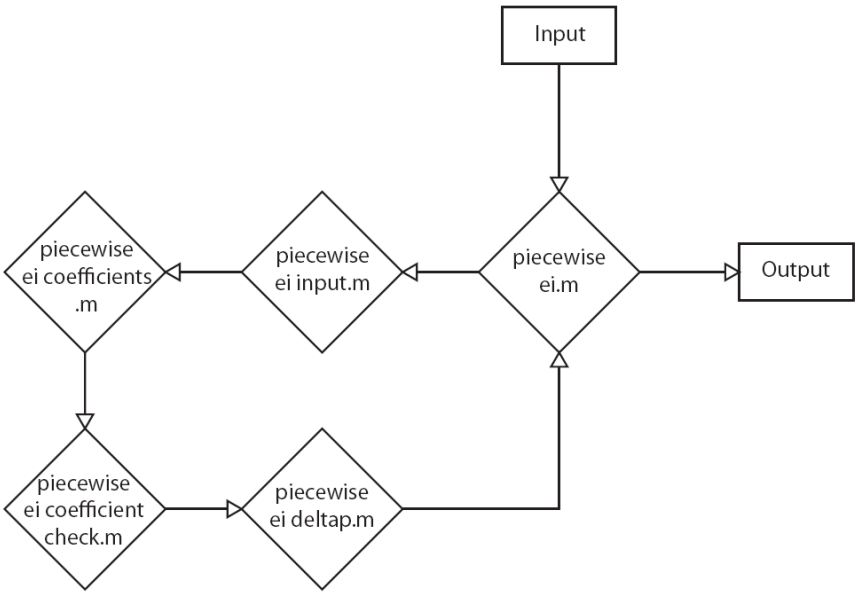

Figure 48: Flowchart for program to determine piecewise flexural stiffness.

The program returns several arrays of data including the following quantities:

- Piecewise flexibility, $\frac{1}{EI}$'s
- Piecewise stiffness, *EI*'s
- Coefficient matrix, A
- Results of checking *A* against the standard deflection equation

The most important output from this program is the full coefficient matrix, *A*. The flexibility values may be the prize at the end of the road, and a standard least-squares technique is used in this program to solve for them. Options for enforcing constraints or initial values are proved to be essential to providing accurate results and will be discussed later.

4.4.4 Determining Initial Values

To solve for the flexibility values, $\frac{1}{EI}$'s, using linear least-squares solvers, their initial values need to be in place. In addition to trying random initial values as in common practice Mat [2008]), initial values of the flexibility $\frac{1}{EI}$'s, or equivalently, those of the stiffness *EI*'s, can be decided through a rational procedure. Note that no precise values are aimed at. Rather, rational but rough estimations of these values are sought after for the optimization to start with.

Assuming a constant value of *EI* across the entire girder and then solving this *EI* value by using a measured $\frac{\Delta}{P}$ and standard elastic deflection equation is a rational approach to derive initial values for the five *EI*'s to be identified. The challenge, however, is to answer which *EI* value out of the five the estimation should be for. To meet this challenge, the sensitivity of a measured $\frac{\Delta}{P}$ with respect

to an $(EI)_i$, where i = 1, 2, 3, 4, 5, is examined. Equation (30) is first rewritten as follows:

$$\frac{\Delta}{P} = \sum_{k=1}^{5} \frac{k_i}{(EI)_i} \quad i = 1,2,3,4,5 \tag{32}$$

The sensitivities if a measured $\frac{\Delta}{P}$ with respect to any $(EI)_i$ can be quantified by using the partial derivatives as shown in Equation (33):

$$\frac{\partial \frac{\Delta}{P}}{\partial (EI)_i} = -\frac{k_i}{[(EI)_i]^2}, \; i = 1,2,3,4,5 \tag{33}$$

If the ranges of EI values are similar, then the maximum value of k_i for a specified load/LVDT case would have the most impact on the value of $\frac{\Delta}{P}$. Consequently, we could assign the calculated uniform EI for this specific case as the initial value for the ith section. In other words, we could find the initial value for $(EI)_i$. An example is shown in Figure 49 where the specified load/LVDT case would be the best to estimate the initial value of $(EI)_3$.

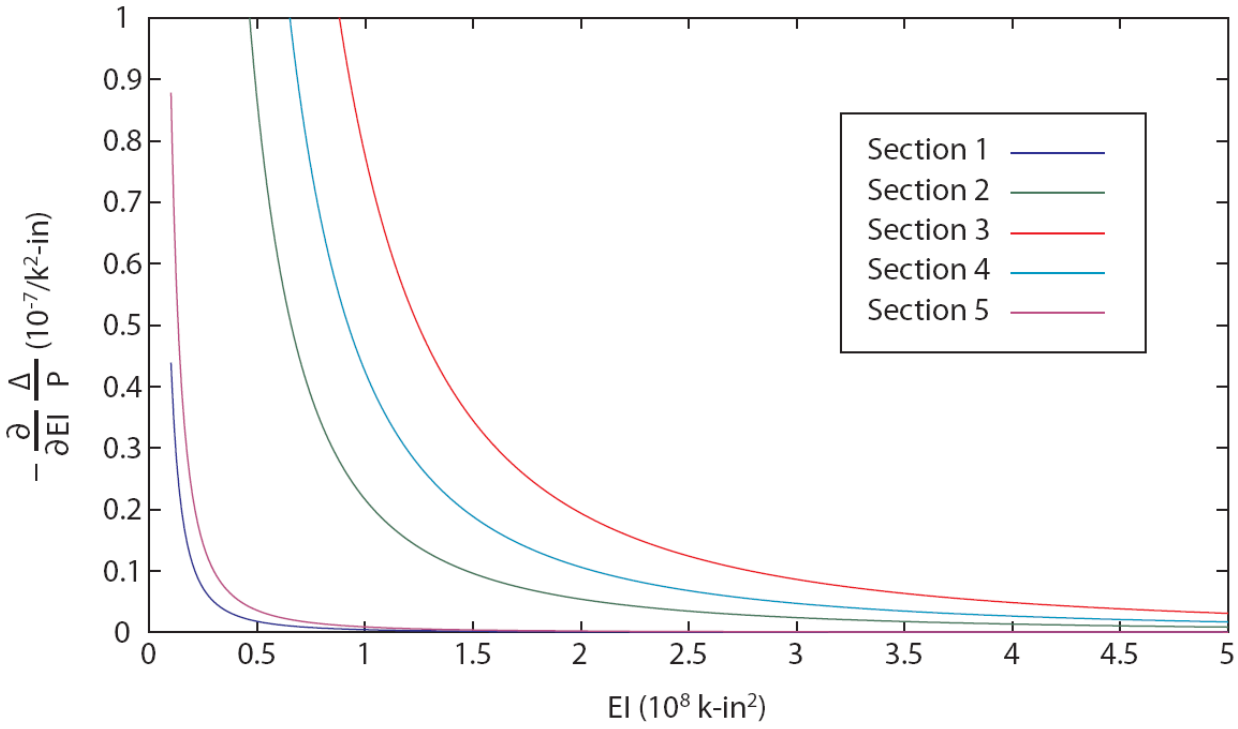

Figure 49: Sensitivity of $\frac{\Delta}{P}$ to each section's stiffness for flexural stiffness test 1A an d LVDT at +5.

Following this analytical approach, all flexural stiffness tests can be utilized to estimate the

initial values of $(EI)_1$ to $(EI)_5$. For the values of $(EI)_2$ to $(EI)_4$, i.e., the *EI* values of the middle three sections of the girder, a range of values for each *EI* is obtained. It is possible that some data needs to be eliminated if it seems to be a statistical outlier. An average value or upper and lower bounds for the initial *EI* of each of these three sections can be obtained. As validation, the initial values can be compared with expected values of *EI* based on the girder's geometry and theoretical values of *E*.

One issue that arose was that there were not any tests in which k_1 or k_5 were the maximum value for a load/LVDT case. This is expected given the analysis presented earlier in Section 4.3.3. This resulted in no basis for determining an initial guess for those sections; however, it can be assumed that they are relatively close to the neighboring sections. Additionally, some scenarios can be run using other assumptions; the stiffness may be higher or lower than the neighboring sections.

4.4.5 Linear Least-Squares Solutions

Applying an unconstrained linear-squares solver to the inverse problem leads to a set of physically meaningless results for the five *EI* values as shown in Figure 50.

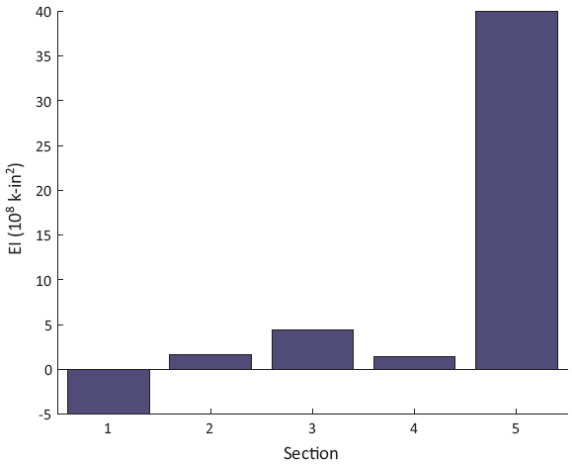

Figure 50: Unconstrained linear least-squares results for piecewise flexural stiffness of the I-244 girder with initial values of zero.

Two MATLAB built-in functions are utilized in this study; *lsqnonneg.m* and *lsqlin.m*. They both use least-squares algorithms to solve the $Ax = b$ problem. *lsqnonneg.m* gives only positive values for the solution. The *EI* values for the ends of the girder took zero values when the initial values were zero, the default option. Manipulating the starting value changes the results, where the end values typically stay pretty close the original guess. The other MATLAB function, *lsqlin.m*, basically does the same except that there is more freedom in the choices of constraints. The most valuable to this study is the ability to set boundaries on the solution. The upper boundary is not of much concern because of the problem's tendency to go towards negative values, although if the upper boundary is set sufficiently close to the results, it will have an impact. As was seen with *lsqnonneg.m*, the values for the ends of the girder stay close to the lower boundary constraint. This is a little troubling because it seems that the solution is artificial. The results are less affected by the lower boundary constraint if it is sufficiently low,

however , this gives values of *EI* that are orders of magnitude larger at the ends than at the middle of the girder.

Figure 51(a) shows ten sets of initial values of the five *EI* value carefully decided in this study, while Figure 51(b) shows their corresponding linear least-squares results using the MATLAB function *lsqlin.m*. The initial guesses were largely left alone through Sections 2 to 4 because data is available to help determine what the initial guess should be in those regions (see Section 4.4.4). Sections 1 and 5 were varied quite a bit, however, because that data was not available. Due to the known damage and repairs done to Section 1, initial guesses were made in that region that were significantly higher and lower than the average of the stiffness values from the sensitivity study. Similar variations were made to Section 5 to see how it would affect the results. When the initial guess for the stiffness of Section 1 was slightly lower or higher than average or much higher than average, the trend was consistent. Stiffness was high in Section 1, low in Section 2, high in Section 3 and descending stiffness in Sections 4 and 5. When stiffness was assumed much lower (45%) in Section 1 than the average, the trend showed low stiffness in Sections 1, 2, 4 and 5 with much higher stiffness in Section 3. Changing the initial guess for stiffness in Section 5 had little impact on the overall trend of stiffness variation.

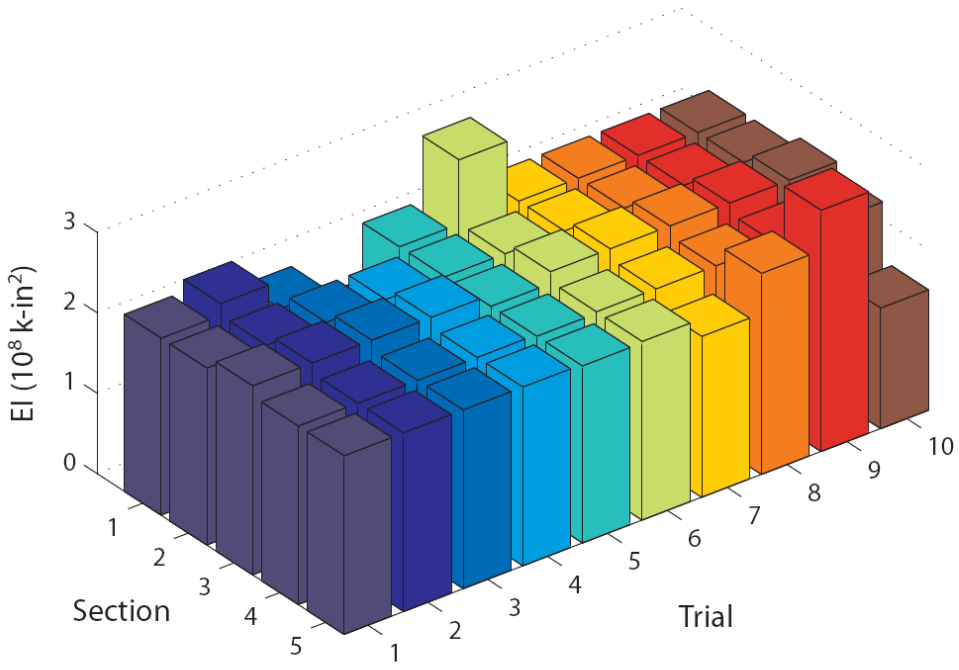

(a)

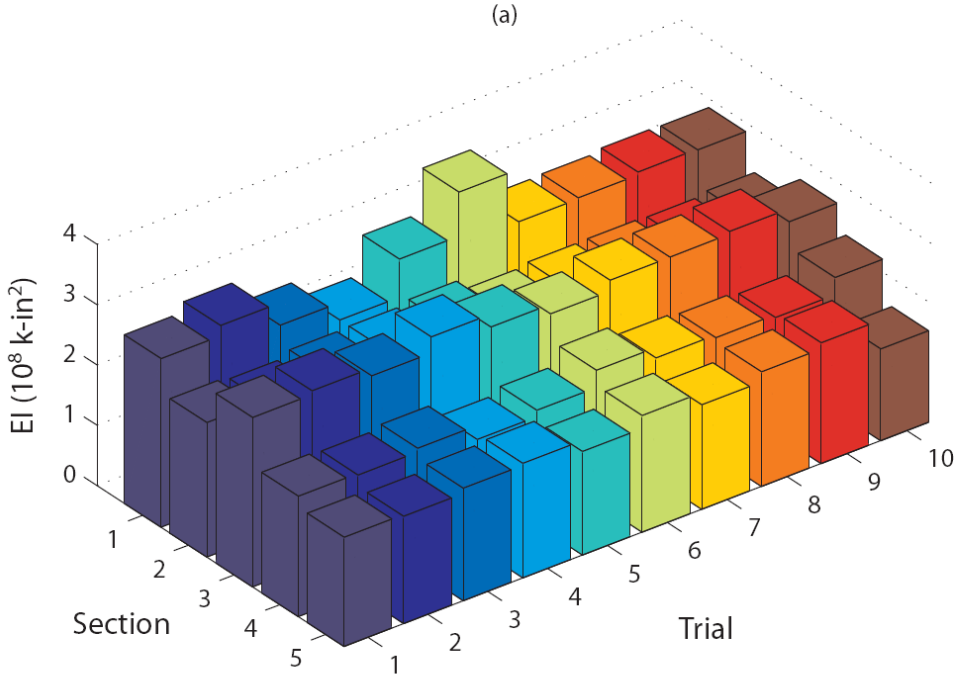

(b)

Figure 51: (a) Various initial values defined in this study, and (b) the results obtained by using the initial values specified in (a).

Random initial values were also attempted so that other possible solutions may be found. The initial values and the results are presented in Figure 52(a) and (b), respectively.

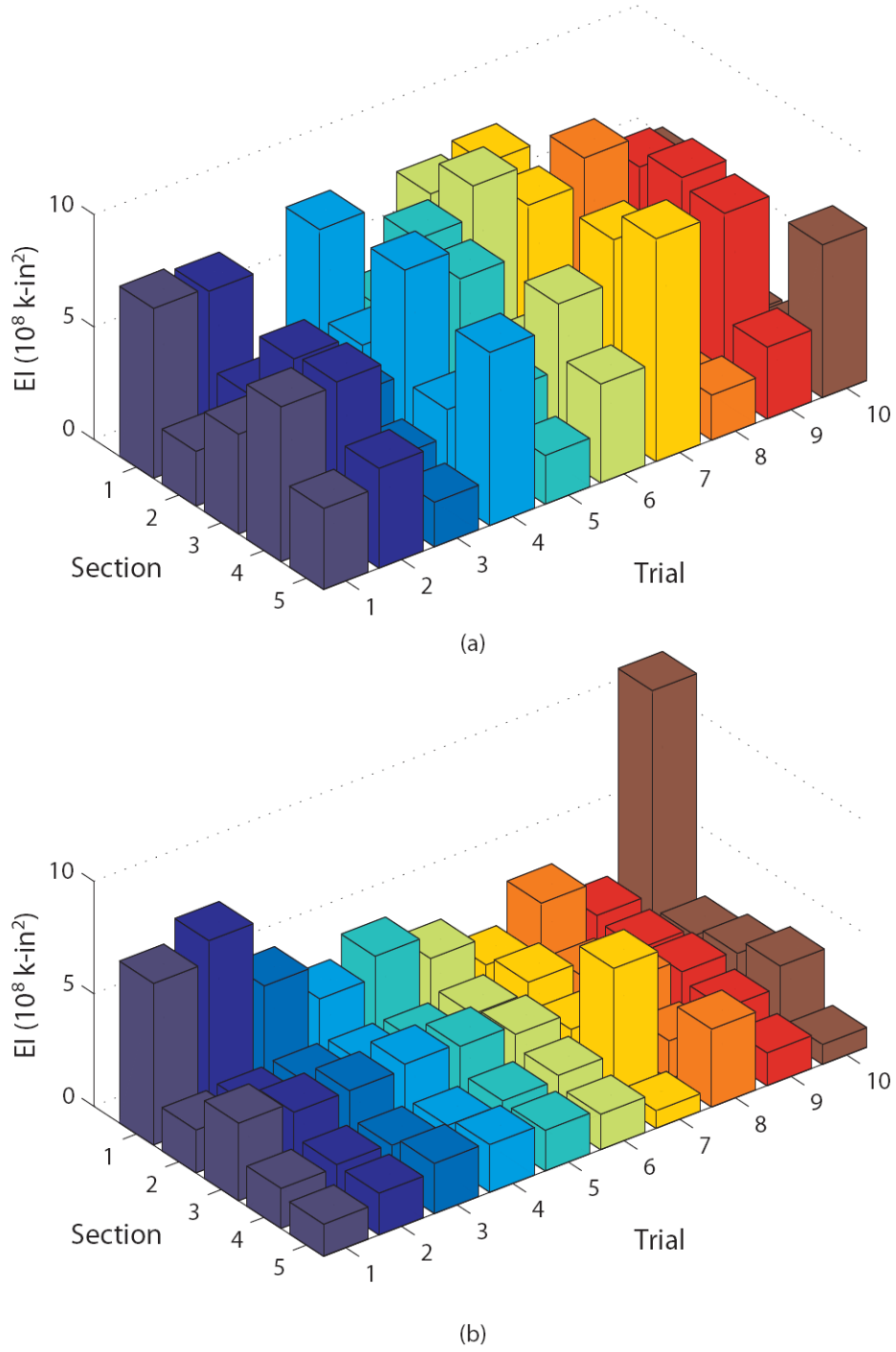

Figure 52: (a) Random initial values adopted in this study, and (b) the results obtained by using the random initial values specified in (a).

These results show a similar trend as those in Figure 51; however, they are not as consistent. The flexural stiffness is generally larger in Sections 1 and 3 than in the other sections.

4.5 Processing Camber Measurements

4.5.1 Review of Time-Dependent Deformation

The very large camber measured from the I-244 Bridge girder has caused a daunting challenge in this inverse analysis - A direct consequence is a very unreasonably high estimated value of effective prestress value (Sandburg [2007]). Possible causes for excessive camber measurements might include the following (and their combinations):

- Creep of concrete and relaxation of tendon
- Aging of concrete that leads to a reduced value of E_c (see Equation (5-1) on pp. 209R-23 in ACI [1997])
- A possible over-design of the girder
- Measurement errors

To better understand the problem at hand (in particular, the effect of creep on camber measurements) and improve the inverse analysis, ACI [1997] and Branson [1977] are reviewed. A summary of the review of ACI [1997] is presented below first followed by another review summary of Branson [1977].

Overall, the prediction of creep of prestressed concrete structures as needed in our study is a complicated issue, however it could be accomplished with reasonable accuracy using a linear combination of various contributing factors. Sections 3.2.1 *Principal facts* and 3.2.2 *Assumptions* on pp. 209R-12 in ACI [1997] are very useful in this regards. In addition, the overall assumptions made in Section 4.1.1 *Assumptions* for long-term deflection and loss of prestress in statically determinate structures on pp. 209R-16 are valuable. They may justify why we can predict the shear capacity of the I-244 girder as if it did not have any creep-related issue.

ACI [1997] emphasizes greatly the influence of environmental factors and loading history to creep (e.g., on pp. 209R-4), which prompts the need to have a proper documentation of (i.e., accurate information on) the history of the I-244 girder. The formulas used can be found in Equations (4-16) for camber at an arbitrary time and (4-17) for ultimate camber in Section 4.4.2 *Camber of noncomposite prestress concrete girders* on pp. 209R-18, Equations (4-21) and (4-22) for unshored and Equations (4-23) and (4-24) in Section 4.5.2 *Camber of composite girders-precast girders* prestressed unshored and shored construction. In particular, Table 4.4.2.1 for instantaneous camber calculation is more comprehensive that those found in Lin and Burns [1981]. The formulas for ultimate camber could be used in this study to help rule out, at least to some extent, the possibility of any over design and severe measurement errors. In addition, nonhomogeneity of creep mentioned on pp. 209R-22 and 209R-23 might be also applicable to the I-244 girder and calls for a better understanding.

Factors contributing to time-dependent deformation of prestressed concrete can be broken down into the following ten parts (Branson [1977], ACI [1997]):

1. Elastic camber due to initial prestress after elastic losses

2. Elastic deflection due to dead load of prestressed concrete girder
3. Creep camber due to prestressing force up until slab casting
4. Creep camber after slab casting
5. Creep deflection from prestressed concrete girder dead load up until slab casting
6. Creep deflection from prestressed concrete girder dead load after slab casting
7. Elastic deflection due to dead load of slab
8. Creep deflection due to dead load of slab
9. Deflection due to differential shrinkage
10. Elastic deflection due to live load

The time-dependent deformation can be multiples of the elastic deflection due to prestressing force and self weight of the girder and slab with the exception of differential shrinkage. Deflections not due to prestressing force may simply be subtracted from the measured deflections, while deflections due to prestressing force may be expressed as a single constant multiplier (that depends on environmental and material conditions) of the prestressing force being calculated.

4.5.2 Overview of Proposed Research

First of all, we communicated with Mr. Bob Rusch and Mr. Walt Peters in the Bridge Division at the ODOT to obtain as much information as possible on the loading and unloading history of the I-244 Bridge girder given the importance of the information on the analysis of time dependent deformation. Following Figure 5-4 on pp. 395 in Branson [1977], a schematic load and unloading history of the real-world girder is illustrated in Figure 53. Note that not all critical information is available to us, such as (1) the time at which the slab was cast, (2) the time at which the overlay was placed and (3) any time that other sustained loading was applied (Peters and Rusch [2006 - 2008]).

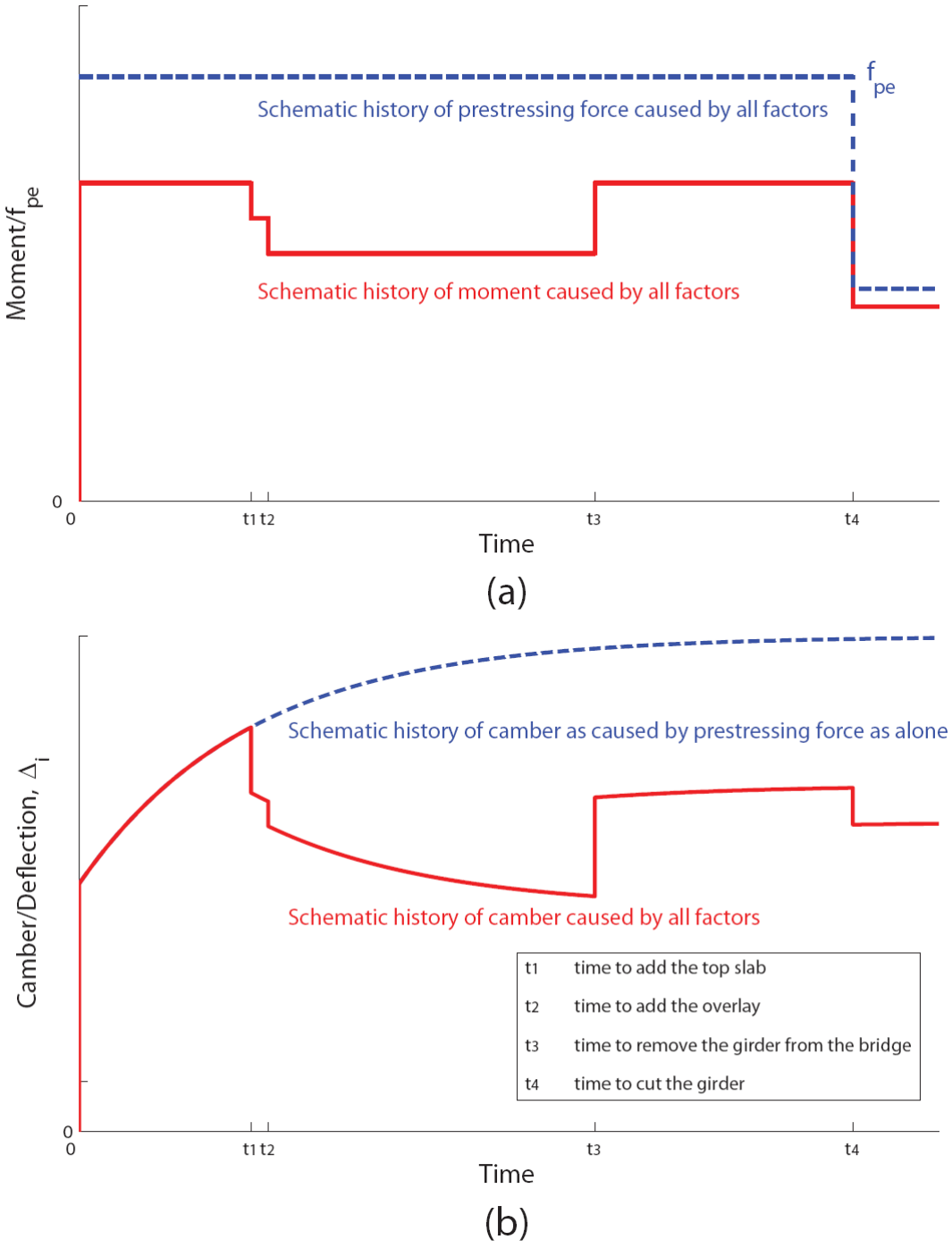

Figure 53: Illustrations of the applied moment and camber histories for the I-244 Bridge girder to the best of our knowledge.

Given the technical challenges elaborated previously, the following aspects are included in this inverse analysis: (1) forward analysis helping the problem formulation and result analysis of the inverse analysis, (2) a numerical process directly to carry out the inverse analysis, and (3) preprocessing.

For the entire project, it seems feasible to carry out forward analysis of time-dependent deformation for (1) the girder fetched from the I-244 Bridge, (2) a generic interior girder on the Little River Bridge, and (3) the girder obtained from Wild Horse Creek Bridge, respectively. In detail, the I-244 Bridge girder may be considered composite unshored construction (Peters and Rusch [2006 - 2008]), (2) the interior girder on the Little River Bridge would be composite unshored construction, and lastly, (3) the girder from Wild Horse Creek Bridge would be a composite girder.

A two-stage strategy is proposed for both forward and inverse analysis: Preliminary analysis is carried out first; it results are reported in Section 4.5.3. Refined analysis is followed; some highlights are included in Section 4.5.4. The basic assumptions made in the preliminary analysis are listed as follows:

1. Self weight uniformly distributed
2. Effect of draped strands neglected
3. A constant EI considered throughout the span using one representative constant EI value or its two bounds

Refined analysis is built upon the following basic assumptions:

1. Self weight uniformly distributed
2. Effect of draped strands considered even including the asymmetrical profile of the harped strands in the shortened I-244 Bridge girder
3. Five different EI values considered throughout the span

There are two distinctive choices to formulate the inverse problem, and they are shown in Equations (32) and (33), respectively. The first method is to directly estimate the effective prestressing stress using eight of the ten terms from Branson [1977], ACI [1997] and listed in Section 4.5.1. The two terms that may be excluded are due to the elastic deflection of the slab and live load because they were not present at the time the measurements were taken. The second method is to estimate the effective prestressing stress considering (1) elastic deflections due to the prestressing stress and dead load of the prestressed concrete girder and (2) a scaling factor to be identified. This scaling factor can be considered a lumped effect of all time-dependent factors. Its identified value will then be validated using the existing knowledge on the topic, say, those in ACI [1997] and Branson [1977].

$$\sum_{i=1}^{8} \Delta_i = \Delta_T \tag{34}$$

$$\sum_{i=1}^{2} \Delta_i = \eta \times \Delta_T \tag{35}$$

where Δ_i and Δ_T stand for estimated individual and measured total camber/deflection, respectively. Note that the prestressing stress to be identified and the flexural stiffness values

are included in Δ_i's. η is the scaling factor to be identified.

The pros and cons of each problem formulation are listed in Table 15:

Equation	Pros	Cons
(34)	No identification of scaling factor	Required thorough understanding of time-dependent effects
	Physical interpretation is clear	Aleatory and epistemic errors lumped together
	Close integration of forward and inverse problem	Challenge to explain result if irrational
(35)	Control over epistemic uncertainties by scaling factor	Fear of wrong impression of fiddling with data
	Reasonable results expected	Challenge to explain results esp. scaling factor

Table 16: Pros and cons of two distinctive choices of problem formulation in inverse analysis.

Figure 54 illustrates a road map in terms of research tasks. Brief descriptions are given as follows:

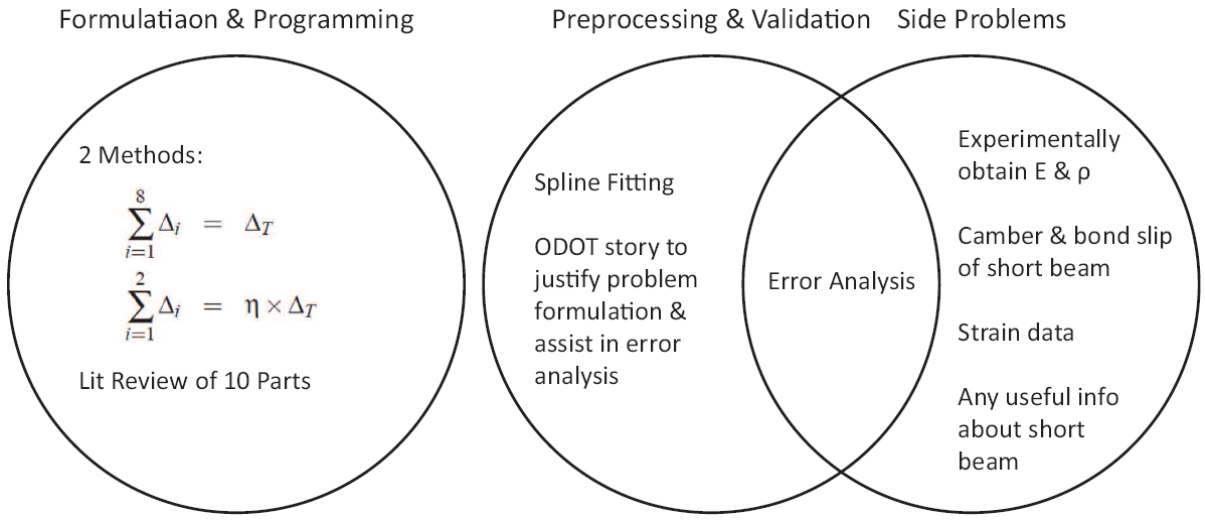

Figure 54: Breakdown of tasks.

Formulation and Programming The above discussions should suffice the problem formulation, while the coding under MATLAB will aim at general-purpose applications whenever possible.

Preprocessing and Validation Preprocessing of camber measurements can be further divided into two parts: (1) correcting the jumps in the camber measurements and (2) spline fitting of the data.

Side Items Side items supplement the analysis of camber measurements to increase understanding and confidence in the result.

4.5.3 Preliminary Analysis

All available camber measurements are summarized in Table 16. Figure 55 presents typical camber profiles obtained from the original and shortened I-244 girder, while in Figure 56 the instantaneous camber profile is simply double integrated from a constant bending moment diagram (with $EI = 2.3 \times 10^8$kip-in^2). The peak camber is proportional to the effective prestressing stress as well as the square of the span.

Girder	Before Shear#1	Before Shear #2	After Shear Tests
I-244 Bridge (Original)	Yes	Yes	No
I-244 Bridge (Shortened)	Yes	Yes	Yes
Wild Horse Creek Bridge	No	Yes	Yes

Table 17: Summary of available camber measurements.

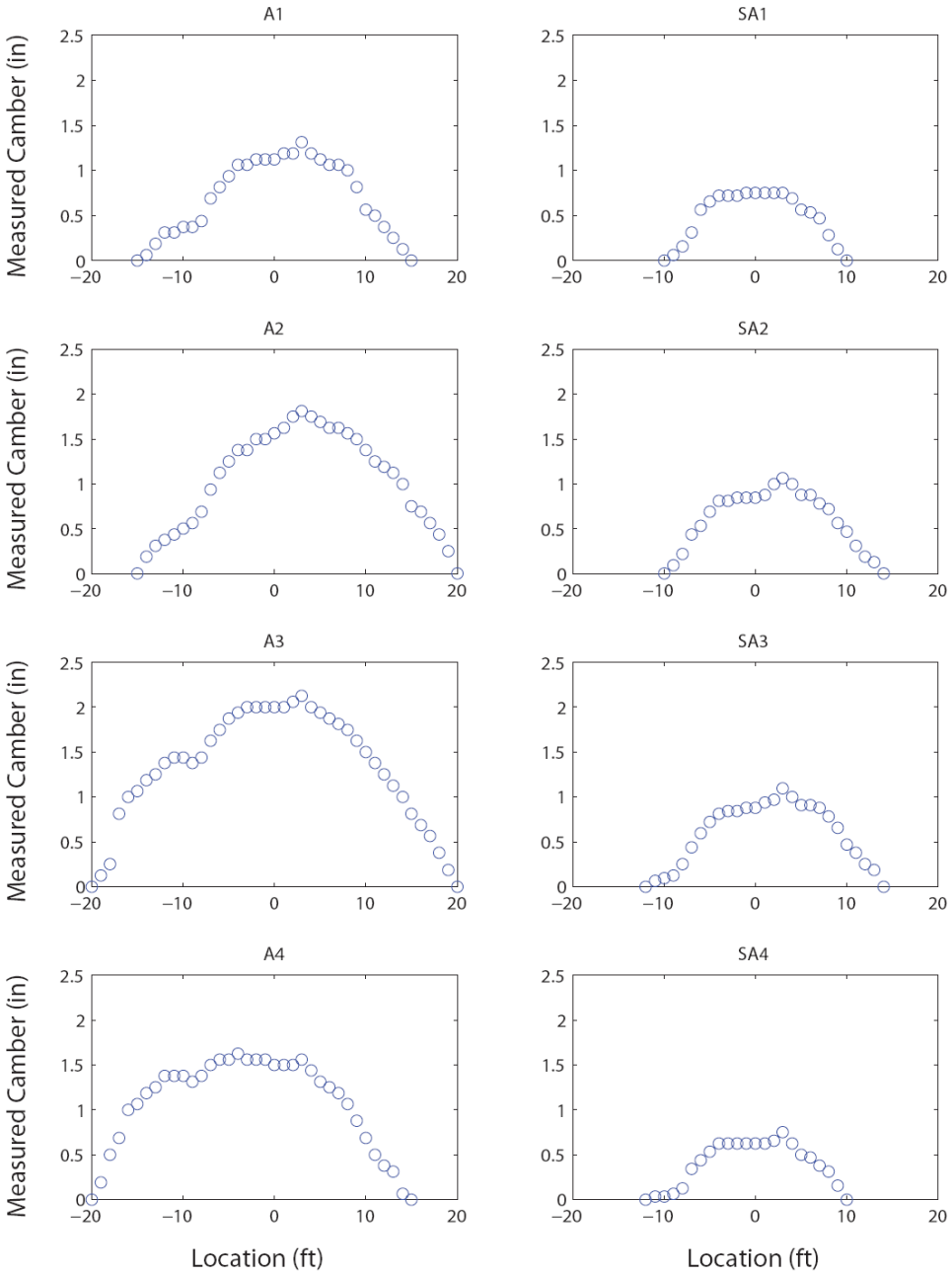

Figure 55: Typical camber profiles of the I-244 Bridge girder in an original and a shortened condition.

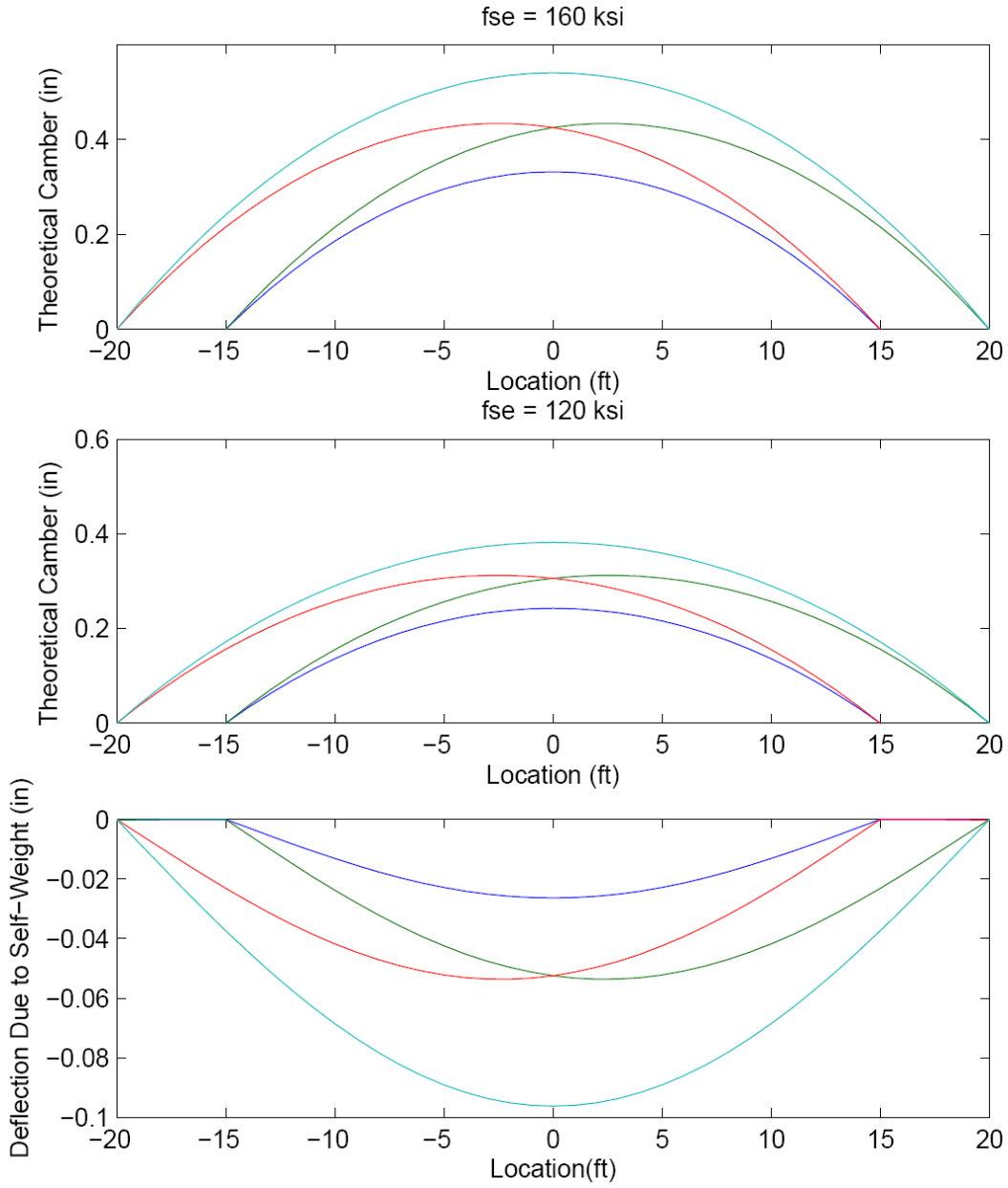

Figure 56: Theoretical values of camber and deflection of the original I-244 girder based on the basic assumptions made for preliminary analysis as in Section 4.5.2.

It can be seen that the measured peak camber can be as high as about four times of the theoretical instantaneous peak camber. This means that, the effect of creep of concrete, relaxation of steel tendons, etc., has significantly amplified the instantaneous camber. Further literature review will confirm if this amplification factor is considered normal. To confirm the significant role played by the abovementioned time-dependent effect, the inter-relations between the camber measurements are explored and presented in Table 17. Strictly speaking, the two sets of ratios in Table 17 cannot be made a light-to-light comparison. Nonetheless, the consistency shows the promise of using the existing formulas (for both instantaneous and creep effect) to analyze the results.

Test ID	A1	A2	A3	A4	SA1	SA2	SA3	SA4
Span	30’	35’	40’	35’	20’	24’	26’	22’
Ratio of span square	0.56	0.76	1	0.76	0.25	0.36	0.42	0.30
Prestressing stress	higher	higher	higher	higher	lower	lower	lower	lower
Anticipated ratio of instanta-neous peak camber	0.56	0.76	1	0.76	<0.25	<0.36	<0.42	<0.30
Peak camber read from Figure 55	1.3125”	1.8125”	2.1250”	1.6250”	0.7500”	1.0625”	1.0938”	0.7500”
Ratio of peak camber	0.6176	0.8529	1.0000	0.7647	0.3529	0.5000	0.5147	0.3529

Table 18: Quick analysis of peak camber measurements in Figure 55.

4.5.4 Refined Analysis

The refined analysis will estimate the piecewise constant *EI* values and effective prestressing stress considering the creep effect. The method used to consider creep and other time-dependent effects will be adopted from Branson [1977]. Equation (5-48) on page 400 provides the most applicable scenario for the I-244 Bridge girder. Some changes need to be made, however, before it can be used. For instance, the elastic deflection due to the slab and live loads need not be considered because they are not present at the time camber measurements were taken. Also, it may be necessary to add in a term or two to account for the high density overlay and transient sandbag loads, which may be borrowed from Equation (5-44) on page 398.

4.6 Discussions

4.6.1 Derivation of Camber Formulas Related to Asymmetrical Strand Profiles

To perform an inverse problem analysis on the shortened I-244 Bridge girder in the future, the asymmetrical draped strand profile needs to be taken into consideration when the camber measurements are analyzed. Presented in this section is a theoretical study for this future work. It is assumed that the modulus of elasticity remains constant throughout the material. The time-dependent effects are not considered. Since the analysis is performed on a real world girder, flexural stiffness will be experimentally determined at a few typical locations along the span.

To start, the principle of virtual force is used to derive the equation for camber. The prestressed girder of interest has straight and asymmetrically draped strands. The equation should be able to handle both types of strands. It will be compared with the following published equations from Lin and Burns [1981]:

$$\Delta = \frac{M_1 L^2}{8EI} \tag{36}$$

$$\Delta = \frac{L^2}{8EI}\left[M_2 + M_1 - \frac{M_1}{3}\left(\frac{2a}{L}\right)^2 \right] \tag{37}$$

where the value for each moment can be expressed as:

$$M_i = F_x y_i \tag{38}$$

Equation (36) applies only to straight strands. Equation (37) is more complicated and applies to symmetrically draped strands. Equation (37) also works for straight strands when the geometry is appropriate. To derive the camber formula for the asymmetrically draped strands consider the free body diagram shown in Figure 57:

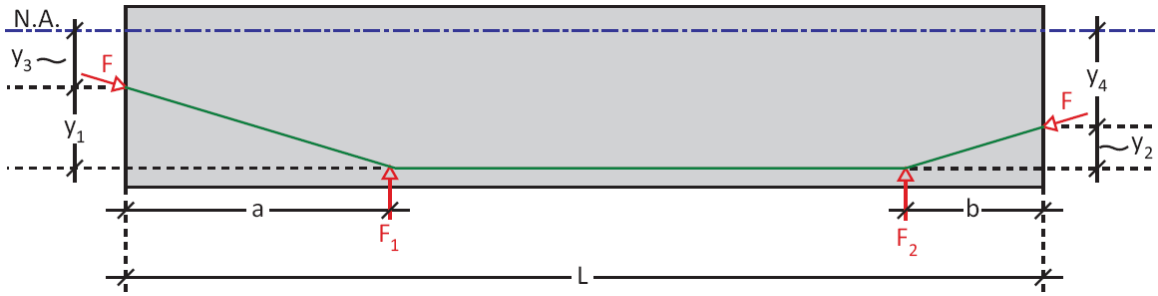

Figure 57: Free body diagram of an asymmetric prestressed girder with draped strands.

When y_1, y_2, a, and b are 0, the prestressing strands are straight. According to Equation (38) this means that $M_1 = 0$ and Equation (37) then reduces to Equation (36). If it can be shown that the derived equation will reduce to Equation (37) when the geometries are correct, the equation will also work for straight strands and symmetrically draped strands. This also provides a means of validation that the derived equation will work for asymmetrically draped strands.

Figure 57 will be decomposed into two free body diagrams containing horizontal and vertical forces which are shown with their corresponding moment diagrams in Figure 58.

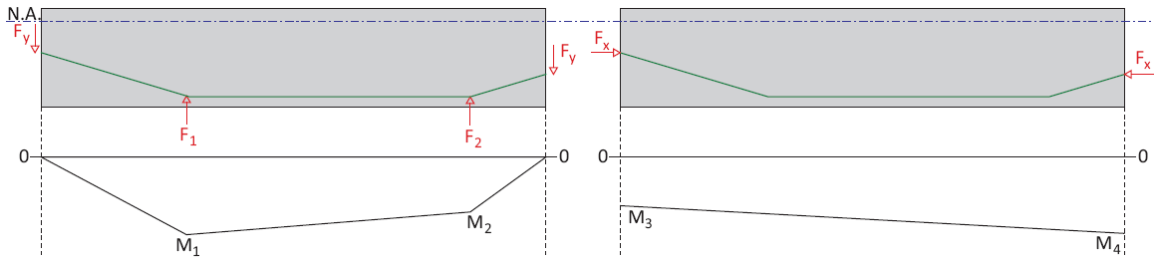

Figure 58: Free body diagram shown in Figure 57 broken down into x- and y-components.

The virtual load will be applied at midspan because Equations (36) and (37) are for deflections at midspan. This has practical benefits as it will simplify the derivation and the deflection at midspan should be large enough to measure on the real girder. An integration table that depends on the shapes of the virtual and real moment diagrams as commonly seen in structural analysis textbooks (e.g., Hibbler [2006]) is used to solve the following integration:

$$\Delta = \int_0^L \frac{mm'}{EI} dx \tag{39}$$

Since there are two moment diagrams that must be accounted for, Equation (39) becomes:

$$\Delta = \frac{1}{EI} \int_0^L \left(\frac{m_1 m'}{EI} + \frac{m_2 m'}{EI} \right) dx \tag{40}$$

Figure 59 shows the moment diagrams from each load case compared with the virtual moment diagram, where the vertical moment diagram is divided into four sections so that the geometries for each moment diagram can be used with the integration table. The same applies to horizontal moment diagram, except that only two sections are needed.

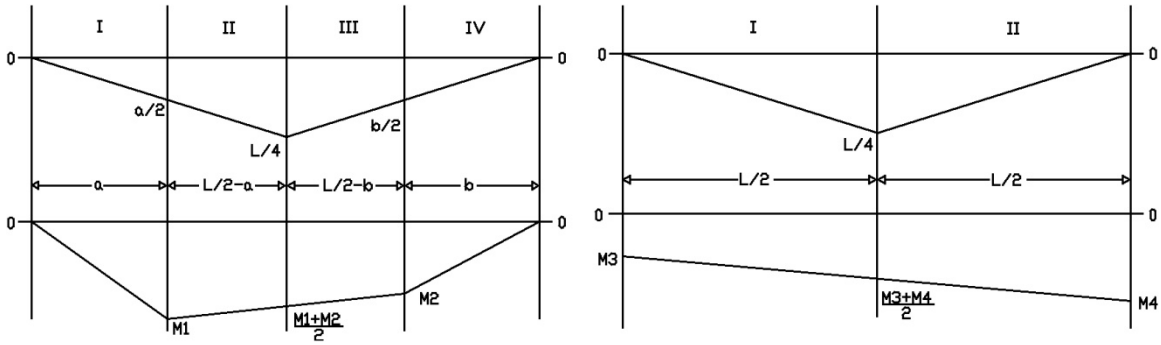

Figure 59: Moment diagrams of real and virtual forces.

Applying the integration table to Equation (40) gives:

$$\Delta = \frac{1}{EI}\left[\begin{array}{c} \frac{1}{3}M_1\frac{a}{2}a + \frac{1}{6}\frac{L}{4}\left[M_3\left(L+\frac{L}{2}\right)+M_4\left(L+\frac{L}{2}\right)\right]\cdots \\ +\frac{1}{6}\left[\frac{a}{2}\left(2M_1+\frac{M_1+M_2}{2}\right)+\frac{L}{4}\left(M_1+M_1+M_2\right)\right]\left(\frac{L}{2}-b\right)\cdots \\ +\frac{1}{6}\left[\frac{L}{4}\left(M_1+M_2+M_2\right)+\frac{b}{2}\left(\frac{M_1+M_2}{2}+2M_2\right)\right]\left(\frac{L}{2}-b\right) \end{array}\right] \quad \textbf{(41)}$$

$$= \frac{1}{48EI}\left[\begin{array}{c} M_1\left(-2a^2+aL+3L^2-bL-2b^2\right)\cdots \\ +M_2\left(-2a^2-aL+3L^2+bL-2b^2\right)+3M_3L^2+3M_4L^2 \end{array}\right] \quad \textbf{(42)}$$

Equation (42) can be checked with the published equations by inputting the appropriate terms for the corresponding geometries. In the symmetrically draped condition $M_1 = M_2$ and $M_3 = M_4$ which reduces Equation (42) to Equation (37).

Each term of the equation depends on F_x, so it can be factored out and solved for by inputting the value for Δ, the deflection due to prestressing force. A summation can be introduced into Equation (42) so that each strand is accounted for as is done in the following equation:

$$F_x = \frac{\Delta}{\frac{1}{48EI}\sum_{j=1}^{n}\left[\begin{array}{c} y_{1j}\left(-2a_j^2+a_jL+3L^2-b_jL-2b_j^2\right)\cdots \\ +y_{2j}\left(-2a_j^2-a_jL+3L^2+b_jL-2b_j^2\right)+3y_{3j}L^2+y_{4j}L^2 \end{array}\right]} \quad \textbf{(43)}$$

where n = the number of prestressing strands in the girder.

4.6.2 Other Means to Estimate Prestressing Stress

Prestressing force can be determined using Mohr's circle if certain data is available. Figure 60 represents Mohr's circle at the neutral axis of a prestressed concrete girder when cracking occurs.

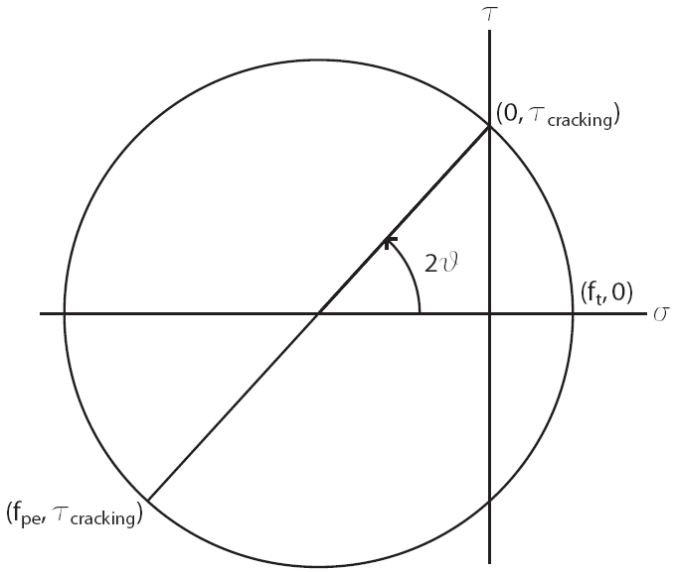

Figure 60: Mohr's Circle of an element at the neutral axis of a prestressed concrete girder when shear cracking begins.

Since there is no moment due to external loads at the c.g.c., the only axial stress present is that from the prestressing strands. This is a combination of the direct axial force and the moment produced by the eccentricity of the strands at the section. Since we know the geometry of the girder, these values can be expressed as a function:

$$f_{pe} = g_1(F) \tag{44}$$

where F is the total force in the prestressing strands.

The shear stress is a function of the shear force due to the external load as well as the prestressing force (because of the moment that it generates). It can be expressed as:

$$\tau_{cracking} = \frac{VQ}{Ib} + g_2(F) \tag{45}$$

where V stands for the applied shear force. Again, since we know the configuration of the girder, g_2 can be found.

Using basic geometry, the following derivation gives a function of prestressing force, applied shear and cracking angle.

$$\tan(2\theta) = \frac{\tau_{cracking}}{f_{pe}/2} \tag{46}$$

$$= \frac{2(\frac{VQ}{Ib} + g_2(F))}{g_1(F)} \tag{47}$$

$$g_1(F)\tan(2\theta) = 2\left(\frac{VQ}{Ib} + g_2(F)\right) \quad \textbf{(48)}$$

Knowing the tension capacity of concrete, f_t, will give the estimation of the total force in the prestressing stands, F:

$$\sin(2\theta) = \frac{\tau_{cracking}}{d/2} \quad \textbf{(49)}$$

$$d = \frac{2\tau_{cracking}}{\sin(2\theta)} \quad \textbf{(50)}$$

$$= \frac{2\left(\frac{VQ}{Ib} + 2g_2(F)\right)}{\sin(2\theta)} \quad \textbf{(51)}$$

$$d = g_1(F) + 2f_t \quad \textbf{(52)}$$

$$d = \frac{2\tau_{cracking}}{\sin(2\theta)} \quad \textbf{(53)}$$

$$= \frac{2\left(\frac{VQ}{Ib} + 2g_2(F)\right)}{\sin(2\theta)} \quad \textbf{(54)}$$

$$d = g_1(F) + 2f_t \quad \textbf{(55)}$$

$$f_t = \frac{d - g_1(F)}{2} \quad \textbf{(56)}$$

4.6.3 Future Work

Complete refined analysis of camber measurements Initially, raw data will be input into a non-linear least-squares solver. Assumptions will fill holes where information is not currently available, however, the analysis may be updated in the future. Preprocessing of the raw data may also be included to an updated analysis in attempt to reduce some of the measurement error.

Perform more data processing to reveal underlying knowledge An example along this line is the deflected shapes of the girder at various time instances during the flexural stiffness tests such as the ones shown in Figures 61 and 62. The potential use of these plots is in the estimation of the initial values for *EI*'s especially the two end values.

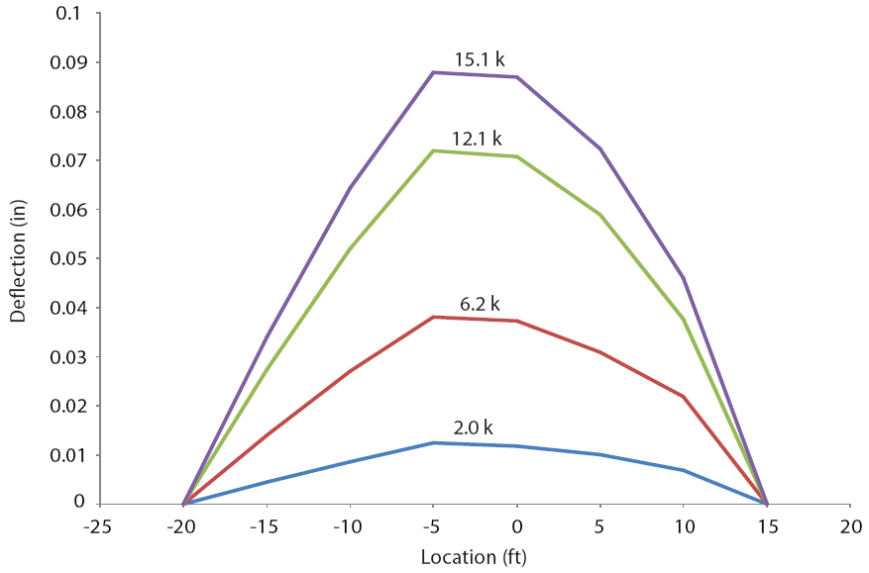

Figure 61: Deflection profile of girder during flexure test 3A at multiple loads.

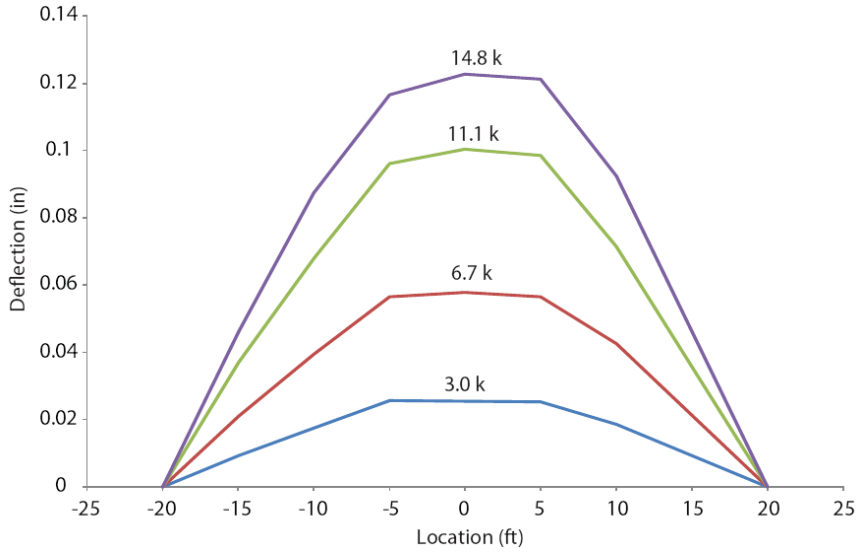

Figure 62: Deflection profile of girder during flexure test 4A at multiple loads.

Conduct more literature review on the identification of f_{se} We will study the traditional methods to determine f_{se}. In addition, we will learn existing work using inverse problem to determine f_{se}.

Understand more on prestressed concrete Topics include but not limited to the effect of debonding to the moment caused by prestressing stress. All these will improve problem formulation and result interpretation of the inverse problem.

Explore new ways to integrate the results of flexural stiffness and camber measurements For the sake of solving the inverse problem, it would be better to decouple these unknown quantities and identify them one by one. In terms of result validation, it would be better to make cross validation. For example, can the camber measurements tell us more about the distribution of the *EI* values? How much information are we supposed to identify out of the data that we have had?

Select the most suitable numerical methods This will be of great importance for us to improve our existing results of the *EI* values and refine the analysis of the camber measurements. Tools to handle the uncertainties in data should be looked into as well.

5 CONCLUSION

In general, AASHTO girders designed under AASHTO-STD may not be conservative according to AASHTO-LRFD and ACI-318. Girders with small transverse reinforcement spacing have the largest difference between margins of safety of AASHTO-STD and current codes because V_s/V_n is relatively large for AASHTO-STD. Girders with large transverse reinforcement spacing are of less concern, however, there is still a significant gap between margins of safety for AASHTO-STD and AASHTO-LRFD.

The interior girders on the Little River Overflow Bridge in McCurtain County, Oklahoma are unconservative according to AASHTO-LRFD but meet the minimum shear capacity according to ACI-318. With a margin of safety of 0.93 for AASHTO-LRFD, the design is close to meeting the requirements. Rating the bridge through LRFR, however, suggests that all AASHTO legal loads are permissible even when the condition is rated as poor. Additionally, there have been no signs of shear distress to the bridge which, in itself, justifies a lack of action.

The limited experimental results indicate the actual shear capacities of the two selected Type II AASHTO girders exceed all estimations put forth by all the above-mentioned codes. However, it should be noted that these experiments were conducted with a point load applied with $a/d \approx 1$ to enable a shear failure. This creates a potential disconnect between the code estimations and results because beam theory may not be applicable. Additionally, there are some girders in use that do not have the same design features as the ones tested in this study such as those on the Little River bridge.

Strut and tie models provide a conservative estimation of failure load in this analysis. The dependence on anchorage length for the prestressing strands limits the estimated capacity of the girder. Even when assuming that the prestressed tie is fully anchored, the applied shear at nominal strut capacity does not exceed that of the standard methods for analysis.

Shear failure may not be of much concern for AASHTO girders because of limited flexural capacity. For the selected I-244 Bridge girder, the applied shear at nominal flexural resistance is not large enough to exceed the nominal shear capacity outside $2d$ from the supports. The analysis may not apply within $2d$ from the supports because of a change in the failure mechanism.

Ongoing refinement of the analysis and data processing may further update these conclusions, most notably with estimated effective prestressing force of the tested real-world girders. Furthermore, it is recommended that additional future experimental tests be conducted to provide data as more evidence to support the analysis. The I-244 Bridge girder tested in this study is somewhat of a special case because its shear capacity was overdesigned for its time. Ideally, future specimens closer represent girders that are in real condition and of real concern for ODOT engineers (e.g., being close to or just under 1.0 for margin of safety under AASHTO-LRFD).

REFERENCE

AASHTO. *Standard Specifications for Highway Bridges*. 11th edition, 1973.

AASHTO. *Interim Revisions to Standard Specifications for Highway Bridges*. 16th edition, 1999.

AASHTO. *LRFD Bridge Design Specifications*. 2004.

AASHTO *Guide Manual for Condition Evaluation and Load and Resistance Factor Rating (LRFR) of Highway Bridges*. 1st edition, 2005.

ACI Committee 209R-92 Report: *Prediction of Creep, Shrinkage, and Temperature Effects in Concrete Structures*. Technical Report, 1997.

ACI Committee 440.2R-02 Report: *Guide for the Design and Construction of Externally Bonded FRP Systems for Strengthening Concrete Structures*. Technical report, 2002.

American Concrete Institute. *ACI Building Code Requirements for Structural Concrete and Commentary*, 2002.

ASTM Committee C09. *Standard Test Method for Compressive Strength of Cylinderical Concrete Specimens*. ASTM C39/C39M-01 edition, 2001.

T.M. Ahlbom. High Strength Prestressed Concrete Bridge Girders. PhD thesis, University of Minnesota, 1953.

E.C. Bentz, F.J. Vecchio, and M.P. Collins. "Simplified Modified Compression Field Theory for Calculating Shear Strength of Reinforced Concrete Elements". *ACI Structural Journal*, 103(4):614– 624, July-August 2006.

E.C. Bentz. AASHTO Calculator for cases with at least minimum reinforcement. http://www.ecf.utoronto.ca/~bentz/aashto.htm, Microsoft Excel, 2000.

D.E. Branson. *Deformation of Concrete Structures*. McGraw-Hill International Book Company, 2nd edition, 1977.

Bridge Diagnostic, Inc. *Strain Transducer for Structural Testing*. 2007.

M.D. Brown and O. Bayrak. "Design of Deep Beams using Strut-and-Tie Models - Part I: Evaluating U.S. Provisions". *ACI Structural Journal*, 105(4):395–404, July-August 2008.

Coreslab Structures (Okla) Inc. *Bridge 'A' Over Wild Horse Creek, Lincoln County, Oklahoma*. BRF-141C(119)CO - State Job No. 20731(04). 2004.

Coreslab Structures (Okla) Inc. Contract Proposal: Quotation on Casting Prestressed Type II Beams. Fax transmittal to University of Oklahoma, March 2006.

D.A. Cumming, C.E. French, and C. Shield. Shear Capacity of High-Strength Concrete Prestressed Girders. Technical report, University of Minnesota, 1998.

T.J. D'Arcy, G.D. Nasser, and S.K. Ghosh. "Building Code Provisions for Precast/Pretressed Concrete". *PCI Journal*, 48(6):116–124, November-December 2008.

D. Duthinh. "Sensitivity of Shear Strength of Reinforced Concrete and Prestressed Concrete Beams to Shear Friction and Concrete Softening According to Modified Compression Field Theory". *ACI Structural Journal*, 96(4):495–508, July 1999.

Forney Inc. *Instructional Manual LC-1 Digitial Load Indicator MN-TA-1237*. www.forneyonline.com, 2005.

M.A. Grubb. "What's up with the Letter 'R' Anyway?" Modern Steel Construction: Bridge Crossings. No. 5, March, 1997.

R.C. Hibbler. *Structural Analysis*. Prentice Hall, 6th edition, 2006. ISBN 0-13-147089-2.

B. Jaramilla, and S. Huo, "Looking to Load and Resistance Factor Rating." Public Roads, Federal Highway Administration, 69 (1): 58-65, 2005.

D. Kuchma, S. Yindeesuk, T. Nagle, J. Hart, and H.H. Lee. "Experimental Validation of Strut-and-Tie Method for Complex Regions". *ACI Structural Journal*, 105(5):578–589, September-October 2008a.

D.A. Kuchma, N.M. Hawkins, S.-H. Kim, S. Sun, and K.S. Kim. "Simplified Shear Provisions of the AASHTO LRFD Bridge Design Specifications". *PCI Journal*, 53(3):53–73, May-June 2008b.

T.Y. Lin and N.H. Burns. *Design of Prestressed Concrete Structures*. John Wiley & Sons, Inc., 1981.

Z. Ma, A.S. Saleh, and M.K. Tadros. "Shear Design of Stemmed Bridge Members: How Complex Should It Be?" *PCI Journal*, 42(5):88–93, September-October 1997.

R.D. Martin. Nominal Shear Capacities and Demands of Real-World PC Girders with Effective Prestressing Force Estimated from Experimental Data (Tentative Title)". Master's thesis, University of Oklahoma, School of Civil Engineering and Environmental Science, May 2009.

The MathWorks**.** *Optimization Toolbox™ User's Guide***,** www**.**mathworks**.**com**,** October 2008**.**

S. Mindess, J.F. Young, and D. Darwin. *Concrete*. Prentice Hall, 2nd edition, 2003.

Oklahoma Department of Transportation (ODOT). *Bridge Repair Details, I-244 over Arkansas River, Tulsa County, Bridges 'A' & 'B'*. July 2004.

Oklahoma Department of Transportation (ODOT), *Project Title to be Determined. Superstructure Sections.* F.A.P. I-244-2(132)093, 2006.

Oklahoma Department of Transportation (ODOT). *Plan of Proposed State Highway McCurtain County, Little River Overflow Bridge, Bridge C, Detail of Super structure & Detail of P.C. Beam*. Oklahoma Department of Transportation. RF-40(53). 1967.

S.E. Olesen, M.A. Sozen, and C.P. Siess. Investigation of Prestressed Reinforced Concrete for Highway Bridges, Part IV: Strength in Shear for Beams with Web Reinforcement. Technical report, University of Illinois, 1965.

W.L. Peters and R.J. Rusch. Conversations and Correspondence with Mr. Walter Peters and Mr. Robert Rusch regarding the Selected I-244 Bridge Girder. 2006 - 2008.

K.-H. Reineck, Editor. *Examples for the Design of Structural Concrete with Strut-and-Tie Models*. ACI SP-208. American Concrete Institute, 2007.

B.W. Russel and N.H. Burns. "Static and Fatigue Behavior of Pretensioned Composite Bridge Girders Made with High Strength Concrete". *PCI Journal*, 38(3):116–128, May-June 1993.

C.J. Sandburg. Shearing Capacity of Prestressed Concrete AASHTO Girders. Master's thesis, University of Oklahoma, School of Civil Engineering and Environmental Science, May 2007.

J.C. Santamarina and D. Fratta. *Discrete Signals and Inverse Problems: An Introduction for Engineers and Scientists*. Wiley, 2005.

J. Schlaich, K. Schäfer, and M. Jennewein, "Towards a Consistent Design of Structural Concrete," *PCI Journal*, 32(3):74-150, 1987.

M.A. Shahawy and B.D. Batchelor. "Shear Behavior of Full-Scale Prestressed Concrete Girders: Comparison between AASHTO Specifications and LRFD Code". *PCI Journal*, 41(3):48–62, 1996.

M.A. Shahawy and B.D. Batchelor. "Reader Comments: Shear Behavior of Full-Scale Prestressed Concrete Girders: Comparison between AASHTO Specifications and LRFD Code". *PCI Journal*, 42: 72–93, May-June 1997.

Sika Corporation. *SikaWrap Hex 100G, Class Fiber Fabric for Structural Strengthening*. http://www.sikaconstruction.com, 7.2003 edition, a. Identification No. 332-15F.

Sika Corporation. *Sikadur Hex 300/306, High-Modulus, High-Strength, Impregnating Resin*. http://www.sikaconstruction.com, 7.2003 edition, b. Identification No. 322-OH.

M.A. Sozen. Strength in Shear of Prestressed Concrete Beams Without Web Reinforcement. PhD thesis, University of Illinois, 1957.

K.S. Tawfiq. Cracking and Shear Capacity of High Strength Bridge Girders. Technical report, FAMU/FSU, 1995.

E.M. Zwoyer. Shear Strength of Simply-Supported Prestressed Concrete Beams. PhD thesis, University of Illinois, 1953.

J.M. Lewis, S. Lakshmivarahan, and S. Dhall. *Dynamic Data Assimilation: A Least Squares Approach*. Cambridge University Press. September, 2006.

APPENDIX A PROJECT TIME LINE

Time	Technical personnel	Milestone, focus and progress
August 2005	Jin-Song Pei, Walt Peters, and Richard Moon	A trip to visit the I-244 Bridge arranged for Dr. Jin-Song Pei by Mr. Walt Peters and Richard Moon where girders were demolished from the bridge
October to December 2005	Jin-Song Pei, Colby Sandburg, and Shannon Norton	Literature on experimental studies of shear capacities of prestressed concrete AASHTO girders searched and studied, and the LRFD example from ODOT studied by the team.
January to March 2006	Jin-Song Pei, Colby Sandburg, Walt Peters, Richard Moon, and Siv Sundaram	An idea of testing the demolished girders from the I-244 Bridge proposed by Dr. Jin-Song Pei. One girder located by Mr. Richard Moon, and its condition studied. The LRFD example using a similar problem programmed by Colby Sandburg. Efforts made by Dr. Jin-Song Pei to contact Krisda Piyawat in Thailand who was the candidate for finite element analysis in this project.
April 2006	Jin-Song Pei, and Colby Sandburg	Concrete Services Corporation (CSC) removed the slab part of the girder with Dr. Jin-Song Pei and Colby Sandburg on site. An idea of retrofitting the damaged end of the I-244 Bridge girder proposed by Dr. Jin-Song Pei. Programming of the LFRF example finished by Colby Sandburg with some questions remaining to consult ODOT engineers. Krisda Piyawat contacted Dr. Jin-Song Pei from Thailand.
May 2006	Jin-Song Pei, and Colby Sandburg	Quote and technical information on FRP obtained from CSC. Programming the Little River Bridge girder started by Colby Sandburg. Priyantha Wijesinghe recruited to the project.

Table 19: Project time line: Part 1 of 6.

Time	Technical personnel	Milestone, focus and progress
June 2006	Jin-Song Pei, Colby Sandburg, Priyantha Wijesinghe, and Christopher Davis	CSC applied FRP to the corroded end of the girder with Christopher Davis on site to document the entire process and the participation of Colby Sandburg for few days. The ACI committee reports on FRP (ACI [1996, 2002]) studied by Dr. Jin-Song Pei, Colby Sanburg and Christopher Davis. Regular conversations started by Krisda Piyawat with Dr. Pei.
July 2006	Jin-Song Pei, Colby Sandburg, Priyantha Wijesinghe, Christopher Davis, and Michael Schmitz	The I-244 Bridge girder delivered to Fears lab at OU and unloaded by Mr. Michael Schmitz, Colby Sandburg and Christopher Davis. Preparation for the testing of the girder started. Intention to return to OU to work on this project stated by Krisda Piyawat.
August 2006	Jin-Song Pei, Colby Sandburg, Priyantha Wijesinghe, Christopher Davis, and Michael Schmitz	A CD containing the work done in Year 1 submitted to ODOT. A presentation to ODOT engineers given by Colby Sandburg at Fears lab. Work on the inverse problem to determine prestressing stress started by Colby Sandburg under guidance by Dr. Jin-Song Pei. Preparation for the testing of the I-244 Bridge girder continued by the team. Paperwork to help Krisda Piyawat's return for the project started by Dr. Jin-Song Pei.
September 2006	Jin-Song Pei, Colby Sandburg, Priyantha Wijesinghe, Christopher Davis, Aaron Landrum, Hungjr Lin, and Michael Schmitz	Estimation of the failure load of the girder refined by Colby Sandburg under guidance by Dr. Jin-Song Pei. Preparation for the testing of FRP coupons started by Christopher Davis under guidance by Michael Schmitz following AST [1995]. Learning strain gauging from Mr. Michael Schmitz started by Priyantha Wijesinghe. Preparation for the testing of the I-244 Bridge girder continued by the team. Krisda Piyawat's return date fixed.

Table 20: Project time line: Part 2 of 6.

Time	Technical personnel	Milestone, focus and progress
October 2006	Jin-Song Pei, Colby Sandburg, Priyantha Wijesinghe, Christopher Davis, Aaron Landrum, Krisda Piyawat, Randy Martin, and Michael Schmitz	Need to determine the values of EI identified by Dr. Jin-Song Pei. FRP coupons prepared by Mike Schmitz. Priyantha Wijesinghe produced principle trajectory plots. Preparation for the testing of the I-244 Bridge girder continued by the team. Work on the finite element analysis for the project started upon the return of Krisda Piyawat. Randy Martin recruited to work on the project.
November 2006	Jin-Song Pei, Colby Sandburg, Priyantha Wijesinghe, Christopher Davis, Aaron Landrum, Krisda Piyawat, Randy Martin, and Michael Schmitz	Flexural stiffness tests started to determine the values of EI led by Colby Sandburg and with assistance by the team. Feasibility of using ANSYS for this project recommended by Krisda Piyawat.
December 2006	Jin-Song Pei, Colby Sandburg, Priyantha B. Wijesinghe, Christopher A. Davis, Aaron Landrum, Krisda Piyawat, Randy Martin, and Michael Schmitz	All flexural stiffness tests completed with significant team effort. Preliminary modal testing of the girder conducted by Priyantha Wijesinghe with assistance by the team. The first shear test conducted with significant team effort. Conversations with Coreslab initiated to obtain the second girder for testing. Finished testing all FRP coupons by Christopher Davis with unreasonable results. Work on ANSYS continued by Krisda Piyawat.
January 2007	Jin-Song Pei, Colby Sandburg, Krisda Piyawat, Priyantha B. Wijesinghe, Aaron Landrum, Randy Martin, and Michael Schmitz	The second shear test conducted with significant team effort. An idea of cutting the tested ends of the girder finalized by Dr. Jin-Song Pei with assistance by Mr. Walt Peters and Mr. Michael Schmitz. Preliminary data cleansing and processing effort started by Colby Sandburg under guidance by Dr. Jin-Song Pei. Priyantha Wijesinghe started to be trained on ANSYS by Krisda Piyawat.

Table 21: Project time line: Part 3 of 6.

Time	Technical personnel	Milestone, focus and progress
February 2007	Jin-Song Pei, Colby Sandburg, Krisda Piyawat, Priyantha B. Wijesinghe, Aaron Landrum, Randy D. Martin, and Michael Schmitz	Two failed ends of the girder removed with cylinder specimens cored at Fears lab as arranged by Mr. Michael Schmitz and with Colby Sandburg on site. A visit to Coreslab led by Randy Martin with Priyantha Wijesinghe's participation. Data cleansing and processing effort continued by Colby Sandburg under guidance by Dr. Jin-Song Pei. Learning MathCAD and project-related knowledge started by Randy Martin. Work on ANSYS continued by Krisda Piyawat and Priyantha Wijesinghe.
March 2007	Jin-Song Pei, Colby Sandburg, Krisda Piyawat, Priyantha B. Wijesinghe, Aaron Landrum, and Randy Martin	Three cylinder specimens cored from one girder end tested by Colby Sandburg. Data cleansing and processing effort continued by Colby Sandburg under guidance by Dr. Jin-Song Pei. Programming TY Lin's camber formulas started by Randy Martin. Work on ANSYS continued by Krisda Piyawat and Priyantha Wijesinghe.
April 2007	Jin-Song Pei, Colby Sandburg, Krisda Piyawat, Priyantha B. Wijesinghe, Aaron Landrum, and Randy Martin	Colby Sandburg's defense for his master's thesis prepared. Preparation for flexural stiffness tests of the shortened I-244 Bridge girder started by Aaron Landrum and Randy Martin. Work on ANSYS continued by Krisda Piyawat and Priyantha Wijesinghe.
May 2007	Jin-Song Pei, Colby Sandburg, Krisda Piyawat, Priyantha B. Wijesinghe, Aaron Landrum, and Randy D. Martin	Master's thesis defended by Colby Sandburg. A summer research schedule made by Dr. Jin-Song Pei with Randy Martin. A term paper on finite element element for the project completed by Priyantha Wijesinghe.
June 2007	Jin-Song Pei, Randy Martin, Priyantha Wijesinghe, and four NSF REU students	Colby Sandburg's master's thesis and defense ppt submitted to ODOT. All flexural stiffness tests of the shortened I-244 Bridge girder conducted by Randy Martin. Efforts made by the team to improve instrumentation for testing.

Table 22: Project time line: Part 4 of 6.

Time	Technical personnel	Milestone, focus and progress
July 2007	Jin-Song Pei, Randy Martin, and Priyantha Wijesinghe, and four NSF REU students	Shear tests completed on the shortened I-244 Bridge girder led by Randy Martin with contribution from the entire team. Dr. Thomas Kang joined the project as Randy Martin's thesis co-advisor. An abstract for an ACI convention submitted for review.
August 2007	Jin-Song Pei, Thomas Kang, Randy Martin, Krisda Piyawat, and Priyantha Wijesinghe	Work with the team started by Dr. Thomas Kang. A plan to write two journal publications made by Dr. Jin-Song Pei and Dr. Thomas Kang. Some progress on finite element analysis made by Krisda Piyawat.
September 2007	Jin-Song Pei, Thomas Kang, Randy D. Martin, Krisda Piyawat, and Priyantha Wijesinghe	Wild Horse Creek Bridge girder delivered from Coreslab to Fears lab. Five typical piecewise constant values for EI proposed by Dr. Jin-Song Pei. A 18-page summary of the finite element analysis work submitted by Krisda Piyawat.
October 2007	Jin-Song Pei, Thomas Kang, and Randy Martin	Five-EI-value codes programmed to MATLAB by Randy Martin. Preparation for testing the Wild Horse Creek bridge girder started.
November 2007 - July 2008	Thomas Kang, Jin-Song Pei, and Randy Martin	Analytical work nearly completed by Randy Martin under guidance by Dr. Thomas Kang. Some progress made on the inverse problem by Randy Martin under guidance by Dr. Jin-Song Pei.
April 2008	Jin-Song Pei, Thomas Kang, and Randy Martin	A presentation at an ACI convention made by Randy Martin for the experimental studies and inverse problem.
June & August 2008	Jin-Song Pei, Thomas Kang, Randy Martin, and Joe Howell	Experimental studies on the Wild Horse Creek Bridge girder completed by Randy Martin with some assistance by Joe Howell, an REU student from OU.

Table 23: Project time line: Part 5 of 6.

Time	Technical personnel	Milestone, focus and progress
August & September 2008	Jin-Song Pei, Thomas Kang, and Randy Martin	A preliminary study on strut-tie model completed.
September 2008	Jin-Song Pei, Thomas Kang, and Randy Martin	A preliminary report detailing the nearly completed analytical work and ongoing inverse problem prepared and submitted to ODOT by Randy Martin under guidance by Dr. Thomas Kang and Dr. Jin-Song Pei.
October 2008	Jin-Song Pei, Thomas Kang, and Randy Martin	Some progress made on the inverse problem by Randy Martin under guidance by Dr. Jin-Song Pei.
November 2008	Jin-Song Pei, Thomas Kang, Randy Martin, and Walt Peters	Detailed feedback provided by Mr. Walt Peters at ODOT on the preliminary report. Efforts started to address the feedback by Randy Martin under guidance of Dr. Thomas Kang. Final project report started to be assembled by Dr. Jin-Song Pei with assistance by Randy Martin.
December 2008	Jin-Song Pei, Thomas Kang, Randy Martin, and Rami Akkari	Feedback on the preliminary report continued to be addressed by Randy Martin under guidance by Dr. Thomas Kang. Final project report assembled by Dr. Jin-Song Pei and Randy Martin with assistance by Rami Akkari on ADA requirements.

Table 24: Project time line: Part 6 of 6